Systematic analysis of the synaptic recruitment and activation kinetics of presynaptic inhibitory group II metabotropic glutamate receptors

Dissertation

zur

Erlangung des Doktorgrades (Dr. rer. nat.)

der

Mathematisch-Naturwissenschaftlichen Fakultät

der

Rheinischen Friedrich-Wilhelms-Universität Bonn

vorgelegt von

Vanessa Rupprecht

aus

Volkmarsen

Bonn, März 2012

Angefertigt mit der Genehmigung der Mathematisch-Naturwissenschaftlichen Fakultät der Rheinischen Friedrich-Wilhelms-Universität Bonn.

Erstgutachter: Prof. Dr. Dirk Dietrich
Zweitgutachter: Prof. Dr. Gerhard von der Emde

Tag der Promotion: 17.8.2012
Erscheinungsjahr: 2012

Table of Contents

Acknowledgements **3**

Table of Contents **4**

Index of Figures **8**

Index of Tables **9**

Abbreviations **10**

Abstract **13**

1 Introduction **15**

1.1 Glutamate 15

1.2 Metabotropic glutamate receptors (mGluRs) 16

1.2.1 History 16

1.2.2 Structure 17

1.2.3 Types, expression and functional relevance 18

1.2.4 Presynaptic group II mGluRs 21

1.3 Hippocampus as a model for the investigation of presynaptic group II mGluR recruitment and kinetics 23

1.3.1 Anatomy 24

1.3.2 Function 26

1.3.3 Hippocampus and presynaptic group II mGluRs 26

1.4 Astrocytes 29

1.4.1 Morphology 29

1.4.2 Transporter mediated glutamate uptake 30

1.5 Aim of the study 32

2 Materials and Methods **34**

2.1 Animals 34

2.1.1 Species 34

2.1.2 Preparation of horizontal hippocampal slices 34

2.2 Solutions 36

2.2.1 Perfusion/ incubation solutions 36

2.2.2 Solutions for Patch clamp recordings 37

2.2.3 Solutions for calcium imaging experiments ... 38
2.2.4 Solutions for histochemical analysis ... 38
2.3 Drugs and reagents ... 40
2.4 Extracellular field potential recordings in the MML (DG) ... 41
2.4.1 Field potential recording setup ... 42
2.4.2 Electrodes ... 42
2.4.3 Positioning of electrodes ... 43
2.4.4 Stimulation protocol ... 43
2.4.5 Experimental procedure ... 43
2.4.6 Application of drugs ... 44
2.4.7 Analysis of fEPSP amplitudes ... 44
2.5 Presynaptic calcium imaging in the MML ... 45
2.5.1 Electrophysiological and imaging setup ... 45
2.5.2 Loading of AM ester calcium indicator dye into the MPP fibre bundle ... 47
2.5.3 Electrodes ... 48
2.5.4 Positioning of electrodes ... 48
2.5.5 Aperture ... 48
2.5.6 Analysis of MPP loading intensity and specificity ... 49
2.6 Caged glutamate ... 49
2.7 Uncaging light source ... 49
2.8 Uncaging protocol design – Method 1: Voltage sensitive dye imaging with RH155 ... 51
2.9 Uncaging protocol design – Method 2: Measuring astrocyte glutamate transporter currents ... 53
2.9.1 Patch clamp setup and experimental procedure ... 53
2.9.2 Astrocyte identification ... 54
2.9.3 Whole cell configuration ... 55
2.9.4 Voltage clamp mode ... 56
2.9.5 UV laser uncaging protocol design ... 56
2.9.6 Application of drugs ... 56
2.9.7 Analysis of glutamate transporter transients ... 57
2.10 Combinatory Ca^{2+} imaging and uncaging protocol ... 57
2.11 GFAP Immunhistochemistry ... 58
2.11.1 Analysis of immunhistochemical treated brain slices ... 59

3 Results ... 60

3.1 Systematic analysis of presynaptic group II mGluR activation by synaptically released glutamate ... 60

3.1.1 mGluR activation by spontaneous, stimulation independent glutamate release ... 60
3.1.2 mGluR activation by stimulation induced synaptic release of glutamate ... 63
3.1.3 mGluR activation depending on stimulation frequency ... 68
3.1.4 mGluR activation dependence on duration of stimulation ... 70
3.1.5 Time course of mGluR mediated feedback inhibition of synaptic transmission ... 73
3.1.6 Influence of repetitive burst stimulation on mGluR activation ... 75
3.2 Presynaptic Ca^{2+} imaging as a tool to directly assess presynaptic inhibition ... 78
3.2.1 Loading of MPP fibres with an AM ester Ca^{2+} indicator dye ... 78
3.2.2 Pharmacological group II mGluR activation depresses the Ca^{2+} signal amplitude ... 81
3.2.3 Influence of glutamate uncaging induced mGluR activation on Ca^{2+} signal amplitude ... 82
3.3 Assessing the time course of extracellular glutamate during uncaging ... 84
3.3.1 Method 1: Voltage sensitive dye imaging with RH155 ... 84
3.3.2 Method 2: Measuring astrocyte glutamate transporter currents ... 87
3.4 Receptor kinetics of presynaptic group II mGluRs ... 90
3.4.1 Latency and activation kinetics ... 90
3.4.2 Deactivation kinetics ... 92
3.5 Collaborative work ... 96
3.5.1 Does mGluR8 activation affect vesicle refilling in lateral perforant path terminals? ... 96
3.5.2 Does frequency facilitation at mossy fibres synchronously go along with an increase in Ca^{2+} influx? ... 98

4 Discussion ... 100

4.1 Limiting factors of presynaptic inhibitory group II mGluR activation ... 100
4.1.1 Performing field potential recordings to systematically investigate group II mGluR activation ... 102
4.2 Kinetics of presynaptic group II mGluR mediated inhibition ... 103
4.2.1 Using Ca^{2+} imaging as a tool to assess the dynamics of mGluR mediated inhibition ... 106
4.2.2 Using flash photolysis to expose mGluRs to glutamate ... 107
4.2.3 Applying voltage sensitive dye imaging to assess extracellular glutamate levels during uncaging ... 108
4.2.4 Performing glutamate transporter current measurements on astrocytes during flash photolysis to evaluate extracellular glutamate levels ... 109

4.3 Pharmacological activation of mGluRs versus endogenous activation by glutamate 109

4.4 How and when could presynaptic inhibitory group II mGluRs activate under physiological conditions? 111

4.5 Potential significance of group II mGluR mediated inhibitory modulation of presynaptic glutamate release in the hippocampus..... 113

4.5.1 mGluR mediated inhibition of glutamate release versus GABAergic inhibition..... 114

5 Summary 116

6 Zusammenfassung 118

7 Perspectives 121

8 References 122

9 Appendix 137

9.1 Curriculum Vitae..... 137

9.2 Erklärung..... 139

Index of Figures

Figure 1. Schematic diagram of the mGluR dimer in different activity states. 18
Figure 2. Localization of glutamate receptors at a theoretical CNS synapse. 21
Figure 3. Schematic view of the hippocampal anatomy and the synaptic connections of the main hippocampal pathway. 25
Figure 4. Distribution of immune-reactivity for mGluR2/3 in rat hippocampus..... 28
Figure 5. Schematic illustration of glutamate uptake. 31
Figure 6. Sectioning-steps during hippocampal slicing procedure. 35
Figure 7. Line drawing illustrating the main hippocampal synaptic connections and the area of stimulation and field potential recording. 41
Figure 8. fEPSP recording setup. 42
Figure 9. Stimulation protocol 44
Figure 10. Imaging and recording setup 47
Figure 11. UV laser flash photolysed CMNB-caged fluorescein – adjustment of imaging and uncaging plane. 50
Figure 12. A schematic example of a voltage imaging system. 52
Figure 13. Imaging and patch clamp setup. 54
Figure 14. Combined stimulation, uncaging and imaging protocol. 58
Figure 15. Glutamate transporter blockade with 100µM DL-TBOA leads to accumulation of spontaneously released glutamate. 62
Figure 16. Glutamate transporter blockade by DL-TBOA facilitates mGluR mediated inhibition of synaptic transmission. 65
Figure 17. GABA receptors do not significantly contribute to LY341495 induced increase in fEPSP amplitude. 68
Figure 18. Group II mGluR activation increases with firing frequency of presynaptic neurons..... 69
Figure 19. Prolonged presynaptic fibre activity strengthens group II mGluR activation. 72
Figure 20. Group II mGluRs activate within 200ms and remain active for at least 800ms. 74
Figure 21. Repetitive burst stimulation does not potentiate mGluR mediated feedback inhibition. inhibitory effect that significantly differs in strength from values obtained in single burst experiments. 77
Figure 22. The Ca^{2+} signal is of presynaptic origin. 80
Figure 23. Activation of group II mGluRs by DCGIV causes a decrease in calcium signal amplitude. 81
Figure 24. Glutamate uncaging induced group II mGluR activation in the MML causes presynaptic calcium signal depression. 83
Figure 25. Voltage sensitive dye imaging with RH155 is not suited to detect astrocyte membrane potential changes during glutamate uncaging..... 86

Figure 26. Astrocyte glutamate transporter current profile is strongly dependent on pharmacology and the UV laser uncaging protocol. 89
Figure 27. Activation kinetics of presynaptic group II mGluRs 91
Figure 28. Persistent glutamate due to slow glutamate reuptake after uncaging possibly interferes with mGluR deactivation. 95
Figure 29. Inhibition of release by mGluR8 allows for a higher potency of transmission during sustained trains of activity. 97
Figure 30. The peak intra-terminal Ca^{2+} level within mossy fibres does not increase during 1Hz facilitation. 99

Index of Tables

Table 1. List of drugs and reagents used in experiments. 40

Abbreviations

ACSF	Artificial cerebrospinal fluid
AM	Acetoxy-methyl
Bicucullin	[R-(*R**,*S**)]-6-(5,6,7,8-Tetrahydro-6-methyl-1,3-dioxolo[4,5-*g*]isoquinolin-5-yl)furo[3,4-*e*]-1,3-benzodioxol-8(6*H*)-one
CA	Cornu Ammonis
cGlut	Caged glutamate
CGP	CGP 54626 hydrochloride, [*S*-(*R**,*R**)]-[3-[[1-(3,4-Dichlorophenyl)ethyl]amino]-2-hydroxypropyl](cyclohexylmethyl) phosphinic acid
γ-CNB-caged L-glutamic acid	L-glutamic acid, γ-(α-carboxy-2-nitrobenzyl) ester, trifluoroacetic acid salt
CMNB caged fluorescein	Fluorescein bis-(-5-carboxymethoxy – 2 – nitroben-zylether, dipotassium salt)
CNS	Central nervous system
DAG	Diacylglycerol
DCGIV	(2*S*,2'*R*,3'*R*)-2-(2',3'-Dicarboxycyclopropyl) glycine
DG	Dentate gyrus
DL-AP5	DL-2-Amino-5-phosphonopentanoic acid
DL-TBOA	L-threo-*β*-Benzyloxyaspartic acid
DMSO	Dimethyl- sulfoxide
EAAT	Excitatory amino-acid transporter
ECS	Extra cellular space
fEPSP	Field excitatory postsynaptic potential
FITC	Fluorescein isothiozyanate
GC	Granule cell
GFAP	Glial fibrillary acid protein
GLAST	Glutamate aspartate transporter

GLT-1	Glutamate transporter 1
GPCR	G protein-coupled receptor
HEPES	4-(2-hydroxyethyl)-1-piperazineethanesulfonic acid
IBI	Inter burst interval
IML	Inner molecular layer
ISI	Inter stimulation interval
L-AP4	L-(+)-2-Amino-4-phosphonobutyric acid
LFS	Low frequency stimulation
L-SOP	L-Serine-*O*-phosphate
LTD	Long term depression
LTP	Long term potentiation
LY341495	(2*S*)-2-Amino-2-[(1*S*,2*S*)-2-carboxycycloprop-1-yl]-3-(xanth-9-yl) propanoic acid
LY367385	(*S*)-(+)-α-Amino-4-carboxy-2-methylbenzeneacetic acid
MAPK	Mitogen-activated protein kinase
MF	Mossy fibre
mGluR	Metabotropic glutamate receptor
MK801	Dizocilpine; (5*S*,10*R*)-(+)-5-Methyl-10,11-dihydro-5*H*-dibenzo[*a*,*d*]cyclohepten-5,10-imine maleate
MML	Middle molecular layer
MPEP	2-Methyl-6-(phenylethynyl) pyridine hydrochloride
MPP	Medial perforant path
NBQX	2,3-Dioxo-6-nitro-1,2,3,4 tetrahydro-benzo[*f*]quinoxaline-7-sulfonamide disodium salt
OGB-1AM	Oregon Green Bapta-1 AM or Glycine,N-[2-[(acetyloxy) methoxy]-2-oxoethyl]-N-[4-[[[3',6'-bis(acetyloxy)-2',7'-difluoro-3-oxospiro[isobenzofuran-1(3H),9'-[9H]xanthen]-5-yl]carbonyl]amino]-2-[2-[2-[bis[2-[(acetyloxy)methoxy]-2-

	oxoethyl]amino]phenoxy]ethoxy]phenyl]-, (acetyloxy) methyl ester
OML	Outer molecular layer
PBI	Post burst interval
PBS	Phosphate buffered saline
PFA	Paraformaldehyde
PLCß	Phospholipase C beta
PPG	(*RS*)-4-Phosphonophenylglycine
PtdIns-3-K	Phosphatidylinositol 3-kinase
PUI	Post uncaging interval
ROI	Region of interest
TBS	Tris buffered saline
TRIS	Tris (hydroxymethyl)-aminomethan
TRITON	Polyethylene glycol p-(1,1,3,3-tetramethylbutyl)-phenyl ether
TTX	Tetrodotoxin; (4*R*,4a*R*,5*R*,6*S*,7*S*,8*S*,8a*R*,10*S*,12*S*)-2-azaniumylidene-4,6,8,12-tetrahydroxy-6-(hydroximethyl)-2,3,4,4a,5,6,7,8-octahydro-1*H*-8a,10-methano-5,7-(epoxymethanooxy)quinazolin-10-olate
UV	Ultra violet
VFD	Venus flytrap domain
VSD	Voltage sensitive dye

Abstract

Pharmacological activation of presynaptic inhibitory group II mGluRs potently modulates excitatory synaptic transmission throughout the brain. However, little is known about the physiological conditions under which these receptors are activated by synaptically released glutamate. To routinely test for activation by action potential driven glutamate release, we applied a conditioning burst (7 stim at 100 Hz) to presynaptic axons in the presence (12.6 ± 1.3%, n=32; 100µM, 17 ± 2.4%, n=13) or absence (5.5 ± 0.9%, n=8) of the glutamate transporter blocker DL-TBOA (40uM) and assessed the resulting receptor activation with the mGluR antagonist LY341495 (3µM). The inhibition reached its maximum with 100µM DL-TBOA. However, strong glutamate transporter blockade did not only facilitate synaptic group II mGluR activation, it caused additionally a stimulation independent activation by accumulated, spontaneously released glutamate alone (19.9 ± 4.5%, n=5), which required the use of a lower DL-TBOA concentration (40µM) to keep mGluR activation facilitated but reduce spontaneous, stimulation independent mGluR effects to an insignificant degree (6.5 ± 1.7%, n=5). Examining the mGluR mediated inhibition on the test fEPSP at different post burst intervals (PBI) revealed a peak depression at 0.2 ms PBI (13 ± 1%, n=34) which was still detectable even after 0.8 s PBI (8 ± 1%, n=7). The maximal inhibition of fEPSPs amounted to 30 ± 6% when applying 100 stim at 100 Hz using 0.2 sec PBI (n=9). Testing different frequencies within the conditioning burst revealed a maximum group II mGluR activation at 200Hz (23 ± 3%, n=10). To investigate the kinetics of group II mGluRs in more detail, we performed glutamate uncaging together with presynaptic Ca^{2+} imaging and assessed mGluR activation via uncaging-induced inhibition of presynaptic Ca^{2+} transients. We designed a laser stimulation protocol which yielded nearly rectangular steps in the extracellular glutamate concentration. Testing the activation time revealed a maximum depressed Ca^{2+} signal amplitude after 450ms (16.7 ± 2.5%, n=3). An upper estimation for the deactivation showed an inhibition of Ca^{2+} entry upon glutamate uncaging slightly dropping to 65.6 ± 4.2% (n=5) 600 ms after uncaging and was still detectable after 2000 ms (16.5 ± 4.4%, n=3). When estimating the lower limit, the inhibition was gone after a 409 ms post-uncaging interval (1.7 ± 0.4%, n=6) (tau= 150ms). Summarizing fEPSP and imaging data, group

II mGluR activation kinetics was shown to be relatively fast (fEPSP rec.: tau= 40 ± 20ms; Ca^{2+} imag.: tau= 150 ± 30ms), whereas the deactivation kinetics were indicated to be slower (fEPSP rec.: 840 ± 230ms; Ca^{2+} imag.: between 150 ± 110ms and 1870 ± 60ms). These data support the idea that the functional significance of mGluRs as presynaptic autoreceptors is not the degree of inhibition, but rather a long duration of inhibition of glutamatergic transmission and that this function is due to intrinsically slow receptor kinetics.

Keywords: presynaptic group II mGluRs, synaptic activation, presynaptic Ca^{2+} imaging, glutamate uncaging, slow receptor kinetics

1 Introduction

1.1 Glutamate

Since the 1930's when Krebs (1935) suggested that glutamate plays an important metabolic role in the brain, glutamate has been studied intensively. A few decades later it emerged that glutamate is the main excitatory neurotransmitter in the vertebrate brain (Fonnum, 1984) acting on three families of ionotropic receptors, named after their preferred agonists, *N*-methyl-D-aspartate (NMDA), 2a-amino-3-hydroxy-5-methyl-4-isoxazolepropionic acid (AMPA) and kainate (Monaghan et al., 1989). Whereas AMPA and NMDA receptors incorporate ligand gated ion channels mainly permeable to Na^+ and Ca^{2+}, and less permeable to K^+ (Asztely and Gustafsson, 1996), kainate receptors are predominantly permable to Na^+ and K^+ and only slightly to Ca^{2+} (Huettner, 2003). NMDA receptors can be distinguished from other types of ionotropic glutamate receptors because they show a voltage sensitive block induced by Mg^{2+} (Meldrum, 2000). This is operative under normal circumstances but is overcome by partial depolarization of the resting membrane potential. Functionally, AMPA receptors are responsible for fast synaptic transmission, NMDA receptors mediate the slower component of the postsynaptic excitatory current, and kainate receptor activation rather seems to have a modulatory effect on synaptic communication (Mayer and Westbrook, 1987, Forsythe and Westbrook, 1988, Boulton et al., 1992, Hollmann and Heinemann, 1994, Castillo et al., 1997, Rodriguez-Moreno and Lerma, 1998, Meldrum, 2000, Huettner, 2003, Lerma, 2003).

Before glutamate mediates synaptic transmission or gets involved in modulatory processes, it is synthesized in the cytoplasm and is stored in presynaptic vesicles for quantal release (Meldrum, 2000, Fremeau et al., 2001). The action potential triggered release of glutamate is Ca^{2+} dependent (Fonnum, 1984) and the removal of glutamate from the extracellular space after release is mediated predominantly by astrocytes (Bergles and Jahr, 1997) and diffusion (Min et al., 1998, Rusakov and Kullmann, 1998).

Another finding that strengthened the dominant role of glutamate was the discovery of glutamate stimulating inositol phosphate formation in striatal neurons (Sladeczek et al., 1985). Later on, it was shown that this process was mediated by a novel type of

glutamate receptor linked to inositol phospholipid metabolism (Sugiyama et al., 1987). The novel receptor was cloned and termed the metabotropic glutamate receptor 1 (mGluR1) (Masu et al., 1991). This discovery dramatically altered the traditional view of glutamatergic neurotransmission because earlier it was believed that the action of glutamate was exclusively mediated by the activation of ionotropic receptors. The newly discovered neuromodulatory glutamate receptors provided a mechanism by which glutamate can modulate cell excitability and synaptic transmission via second messenger systems (Conn and Pin, 1997). It became evident, that glutamate activates a large family of glutamate receptors, mediating and modulating most of the excitatory neurotransmission in the mammalian central nervous system (CNS) (Ozawa et al., 1998).

1.2 Metabotropic glutamate receptors (mGluRs)

1.2.1 History

As mentioned in the previous section, metabotropic glutamate receptors were discovered in the mid 1980's. A first hint was the finding that glutamate induced formation of inositol phosphate belonging to a major second messenger system (Sladeczek et al., 1985), indicating that glutamate does not act exclusively on ionotropic glutamate receptors. Additionally, a pharmacological study performed by Carl Cotman and colleagues (Cotman et al., 1986) demonstrated that L-2-amino-4-phosphonobutyrate (L-AP4) and L-serine-0-phosphate (L-SOP) reduced synaptic transmission without affecting the membrane potential or the input resistance of the recorded cell. Based on these findings they concluded that the site of action for the L-glutamate analogue L-AP4 and its structural analogue L-SOP must be presynaptic. These antagonist had no effect on any of the excitatory amino acid receptors (AMPA-R, NMDA-R, Kainate-R) known so far. Thus, they were suggested to act on a fourth class of receptors but detailed descriptions were not made. Later studies provided evidence that under endogenous conditions, these modulatory effects are mediated by novel glutamate receptors (Masu et al., 1991), firstly described in 1987 (Sugiyama et al.). Later, the terminology "metabotropic glutamate receptor" was created and further important steps were the

cloning of the first mGluR (Masu et al., 1991) and the description of the whole mGluR family in the early 1990s (Bockaert et al., 1993).

Functionally, mGluRs are believed to modulate synaptic transmission (Pin and Duvoisin, 1995, Cartmell and Schoepp, 2000), but despite three decades of intensive research on mGluRs, little is known about the physiological action of these receptors and which endogenous mechanisms control their activation.

1.2.2 Structure

mGluRs belong to the class C G-protein coupled receptor (GPCR) super-family which also includes $GABA_B$ receptors, calcium sensing receptors, pheromone receptors and taste receptors (Pin et al., 2003). GPCRs in general are membrane bound proteins and activated by extracellular ligands. These receptors are composed of an N-terminal domain, 7-transmembrane-spanning domains and an intracellular C-terminal domain.

"Metabotropic/glutamate/pheromone"-class C GPCRs differ from the other main families: "rhodopsin-like"-class A and "secretin-like"-class B GPCRs (Fredriksson et al., 2003, Chou, 2005). They possess a larger N-terminal domain that contains the endogenous ligand binding site. This part of the receptor is termed the Venus Flytrap Domain (VFD). Each VFD consists of two lobes sitting on top of each other with the ligand bound between them (Pin et al., 2004).

A trait that distinguishes mGluRs from other class C GPCRs is the deviating coding sequence for the 7-transmembrane spanning domains. This part of the receptor is shown to be involved in G-protein coupling and coupling selectivity (Pin et al., 2003). The intracellular C-terminal end of the receptor mediates and modulates G protein coupling.

Metabotropic glutamate receptors can form homo- as well as hetero-dimers (Romano et al., 1996, Doumazane et al., 2011). In the dimerized form, three conformational or activation states can be distinguished (Figure 1): the open-open (glutamate is not bound), open-closed (glutamate is bound to one VFD) and closed-closed (both VFDs are bound to glutamate) state (Niswender and Conn, 2010).

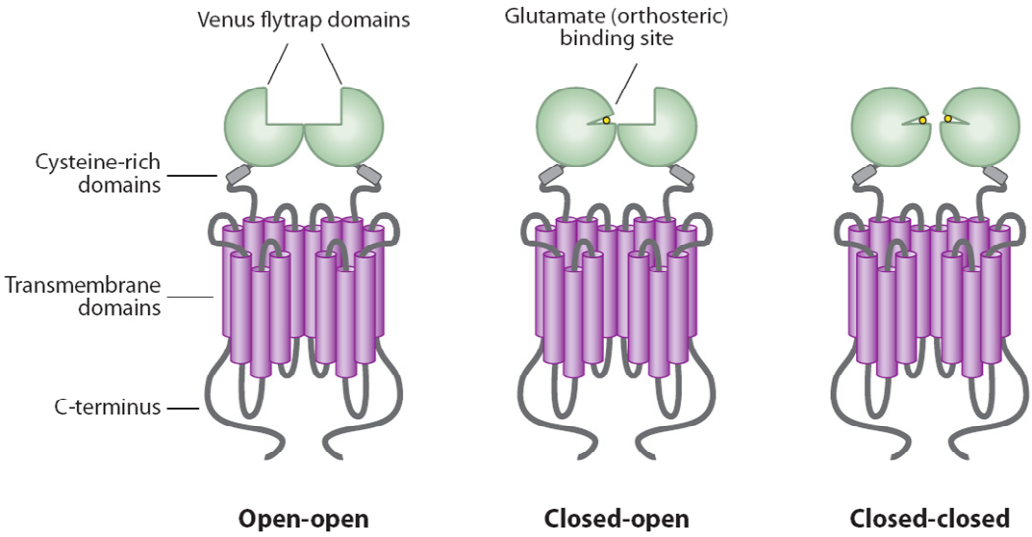

Figure 1. Schematic diagram of the mGluR dimer in different activity states. The two large extracellular domains of an mGluR dimer are called Venus Flytrap domains (VFDs). These domains bind glutamate and other orthosteric ligands. Seven transmembrane spanning domains are linked to the VFDs via cysteine-rich domains. The C-terminus faces intracellularly and is often subject to alternative splicing to generate different C-terminal protein tails. The open-open conformational state on the left side is the inactive state and can be stabilized by antagonists. A glutamate binding to either one or both VFDs results in a receptor activation. Picture is adapted from: Niswender and Conn, Annu. Rev, Pharmacol. Toxicol., Vol. 50, pp. 295 – 322, 2010

1.2.3 Types, expression and functional relevance

The ubiquitously expressed mGluR family composed of eight different subtypes is divided into three subgroups (group I-III) depending on sequence similarities, pharmacological profile and signal transduction mechanism (Nakanishi, 1994). mGluR type 1 and 5 belong to group I, type 2 and 3 constitute group II and the remaining types 4, 6, 7 and 8 are allocated to group III. Whereas group I mGluRs are predominantly post-synaptically localized, group II and III mGluRs are dedicated to presynaptic sites (Figure 2) (Cartmell and Schoepp, 2000). Moreover, postsynaptic group I and presynaptic III mGluRs prevail in the terminal zone of synapses, facing towards the synaptic cleft and presynaptic group II mGluRs are mainly restricted to the pre-terminal site of the synapse, closer to the axonal part of the neuron and further away from the glutamate release site (Shigemoto et al., 1997).

As mentioned in the previous section, mGluRs are coupled to G proteins. Characteristically, subtypes mGluR 1 and 5 (group I) are primarily coupled to Gq/G11 proteins (Masu et al., 1991). In most cases, receptor activation stimulates phospholipase

Cβ (PLCβ) and causes formation of inositol-1,4,5-trisphosphate (IP3) and diacylglycerol (DAG). Ins-1,4,5-P_3 releases Ca^{2+} from intracellular stores and DAG activates protein kinase C. Via this second messenger cascade group I mGluRs positively trigger the excitability of the postsynaptic cell (Cartmell and Schoepp, 2000). Presynaptic group II mGluRs are coupled to Gi/Go proteins (Tanabe et al., 1993, Chavis et al., 1994, Kammermeier et al., 2003). Their activation inhibits cAMP formation and N or P/Q-type voltage sensitive Ca^{2+} channels, activates K^+ channels and can also activate the MAPK and the phosphatidylinositol-3-OH-kinase [PtdIns(3)K]-mediated pathway (Pin and Duvoisin, 1995, Anwyl, 1999). These signalling pathways are negatively linked to synaptic transmission. Like group II mGluRs (type 2, 3), group III mGluRs (Type 4, 6, 7, 8) are also coupled to Gi/Go proteins and negatively regulate glutamate release from the presynapse (Pin and Duvoisin, 1995, Niswender and Conn, 2010).

In general it is believed that mGluRs inhibit synaptic transmission via the blockade of Ca^{2+} entry but recently, it was shown that the group III subtype mGluR8 acts without affecting Ca^{2+} influx (Erdmann et al., 2011). Rather, the inhibition could be explained by a decrease in the Ca^{2+} affinity of the release sensor and to a lesser extent by a reduction of the maximal release rate. The mGluR6 subtype differs from other group III mGluRs because the receptor is exclusively localized on the dendrites of ON bipolar cells of the retina. It responds to glutamate released from rod and cone receptor cells in the dark. There the activation of the mGlu6 receptor reduces excitability of ON bipolar cells by negatively regulating a membrane non-selective cation channel (Nakajima et al., 1993, Nomura et al., 1994, Vardi et al., 2000).

It is important to mention that expression of mGluRs is not exclusively restricted to neurons. mGluR 5 (group I) and mGluR 3 (group II) can be expressed in glial astrocytes as well (Ohishi et al., 1993, Tanabe et al., 1993, Balazs et al., 1997, Aronica et al., 2000).

As already mentioned, mGluRs are broadly distributed throughout the CNS and are specifically localized at discrete synaptic and extra-synaptic sites in both neurons and glia. This variety implies that mGluRs must be involved in numerous functional processes in the brain. It is already known that, activation of mGluRs results in diverse actions on neuronal excitability and synaptic transmission due to modulation of ion channels and other regulatory signalling proteins (Niswender and Conn, 2010).

Moreover, the physiological role of an mGluR subtype is highly specific to the neuronal population and the sub-cellular location. For example postsynaptic group I mGluRs can induce hyperpolarization in midbrain dopamine neurons (Valenti et al., 2002), whereas elsewhere they can potentially act presynaptically to either decrease or increase transmitter release via the release of retrograde messengers like endocannabinoids (Maejima et al., 2001, Varma et al., 2001) and may even be located presynaptically (Schwartz and Alford, 2000).

The widespread and heterogeneous distribution of mGluRs in the brain also makes them attractive drug targets because it was shown that mGluR function seems to be more or less critically involved in various neurologic and psychiatric disorders like epilepsy (Alexander and Godwin, 2006), anxiety (Swanson et al., 2005), schizophrenia (Moghaddam, 2004), depression (Pilc et al., 2008), pain syndromes (Bleakman et al., 2006), Alzheimer's disease (Lee et al., 2004) and Parkinson's disease (Conn et al., 2005). However, it has to be taken into account that most of these finding about potential functional roles of mGluRs are based on pharmacological rather than on physiological studies via testing the activation by the endogenous ligand glutamate.

Indeed, there are a few *in vitro* studies dealing with synaptic activation of, for example, group II mGluRs via glutamate (Scanziani et al., 1997, Dube and Marshall, 2000, Awatramani and Slaughter, 2001, Kew et al., 2001) and *in vivo* studies that indicate an involvement of mGluRs in important neuronal processes (Grueter et al., 2008, Carzoli and Hyson, 2011). In the end it is important to perform a systematic analysis in order to find out how and when mGluRs activate under natural conditions and to shed light on the question of which physiological processes they might be involved in as modulatory triggers.

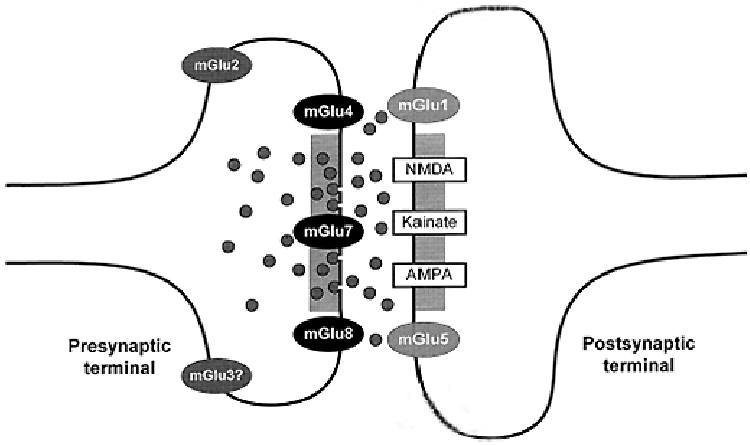

Figure 2. Localization of glutamate receptors at a theoretical CNS synapse. Group I mGluRs are predominantly localized postsynaptically facing towards the synaptic cleft. In contrast, group II and III mGluRs are located presynaptically, group II at the axonal, pre-terminal site and group III terminally. Whereas all types of ionotropic glutamate receptors are situated in the active zone of the postsynapse, only mGluR 7 (group III) is located in the vesicle release area of the presynapse. Picture is adapted from: Cartmell and Schoepp, J. Neurochem., Vol. 75, No. 3, 2000

1.2.4 Presynaptic group II mGluRs

Many studies support the hypothesis that group II mGluRs function as a presynaptic regulatory mechanism to control neurotransmitter release (Pinheiro and Mulle, 2008) . Their predominant extra-synaptic location implies that they detect the extracellular build-up of glutamate, therefore acting as autoreceptors (Kew et al., 2001, Nicoll and Schmitz, 2005, Kwon and Castillo, 2008).

Apart from that, it has been shown that presynaptic group II mGluRs can also act as hetero-receptors, controlling the release of GABA by inhibitory interneurons (Mitchell and Silver, 2000). Some other studies state for example, that most likely all group II mGluRs are activated by glutamate spillover and act exclusively hetero-synaptically (Scanziani et al., 1997, Pinheiro and Mulle, 2008).

In the past decades, a multitude of studies tried to discover the potential roles presynaptic group II mGluRs might play in neuronal processes. Most of these studies were performed with selective pharmacological agents. One interesting finding is that group II mGluRs seem to be involved in different forms of short- and long-term plasticity (Pinheiro and Mulle, 2008). For example, at hippocampal mossy fibres/CA3 pyramidal cell synapses they decrease frequency facilitation (Scanziani et al., 1997), whereas at thalamocortical synapses onto layer IV barrel cortex neurons (Mateo and

Porter, 2007), at the calyx of Held (von Gersdorff et al., 1997) and at the medial perforant path/granule cell synapse (Brown and Reymann, 1995) group II mGluRs contribute to the regulation of synaptic short-term depression. Moreover, compelling evidence has been provided that metabotropic glutamate receptors are essential for the induction of long-term potentiation (LTP) and long-term depression (LTD) in the hippocampus (Huang et al., 1997, Bortolotto et al., 1999). Further, in the case of group II mGluRs, it has been found that they are required for persistent LTD, but not for LTP in the hippocampal CA1 region (Altinbilek and Manahan-Vaughan, 2009). Generally, there are two forms of LTD group II mGluRs are required for: an electrically-induced LTD in the CA1 region that is protein synthesis-dependent (Manahan-Vaughan et al., 2000) and a chemically-induced LTD in the dentate gyrus that is protein synthesis-independent (Poschel and Manahan-Vaughan, 2005). Another study indicated that group II mGluRs could also be involved in mossy fibre LTD as evidenced by the lack of the mGlu 2 receptor in a knock-out mouse (Yokoi et al., 1996) but a re-examination of the group II mGluR role for mossy fibre LTD showed that group II mGluRs are neither necessary nor sufficient for the induction (Wostrack and Dietrich, 2009).

As mentioned in the previous section, group II mGluRs seem to be also critically involved in a variety of neuronal disorders. For example, it is indicated that group II mGluRs might play a role in at least one form of epilepsy which is accompanied by a degeneration of the hippocampus because a pharmacological treatment with group II mGluR agonists revealed anticonvulsive effects (Dietrich et al., 2002). Additionally, mGluR2/3 agonists have been shown to decrease glutamate release in brain regions associated with fear and anxiety (Swanson et al., 2005). Adjacent to these effects, a group II mGluR mediated influence on neuronal excitability can in turn cause alterations in LTD or LTP (Anwyl, 1999) accompanied by changes in cognitive processes such as memory retention (Mathis and Ungerer, 1999) and spatial awareness (Altinbilek and Manahan-Vaughan, 2009). Indeed, group II mGluRs are not essential for the encoding of information, but they seem to be vital for the consolidation of memory (Riedel et al., 2003). Further, mGluR 2/3 receptors potentially play a role in the altered neurotransmission which might be part of the cause of schizophrenia. mGluR 2 can form a complex with the serotonin 5-HT_{2a} receptor, and it is suggested that a change in expression of both receptors could lead to altered signalling which may contribute to the manifestation of psychotic symptoms characterising schizophrenia (Gonzalez-

Maeso et al., 2008). Neuronal circuits that might be altered through substance abuse also reflect a potential point of action for group II mGluRs (Olive, 2009) as well as physiological and behavioural processes influenced by depression (Chaki et al., 2004).
Most of these findings on group II mGluRs and about mGluR types in general are based on pharmacological studies as mentioned in the previous section. This can be critical because too little is known about the physiological conditions under which these receptors might be activated and whether they really fulfil the potential (proposed?) functional role they are believed to have. So long as it is unknown whether endogenous group II mGluR activation corresponds to pharmacological activation, the possibility cannot be excluded that mGluRs do not act as autoreceptors. Eventually, the functional relevance of group II mGluRs must be reconsidered depending on future findings.

1.3 Hippocampus as a model for the investigation of presynaptic group II mGluR recruitment and kinetics

The hippocampus is one of the best investigated regions of the brain. The earliest description came from the Venetian anatomist Julius Caesar Aranzi (circa 1564). He was the first to coin the expression “hippocampus“, due to the enormous similarity to the tropical fish. After the advent of microscopy, it became possible to investigate the hippocampal anatomy on the cellular level. Camillo Golgi developed a new technique to illustrate the unique organization of this brain structure (1886) and Santiago Ramon y Cajal’s pioneering anatomical study on the stratification of the various afferent systems paved the way for later scientists to clarify the question of which functional role(s) the hippocampus plays in brain function (Andersen, 2007).
Two reasons support the selection of the hippocampus for our study. First, the laminar arrangement of cellular pathways makes it a nearly perfect open-field structure (Johnston and Wu, 1995), allowing stimulation and recording from specific types of cells and second, the strong expression of group II mGluRs on medial perforant path fibres terminals (Shigemoto et al., 1997).

1.3.1 Anatomy

The hippocampus is a paired structure located inside the medial temporal lobe and belongs functionally to the limbic system. The hippocampal region includes two sets of cortical structures, the hippocampal formation and the parahippocampal region. Important defining differences between the two are the number of cortical layers and the connectivity.

Most commonly, the hippocampal formation is divided into three regions depending on the cytoarchitecture: dentate gyrus (DG), hippocampus proper (or Ammon's horn) which is subdivided into three fields (CA3, CA2 and CA1), and subiculum. All three areas share the three layered structure and the unipolar connectivity (Witter, 1995). Here, the term hippocampus is used for the structure formed by the dentate gyrus and Ammon's horn.

The parahippocampal region includes the entorhinal, perirhinal and postrhinal cortices as well as the presubiculum and parasubiculum (Furtak et al., 2007). The latter two areas share the laminar organization, have more than three layers and are reciprocally connected with the subiculum (Scharfman et al., 2000).

The three dimensional form of the rodent hippocampus is a relatively complex elongated structure with the long axis referred to as the septotemporal axis and the orthogonal axis as the transverse axis. The long axis is bent in a C-shape .

The organisation of the major intrinsic hippocampal connections is described as a trisynaptic circuitry and characterized by the laminar arrangement of each group of these neurons (Figure 3) (Amaral and Witter, 1989). Strictly speaking, this is a simplified description of the main pathways involved in signal transmission and processing; however, it is sufficient to get an overview of the anatomical structure of the hippocampus. Originating in the entorhinal cortex, perforant path fibres project to the outer two-thirds of the dentate gyrus molecular layer, forming asymmetrical synapses with granule cell dendrites. The myelinated axons of the perforant path are on average 0.1µm thin and show periodic varicosities with a thickness of 0.5 to 1.0µm (Amaral et al., 2007). Fibres that emanate from the lateral entorhinal area terminate in the most superficial third of the molecular layer, whereas fibres that originate from the medial entorhinal area terminate in the middle-third of the molecular layer. Elongated, un-myelinated axons of granule cells, called mossy fibres, project to CA3 pyramidal neurons. These fibres give rise to unique complex presynaptic terminals called mossy

fibre expansions (or boutons). One feature that makes them unique is their size; they can be as large as 8µm in diameter, but typically they range from 3 to 5µm (Bischofberger et al., 2006). Axon collaterals given off by CA3 pyramidal neurons, called Schaffer collaterals, build connections with CA1 pyramidal neurons. A feature of these myelinated projections is that the axons vary in thickness. Lastly, the processed information propagates via the subiculum back to the entorhinal cortex (Amaral and Witter, 1989).

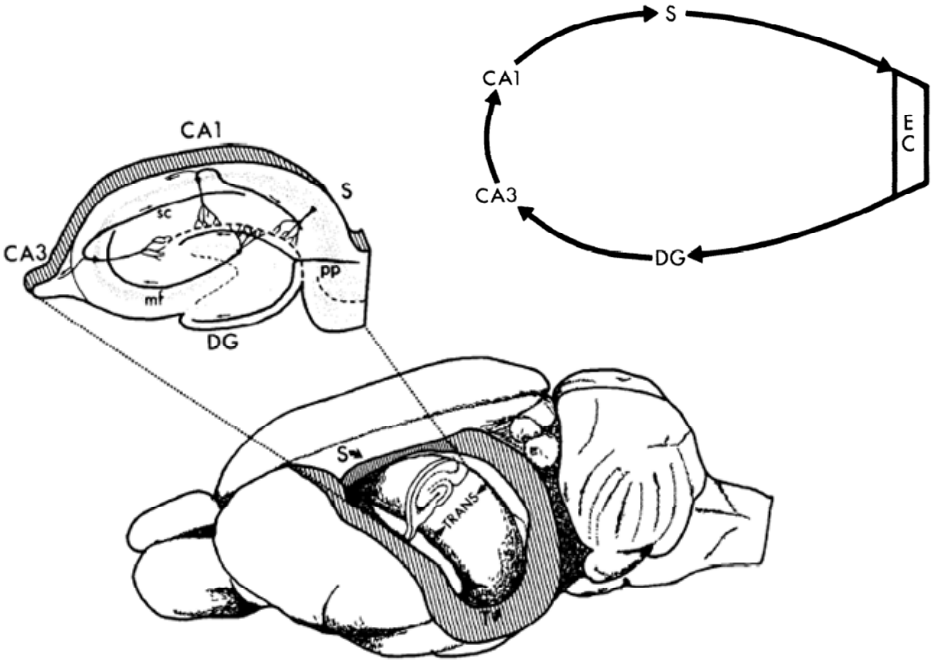

Figure 3. Schematic view of the hippocampal anatomy and the synaptic connections of the main hippocampal pathway. Shown in the middle is a preparation in which the cortical surface overlying the hippocampus has been removed. The hippocampus is an elongated, C-shaped structure with the long or septotemporal axis running from the septal nuclei rostrally (S) to the temporal cortex (T) ventrocaudally. The short or transverse axis (TRANS) is oriented perpendicular to the septotemporal axis. The slice pictured at top left is a representation of the major neuronal elements and intrinsic connections of the hippocampal formation. Schematized in the top right corner is a simplified diagram of the intrinsic circuitry of the hippocampal formation. Each of the fields is linked by unidirectional excitatory projections. Abbreviations: CA, Cornu Ammonis; DG, dentate gyrus; EC, entorhinal cortex; mf, mossy fibers; pp, perforant path; S, subiculum (upper circuitry schemes); S, septal nuclei (lower brain scheme); SC, Schaffer collaterals. Picture (modified) is adapted from: Amaral and Witter, Neuroscience Vol. 31, No. 3, pp. 571-591, 1989

1.3.2 Function

The hippocampus was believed to play an important role in certain forms of learning and memory. This assumption was intensified when case studies from patients who suffered from severe epilepsy showed a profound and selective loss of memory after surgical removal of the whole hippocampus (Scoville and Milner, 1957). H. M., the most famous of these patients, was impaired in a broad range of memory functions, including recognition of previously presented words or figures, free recall of noun pairs, and memory for the position of objects (Milner, 1965, Milner et al., 1968).

Consistent evidence for hippocampal involvement in memory formation has also been obtained in tasks in which animals or humans used spatial memory for navigation (O'Keefe and Conway, 1978, Nadel, 1991). For example, it could be shown in rats that a significant portion of pyramidal cells have spatial firing correlates (O'Keefe and Dostrovsky, 1971, Muller, 1996). These so called “place cells“ show a spatially restricted firing pattern.

The importance of the hippocampus for spatial mnemonic operations was also supported by findings showing that specific lesions of the hippocampal formation severely disrupted acquisition of spatial navigation tasks. Rats with such lesions, performing tasks in radial mazes failed to learn which arms were baited with food and which were not. They re-entered arms from which they had already collected food (Jarrard, 1978, Olton et al., 1978).

It has been postulated that the brain uses short- and long-lasting modifications of synaptic strength in critical neuronal circuits to accomplish the processing and storage of information (Siegelbaum and Kandel, 1991, Malenka, 1994, Bear and Abraham, 1996). Information that enters the hippocampus can underlie such changes caused by long-term plasticity effects as already described in section 1.2.4. Long lasting processes like LTD or LTP build on shorter-term processes to span the gap between synaptic plasticity and permanent structural changes involved in long-term memory (Zucker, 1989) .

1.3.3 Hippocampus and presynaptic group II mGluRs

In the hippocampus of the rat, mGluRs are located fibre tract specific at the main synapses of the trisynaptic circuitry (Shigemoto et al., 1997). First evidences for group II mGlu receptor action at medial perforant path fibres in the dentate gyrus were

provided in 1996 (Macek et al.). At this location, group II mGluRs mediate inhibitory presynaptic modulation of synaptic transmission (Dietrich et al., 1997, Kew et al., 2001) and at mossy fibre synapses connecting CA3 pyramidal cells (Scanziani et al., 1997, Dietrich et al., 2003).

In my project I focused on mGluR2/3 located at medial perforant path (MPP) extra-synaptic sites because the expression level of group II mGluRs on this fibre tract is very high (Figure 4) (Shigemoto et al., 1997) and the laminar arrangement of the MPP fibre tract makes it best suited for electrophysiological recordings.

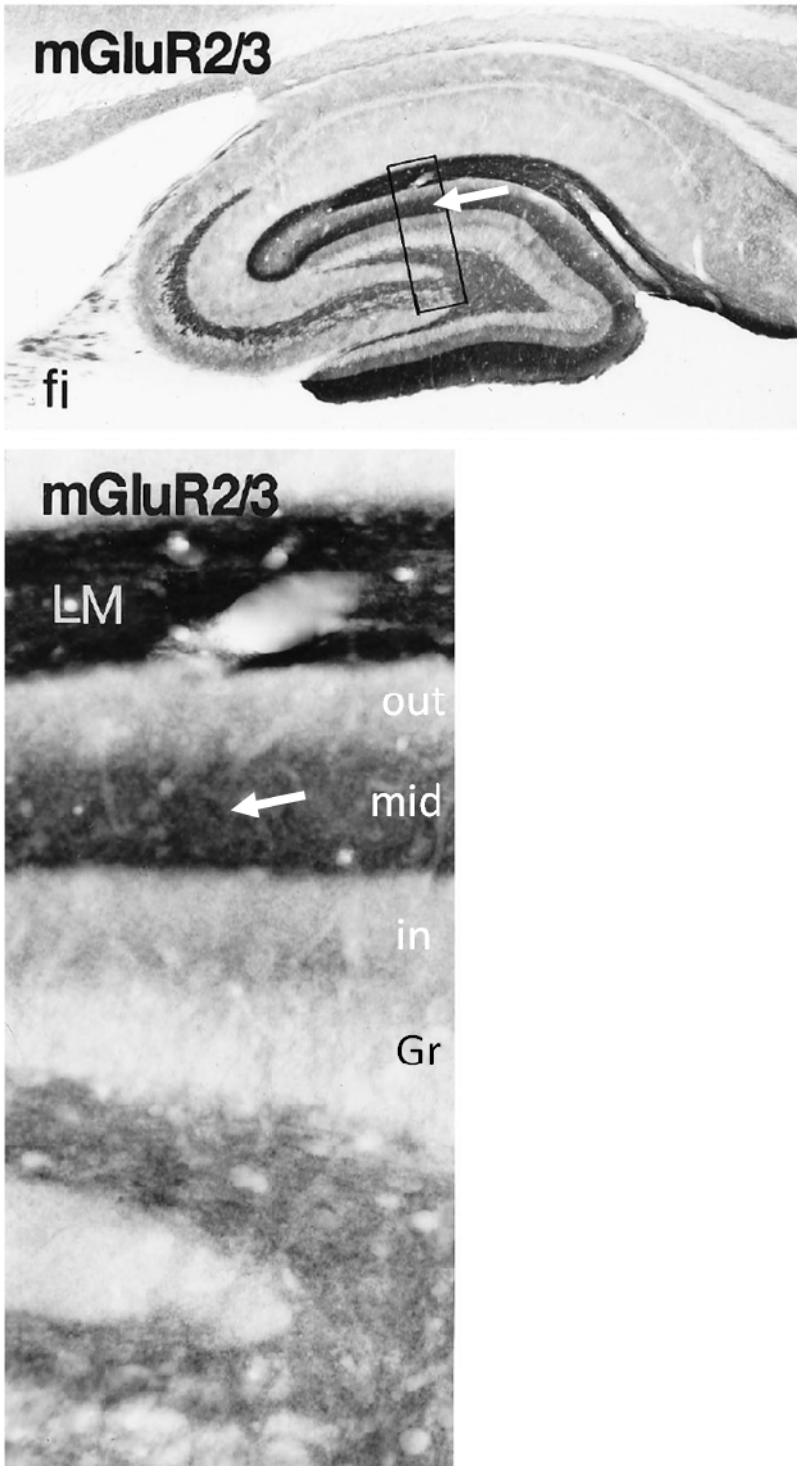

Figure 4. Distribution of immune-reactivity for mGluR2/3 in rat hippocampus. Shown on the upper part is a parasagittal section of the hippocampus reacted with a specific antibody for group II mGluRs. The immune-reactivity is restricted to the terminal zones of perforant path and mossy fibres. Marked by an arrow in the upper as well as in the lower part is the medial perforant path region where the expression level is most prominent. *fi*, fimbria; *LM*, stratum lacunosum moleculare; *out*, outer molecular layer; *mid*, middle molecular layer; *in*, inner molecular layer; *Gr*, granule cell layer. Picture (modified) is adapted from: Shigemoto et al., J. Neuroscience, Vol. 17, No. 17, pp. 7503-7522, 1997

1.4 Astrocytes

Neuroglia were discovered in the late 1800's (Montgomery, 1994) and Mihaly von Lenhossek was the first who used the expression 'astrocyte' in 1895 to describe this specific class of glia cells. He intended to avoid the term glia that primarily implied a passive function for these cells. The name astrocyte is based on morphology because the round shape of the cell body and the outgrowing processes reminded Lenhossek (1895) of a cartoon of a star. However, the truth is that astrocytes are highly fibrous cells of great structural complexity and uniquely characterized by a dense array of processes (Nedergaard et al., 2003, Ransom et al., 2003).

Together with oligodendrocytes, astrocytes constitute the major glial cell types within the central nervous system (CNS) (Jessen, 2004). They build a heterogeneous class of cells (Hansson, 1990, Zhang and Barres, 2010) with diverse functions similar to neurons (Sontheimer, 1992). Emsley and Macklis (2006) divided them into 9 classes based on immune-labelling methods (Matyash and Kettenmann, 2010).

1.4.1 Morphology

The morphology of astrocytes is determined by the cytoarchitecture of a given brain region. Depending on where astrocytes are located, the density can vary by a factor of 1000 (Emsley and Macklis, 2006). Within one brain region several types of astrocytes can coexist (Matyash and Kettenmann, 2010). Common features of astrocytes are the expression of intermediate filaments which form the cytoskeleton. The main type of astroglial intermediate filament proteins is the glial fibrillary acid protein (GFAP) (Eng, 1985). GFAP is commonly used as a specific marker to identify astrocytes (Raff et al., 1979). Other characteristic features are a small soma diameter (~10µm), a low input resistance (≤ 30MΩ), a high resting potential (~ -95mV) and passive membrane properties (Diamond and Jahr, 2000).

In contrast to other glia cells, astrocytes are characterized by the formation of end-feet that contact a basal lamina around blood vessels, the pia mater, or the vitreous body of the eye (Reichenbach, 2004).

Depending on the brain region, astrocyte processes surround pre- and postsynapses to a varying extent. In the hippocampus, 57% of the synapses are associated with the process of an astrocyte (Ventura and Harris, 1999). This form of neuron-glia assembly is termed the ‚tripartite synapse', a functional system where bidirectional information flow between astrocytes and neurons takes place (Araque et al., 1999). The role of astrocytes in this formation is to exchange information with the synaptic neuronal elements, to respond to synaptic activity, and in turn to regulate synaptic activity (Perea et al., 2009). It is important to mention that astrocyte processes do not fully insulate a synapse from the surrounding environment. They allow some flow into and out of the synaptic cleft. Some hippocampal synapses, for example, are astrocyte-free ranges. Potentially, substances could escape from these areas and activate receptors located extra-synaptically or at neighbouring synapses (Ventura and Harris, 1999).

Another feature of astrocytes is the expression of gap junctions mainly formed from the protein connexin 43. Gap junctions mediate intracellular communication by providing ultra-structural cytoplasmic continuity and allow astrocytes to form a functional syncytium (Bennett et al., 2003).

The astroglial types which have been described so far include: the main types called protoplasmic astrocytes (Eng, 1985) and fibrous astrocytes (Hildebrand et al., 1985) and the other types named tanycytes (Bruni et al., 1983), 'radial' cells (Kosaka and Hama, 1986), Bergmann glia (Das, 1976), velate glia (Valverde and Lopez-Mascaraque, 1991), marginal glia (Braak, 1975), perivascular glia (Schnitzer, 1987), and ependymal glia (Reichenbach, 2004). In the molecular layer of the dentate gyrus, protoplasmic astrocytes predominate. The distribution of the cells is influenced by the boundary that separates the associational/commisural and the perforant path afferents (Bushong et al., 2003).

1.4.2 Transporter mediated glutamate uptake

The main astrocyte functions range from guidance and support of neuronal migration during development, to modulation of immune-reactions, to maintenance of the neuronal microenvironment (Montgomery, 1994). Although astrocytes are assigned to different functional processes, their roles in these processes often overlap.

One of the most important processes astrocytes are involved in is glutamate clearance after synaptic release. The uptake of glutamate from the extracellular space is

transporter mediated and electrogenic because the glutamate translocation is coupled to the electrochemical gradient for Na^+, K^+, and H^+. During each transport cycle net positive charge is translocated across the membrane (three Na^+ and one H^+ into the cell and one K+ ion out of the cell for every molecule of glutamate by each transporter, (Figure5) which makes it possible to monitor glutamate transport electrophysiologically.

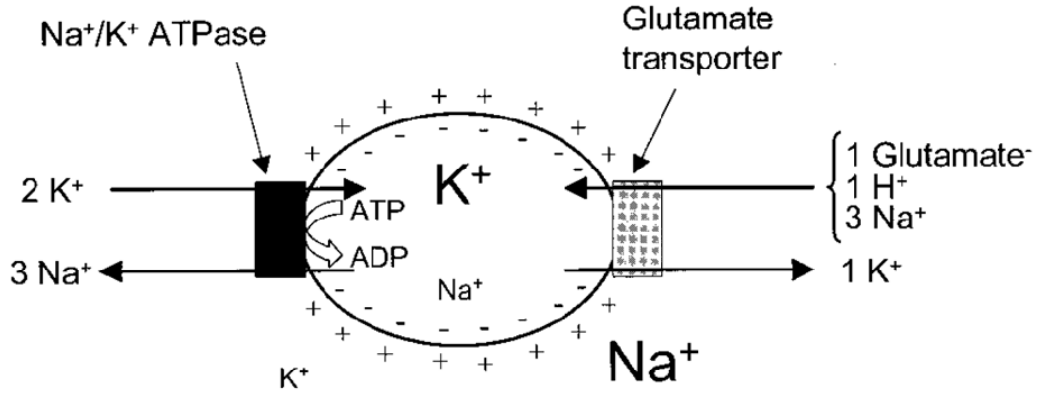

Figure 5. Schematic illustration of glutamate uptake. The coupled transport of Na^+ and K^+ drives the uptake of glutamate and H^+ down their concentration gradient. The cell membrane potential contributes to the uptake driving force due to a net inward movement of positive charge with each glutamate transported. Picture is adapted from: Anderson and Swanson, GLIA Vol. 32, pp. 1–14, 2000

Astrocytes express the excitatory amino acid transporter (EAAT) termed GLAST (Glutamate aspartate transporter) (or EAAT1) and the glutamate transporter GLT-1 (or EAAT2) (Swanson et al., 1997, Anderson and Swanson, 2000). The high-affinity uptake of glutamate by GLAST and GLT-1 is the primary mechanism by which extracellular glutamate is maintained at low levels (< 1μM) (Meldrum, 2000). This is of great importance because the concentration of extracellular glutamate determines the extent of receptor activation. By limiting the extra-synaptic diffusion of glutamate, it is ensured that synaptic transmission occurs in a point-to-point fashion and that cross-talk between neighbouring excitatory synapses is minimized (Anderson and Swanson, 2000). Apart from that, high levels of extracellular glutamate can cause excitotoxic effects (Danbolt, 2001).

It is also important to mention that astrocytes-mediated glutamate uptake is highly temperature dependent (Asztely et al., 1997) and the transport process is accompanied

by pH changes, an alkalinisation of the outside and acidification of the inside of the cell (Bouvier et al., 1992, Amato et al., 1994).

The degree to which the transporters shape the extracellular glutamate transient may also dependent on synapse geometry, transporter density and other varying factors among synapses (Bergles and Jahr, 1997).

Clearance of extracellular glutamate by astrocyte glutamate transporters essentially limits the activity of metabotropic glutamate receptors at excitatory synapses (Huang et al., 2004), especially when the receptors are located extra-synaptically like group II metabotropic glutamate receptors.

1.5 Aim of the study

Pharmacological activation of presynaptic inhibitory group II mGluRs potently modulates synaptic transmission. However, little is known about the physiological conditions and the temporal and spatial pattern of glutamate release mediating group II mGluR receptor activation. Whereas ionotropic glutamate receptors can be activated by a single action potential, metabotropic glutamate receptors do not activate, even by a single vesicle (Manzoni et al., 1995, Dietrich et al., 1997, Scanziani et al., 1997). In a few studies, group II mGluR activation has been tested and it could be shown that repetitive stimulation is necessary to activate the receptors (Scanziani et al., 1997, Kew et al., 2001). Strikingly, the inhibition was drastically smaller compared to pharmacological activation. Despite this enormous discrepancy, nobody has performed a systematic analysis of group II mGluR activation.

I sought to resolve this ambiguity and tested mGluR activation in detail by performing field potential recordings in the middle molecular layer of the dentate gyrus in horizontal hippocampal brain slices of Wistar-rats. My goals were to determine the presynaptic activity required for triggering group II mGluR activation, to find out how fast they activate and how long the activation lasts, and to determine which presynaptic factors substantially limit mGluR activation.

In general, synaptic activation of presynaptic group II mGluRs is complex and influenced by many factors such as sub-cellular localization, the glutamate affinity and the glutamate accumulation in the ECS. To activate extra-synaptic group II mGluRs at

pre-terminals, a form of presynaptic activity is needed that causes strong extracellular glutamate dynamics after synaptic release, so that glutamate gets the chance to overcome the homeostasis between release and removal to diffuse and bind to the metabotropic glutamate receptor. The latter is predominantly controlled by astrocytes that perform fast electrogenic glutamate uptake after synaptic release (Takahashi et al., 1997). This transporter mediated glutamate uptake plays a prominent role in mGluR activation because it limits glutamate concentration and diffusion distance in the ECS. It has been shown that, at physiological temperatures, synaptically released glutamate is rapidly removed from the extracellular space (Borg et al., 1976, Asztely et al., 1997), restricting the activation of pre-synaptically and pre-terminally located group II mGluRs (Huang and Bergles, 2004).

The aim was to clarify how strongly mGluR activation is influenced by astrocyte glutamate uptake. In this study we tested, how strong mGluR activation is under physiological conditions and how the activation changes when the glutamate transporter blocker DL-TBOA is added in different concentrations to facilitate mGluR activation.

In order to draw conclusions about the mGluR mechanism of action on synaptic transmission, it is important to resolve the kinetics of the inhibitory process. The shorter the time mGluRs need to activate fully, the shorter the required exposure to glutamate. Moreover, the characterisation of the deactivation kinetics would make clear whether the deactivation is determined by the glutamate level in the ECS or the intrinsic receptor and signal cascade kinetics.

Finally, the systematic analysis of the inhibitory presynaptic group II mGluR activation and kinetics allowed more detailed assumptions to be drawn about the potential role of these modulatory receptors in neuronal processes and what it could imply for brain function.

2 Materials and Methods

2.1 Animals

2.1.1 Species

Male Wistar rats between postnatal day 20 and 40 (nomenclature: Crl WI, Charles River, Sulzfeld, Germany) were used for field potential experiments as well as for combined Ca^{2+} imaging and glutamate uncaging experiments. Patch clamp recordings were performed on brain slices from rats between P20 and P30.

2.1.2 Preparation of horizontal hippocampal slices

Rats were anesthetized in a covered glass beaker using Isofluran (1-Chloro-2, 2, 2,-trifluoroethyldifluoromethylether, Abbott GmbH & Co KG, Wiesbaden, Germany) and decapitated with a small rodent guillotine (DCAP, World Precision Instruments, Sarasota, FL, USA). The brain was transferred into ice cold ACSF (in mM): 87 NaCl; 2.5 KCl; 1.25 NaH_2PO_4, 7 $MgCl_2$; 0.5 $CaCl_2$; 25 $NaHCO_3$; 25 Glucose; 75 Sucrose (pH 7.4) equilibrated with 95% O_2/5% CO_2 mixture. On a cooled, ACSF filled metal plate, the cerebellum was removed from the cerebrum and olfactory bulb (Figure 6A). The remaining two hemispheres were separated. A piece of the cortex was removed along the cranial-caudal axis (Figure 6B) and a piece of the basal forebrain was removed along the dorsal-ventral axis (Figure 6C). The prepared hemispheres were glued on a vibratome tissue holder, the cortex side being the glue site. 400µm (field potential recording) or 300µm (calcium imaging, patch clamp recording) horizontal hippocampal slices (Figure 6D) were prepared on a vibratome (Leica VT 1200S, Leica Microsystems GmbH, Wetzlar, Germany), transferred onto a net within a beaker filled with ACSF (in mM): 87 NaCl; 2.5 KCl; 1.25 NaH_2PO_4, 7 $MgCl_2$; 0.5 $CaCl_2$; 25 $NaHCO_3$; 25 Glucose; 75 Sucrose (pH 7.4), equilibrated with 95% O_2/5% CO_2 mixture and heated up to 35°C. After 30 minutes the slices were transferred to another beaker filled with ACSF (in mM): 124 NaCl; 3 KCl; 2 $CaCl_2$, 2$MgCl_2$; 1.25 NaH_2PO_4; 26 $NaHCO_3$; 10 Glucose (pH 7.4), equilibrated with 95% O_2/5% CO_2 mixture and kept at room temperature. All beakers were covered with parafilm (Pechiney Plastic Packaging, Chigago, IL, USA).

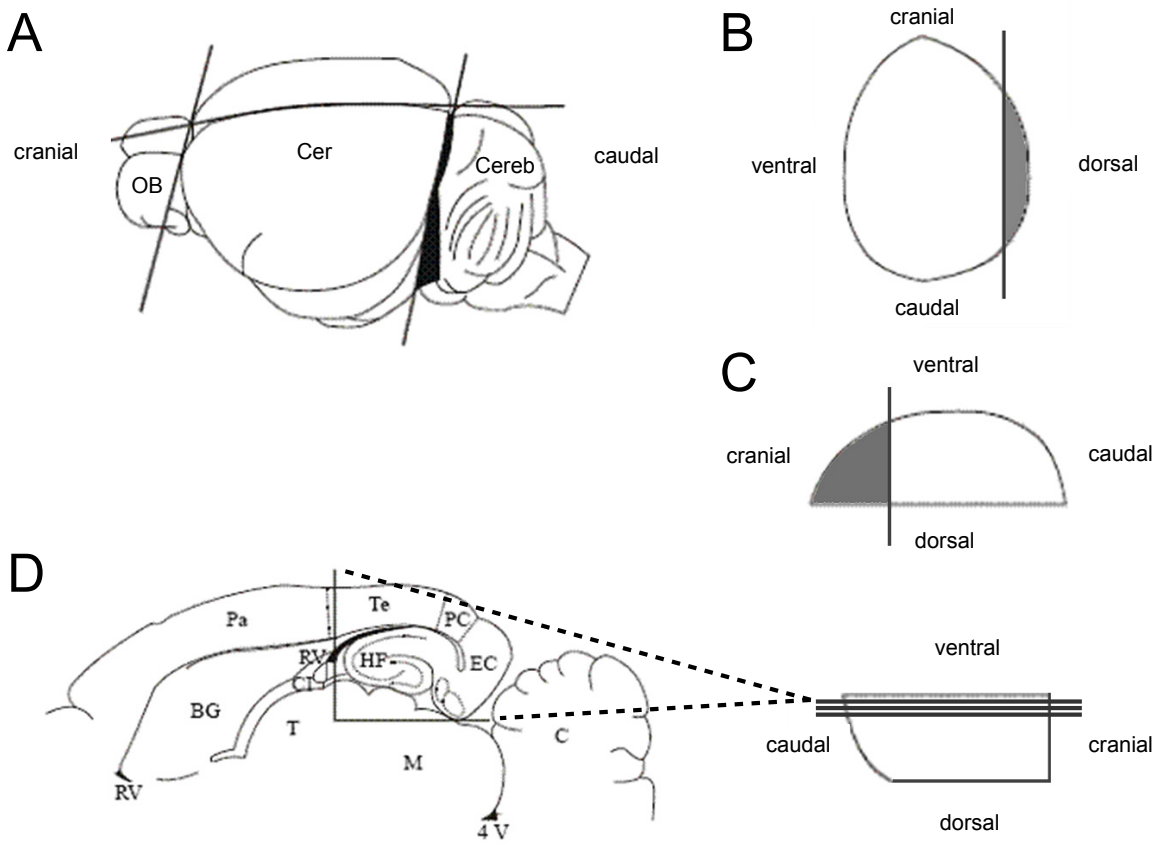

Figure 6. Sectioning-steps during hippocampal slicing procedure. (A) The cerebrum (Cer) is separated from cerebellum (Cereb) and olfactory bulb (OB) **(B)** a piece of the cortex along the cranial-caudal and **(C)** a part of the basal forebrain along the dorsal-ventral axis are removed (D) hippocampal slices are made along the cranial-caudal axis

2.2 Solutions

2.2.1 Perfusion/ incubation solutions

Artificial cerebrospinal fluid (ACSF) for room temperature (RT)	124 mM	NaCl
	3 mM	KCl
	1.25 mM	NaH_2PO_4
	2 mM	$MgCl_2$
	2 mM	$CaCl_2$
	26 mM	$NaHCO_3$
	10 mM	Glucose
Sucrose preparation solution ("Messy-Ringer")	87 mM	NaCl
	2.5 mM	KCl
	1.25 mM	NaH_2PO_4
	7 mM	$MgCl_2$
	0.5 mM	$CaCl_2$
	25 mM	$NaHCO_3$
	25 mM	Glucose
	75 mM	Sucrose
Artificial cerebrospinal fluid (ACSF) for physiological temperatures (35°C)	24 mM	NaCl
	3 mM	KCl
	1.25 mM	NaH_2PO_4
	2 mM	$MgCl_2$
	2 mM	$CaCl_2$
	26 mM	$NaHCO_3$
	10 mM	Glucose

Artificial cerebrospinal fluid (ACSF) for physiological temperatures (35°C) - "low calcium"	24 mM	NaCl
	3 mM	KCl
	1.25 mM	NaH_2PO_4
	3 mM	$MgCl_2$
	1 mM	$CaCl_2$
	26 mM	$NaHCO_3$
	10 mM	Glucose

2.2.2 Solutions for Patch clamp recordings

Pipette solution	130 mM	K-gluconate
	0.5 mM	$MgCl_2$
	4 mM	NaCl
	5 mM	KCl
	4 mM	Na_2ATP
	10 mM	HEPES
	0.1%	Lucifer Yellow

Sucrose preparation solution with astrocyte marker	87 mM	NaCl
	2.5 mM	KCl
	1.25 mM	NaH_2PO_4
	7 mM	$MgCl_2$
	0.5 mM	$CaCl_2$
	25 mM	$NaHCO_3$
	25 mM	Glucose

	75 mM	Sucrose
	1µM	Sulforhodamine 101

2.2.3 Solutions for calcium imaging experiments

Stock solution for dilution of calcium AM dyes	250mg	Pluronic acid
	1ml	DMSO
Pipette solution with calcium AM dye for positive pressure loading	30µl	25% pluronic acid/ DMSO
	200µl	ACSF (35°C)
	50µg	Magnesium green AM
Pipette solution with calcium AM dye for positive pressure loading	30µl	25% pluronic acid/ DMSO
	200µl	ACSF (35°C)
	50µg	Oregon green BAPTA 1 AM

2.2.4 Solutions for histochemical analysis

TRIS buffer (TBS) 0.1 M	12.12 g	TRIS
	9 g	NaCl
	1000 ml	Aqua dest

pH adjustment with 1 M NaOH or 1 M HCl to 7.6

Phosphate buffer saline (PBS) 10mM	150 mM	NaCl
	1.9 mM	NaH_2PO_4

	8.1 mM	Na_2HPO_4

pH adjustment with 1 M NaOH or 1 M HCl to 7.6

PFA 8%	8 g	PFA
	100 ml	1 mM PBS
	12 drops	1 M NaOH
	6 drops	1 M HCl

pH adjustment with 1 M NaOH or 1 M HCl to 7.4

Staining protocol: GFAP gt anti-rb RRX

Day 1	3 x 10 min wash with 0.1 M TBS		
	50µM thick slices of embedded (agarose) tissue		
	1 x 10 min wash-in 0.1 M TBS		
Day 1	3 slices per micro dish		
	Overnight 4°C:	485 µl	TBS 0.1 M
		1 µl	anti-GFAP
		10 µl	Triton X 10%
Day 2	3 x 10 min wash with 0.1 M TBS		
	3 hours at 35°C:	485 µl	TBS 0.1 M
		2.5 µl	gt anti-rb RRX
		10 µl	Triton X 10%

2.3 Drugs and reagents

Table 1. List of drugs and reagents used in experiments.

Site of action	Way of action	Substance	Vendor	Solvent	Final concentration
Group II mGluRs	Agonist	DCG IV	Tocris, Bristol, UK	Water, ACSF	1µM
Group II mGluRs	Antagonist	LY 341495	Tocris, Bristol, UK	DMSO, NaOH	3µM
mGluR 8 (group III)	Agonist	PPG	Tocris, Bristol, UK	NaOH	3µM
mGluR 5 (group I)	Antagonist	MPEP	Tocris, Bristol, UK	Water, DMSO	10µM
mGluR I (group I)	Antagonist	LY 367385	Tocris, Bristol, UK	NaOH, Water	50µM
$GABA_A$-R	Antagonist	Bicuculline	Tocris, Bristol, UK	Ethanol, DMSO	10µM
$GABA_B$-R	Antagonist	CGP	Tocris, Bristol, UK	DMSO, Ethanol	2µM
AMPA-R	Antagonist	CNQX	Tocris, Bristol, UK	Water	30µM
AMPA-R	Antagonist	NBQX	Tocris, Bristol, UK	NaOH, DMSO	10µM
NMDA-R	Antagonist	DL-AP5	Tocris, Bristol, UK	Water, NaOH	30µM, 50µM or 100µM
NMDA-R	Antagonist	MK 801	Tocris, Bristol, UK	Water, DMSO	50µM
GLAST, GLT-1	Blocker	DL-TBOA	Tocris, Bristol, UK	DMSO, Water	10µM, 40µM or 100µM
Na^+_v channels	Blocker	TTX	Alomone Labs, Jerusalem, Israel	Water	1µM
Ca^{2+}_v channels	Blocker	Cobalt	Sigma, St. Louis, MO	Water	600µM
Glutamate receptors	Ligand	γ-CNB-caged L-glutamic acid	Invitrogen, Grand Island, NY	ACSF	250µM

2.4 Extracellular field potential recordings in the MML (DG)

Field potentials are electrical signals measured between two points in the extracellular space and generated by electrical fields produced by the activity of a single neuron or a group of neurons. A field potential is composed of a presynaptic (fibre volley) and a postsynaptic component (population spike (pspike)).

Depending on the geometric arrangement of neurons, three characteristic types of field potentials can be distinguished: the open field, the closed field and the open-closed field. The simplest form is the open field structure because the somas of laminarly organized neurons face in one direction and the dendrites in the other. The hippocampus is a typical representative for this arrangement (Johnston and Wu, 1995).

In this study, field potential recordings were performed in the middle molecular layer (MML) of the rat hippocampal dentate gyrus (Figure 7). Medial perforant path fibres were stimulated and group II mGluR activation was assessed via the inhibition of the postsynaptic field potential component.

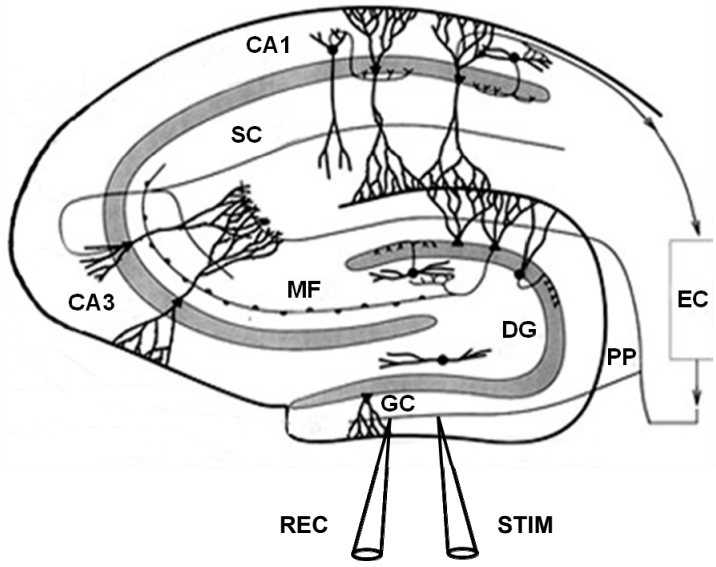

Figure 7. Line drawing illustrating the main hippocampal synaptic connections and the area of stimulation and field potential recording. Both pipettes were positioned within the middle molecular layer to stimulate the medial perforant path projection incoming from the entorhinal cortex and to record the corresponding postsynaptic answer of the granule cells extra-synaptically. Picture (modified) adopted from: The Rat Nervous System, 3rd Edition, 2004 by George T. Paxinos, Academic Press

2.4.1 Field potential recording setup

The electrophysiological setup for field potential recordings (Figure 8) can be described as follows: horizontal hippocampal slices (thickness: 400µm) positioned on a piece of lens paper were laid on a net in an interface chamber, were perfused with 35°C warm ACSF equilibrated with 95% O_2/5% CO_2 mixture. Slice and electrode positioning, as well as the observation of the perfusion rate, were managed with the help of a stereomicroscope (Stemi 1000, Zeiss, Göttingen, Germany). A digital signal was transformed via an interface (ITC 16, Instrutech cooperation, Long Island, NY, USA) into an analog signal and sent to an isolated stimulator (custom made) to trigger stimulation. Signals detected by the recording pipette were pre-amplified (custom made), amplified (SEC-05 LX, npi, Tamm, Germany) and filtered at 3kHz. Data were sampled at 8kHz and stored on a computer for further analysis.

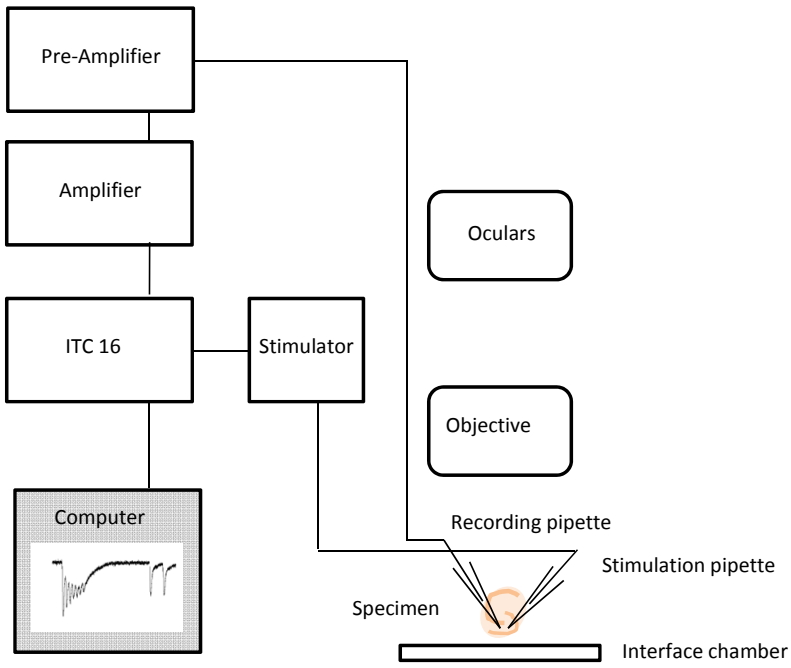

Figure 8. fEPSP recording setup.

2.4.2 Electrodes

1mm thick glass capillaries (GB150F-8P, Science products, Hofheim, Germany) were used to pull pipettes for stimulation and recording (pipette resistance: ~1-3MΩ). The glass capillary was fixed upright in a vertical puller (Model PP-830, Narishige, Japan)

and pulled in two steps. The heating temperature of the first pull-step mainly determined the angle of aperture and the heating temperature of the second pull step the diameter of the pipette tip. For extracellular stimulation and recording the pipettes were filled with ACSF (for physiological temperatures) and mounted on a cloridized silver wire fixed on a holder, so that the tip of the silver wire touched the ACSF.

2.4.3 Positioning of electrodes

The stimulation and recording electrode were positioned in the MML parallel to the medial perforant path fibre tract. Paired-pulse stimulation (stim: 0.1ms, 40ms IPI, ISI 30s) was performed and fEPSPs were accepted for an experiment if they showed paired-pulse depression to ~80% and if the amplitudes were stable between approximately 5 to 20 minutes. The peak amplitude of fEPSPs usually exceeded 1mV.

2.4.4 Stimulation protocol

A flexible burst protocol programmed in Igor PRO (Wavemetrics Inc, Portland, OR, USA) was used to create different stimulation pattern, varying in burst length, number of given bursts, frequency, inter-burst interval (IBI) and post-burst interval (PBI). In general, the protocol was composed of a conditioning burst to activate group II mGluRs, and a test-stimulus to assess the mGluR effect on the field potential response.

2.4.5 Experimental procedure

Slices were transferred to the interface chamber and incubated for one hour before the measurement started. Stimulation and recording pipettes were positioned in the MML of the DG and the paired pulse plasticity was monitored for at least 20 minutes. After reaching a stable baseline, a conditioning burst was applied followed by a test-stimulus. Then the group II mGluR antagonist LY341495 was added and as soon as a steady-state of the blocking effect was reached the same stimulation protocol was applied again (approximately after ten minutes) (Figure 9). The mGluR activation was assessed by the antagonist (LY341495) mediated increase of the test-stimulus fEPSP and calculated by the following formula:

$$\frac{\text{fEPSP peak}_{\text{test}} / \text{fEPSP peak}_{\text{cond\_1st}}}{\text{fEPSP peak\_LY}_{\text{test}} / \text{fEPSP peak\_LY}_{\text{cond\_1st}}}$$

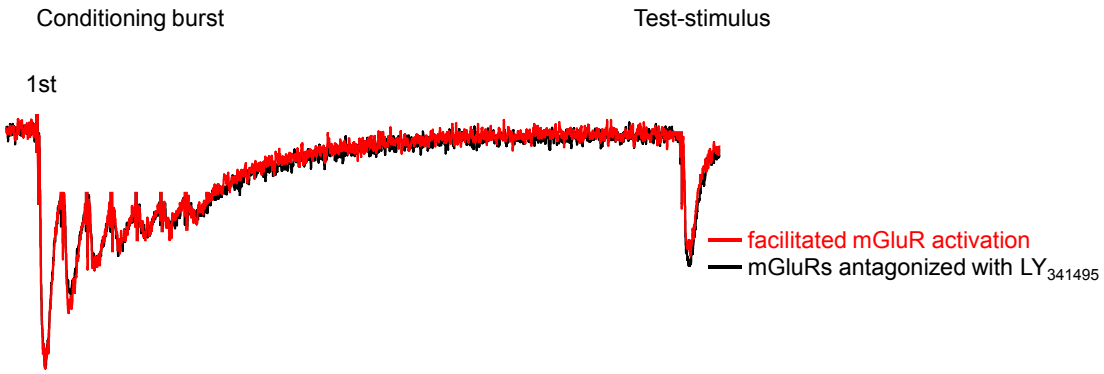

Figure 9. Stimulation protocol

2.4.6 Application of drugs

Pharmacological substances were added to the bath solution (ACSF for 35°C) in a separate reservoir by perfusion (rate: 2ml/min). The solution was bubbled with carbogen. NMDA receptor blockers (DL-AP5 30-100µM and/or MK 801 50µM) were added in every field potential experiment to prevent LTP during high frequent repetitive stimulation.

2.4.7 Analysis of fEPSP amplitudes

Data were analyzed with custom macros in Igor PRO as well as in Excel and are presented as average ± standard error of the mean (SEM).

2.5 Presynaptic calcium imaging in the MML

A procedure that can be used to study presynaptic calcium transients in rodent brain slices is monitoring presynaptic calcium dynamics with membrane permeable indicators. Rather than attempting to measure calcium levels in individual terminals, the strategy is to make an aggregate measurement from many presynaptic terminals. I utilized this method to investigate the temporal dynamics of group II mGluR mediated inhibition of synaptic transmission in detail.

2.5.1 Electrophysiological and imaging setup

The rat hippocampal brain slice (300µm) was positioned in a submerge chamber of an upright fluorescence microscope (Eclipse E600-FN, Nikon Instruments Inc., Melville, NY, USA) and held in place with a nylon harp fixed on a flattened platinum wire. The loading pipette and the stimulation electrode were mounted on a manipulator and driven by a stage control unit (SM. I, Luigs & Neumann, Ratingen, Germany).

To stimulate the Ca^{2+} AM-ester-dye-loaded medial perforant path fibre tract (Magnesium Green AM or Oregon Green BAPTA-1 AM, Invitrogen, Molecular Probes, Darmstadt, Germany), a digital trigger signal was sent via the recording software TIDA (HEKA Elektronik Dr. Schulze GmbH, Lambrecht, Germany) to the interface (ITC16, Instrutech cooperation, Long Island, NY, USA) which converted the digital input into an analogue output and forwarded the signal to the isolated pulse stimulator (model 2100, A-M SYSTEMS, Sequim, WA, USA). The stimulator sent a voltage pulse of defined duration (0.2-0.4ms) and strength (40-50V) to the stimulation electrode. Stimulation generated presynaptic action potentials in the MPP causing presynaptic Ca^{2+} influx. Within the terminals, Ca^{2+} binding to the fluorescent dye lead to a fluorescence emission increase. The fluorescent Ca^{2+} indicator was excited by light with 470nm wavelength (bandwidth ±30nm) (def.: light exhibits properties of waves and a wavelength is usually considered as distance between consecutive corresponding points of the same phase in such a sinusoidal wave. Light of specific colour matches a specific wavelength or a wavelength range) emitted from an LED light source (OptoLED, Cairn-Research, Faversham, Kent, UK).

Fluorescent, band-pass filtered light (530 ± 43nm, AHF Analysetechnik AG, Tübingen, Germany) was detected by a light sensor (photodiode detector, Till Photonics GmbH, Gräfelfing, Germany) through a 60x objective (60x Fluor, DIC H, NA 1.00, WD 2.0, Nikon Instrutech cooperation, Long Island, NY, USA) and monitored with a CCD camera (model FK 7512 IQ, Pieper GmbH, Schwerte, Germany). A beam splitter unit mediated the dispersion of the corresponding light (model DCXRUV, AHF Analysetechnik AG, Tübingen, Germany).

Fluorescent signals could be either amplified by increasing the gain of the voltage converter unit (Till Photonics GmbH, Gräfelfing, Germany) or by enhancing the gain of the amplifier (model EPMS 07, npi electronic GmbH, Tamm, Germany).

The ITC 16 was supplied with the amplified voltage signal which in turn was transformed into a digital signal displayed on the oscilloscope and computer with the respective software (see the upper part of the section).

If presynaptic Ca^{2+} imaging experiments were performed in combination with glutamate uncaging, a light fibre connected to a UV laser system (DPSL, Rapp OptoElectronic GmbH, Hamburg, Germany) was intercalated in the light path. A dicroic beam splitter within the optical system of the microscope was necessary to center the UV light with the excitation light on the specimen. In the lower graphic a schematic drawing of the imaging and recording setup is illustrated (Figure 10).

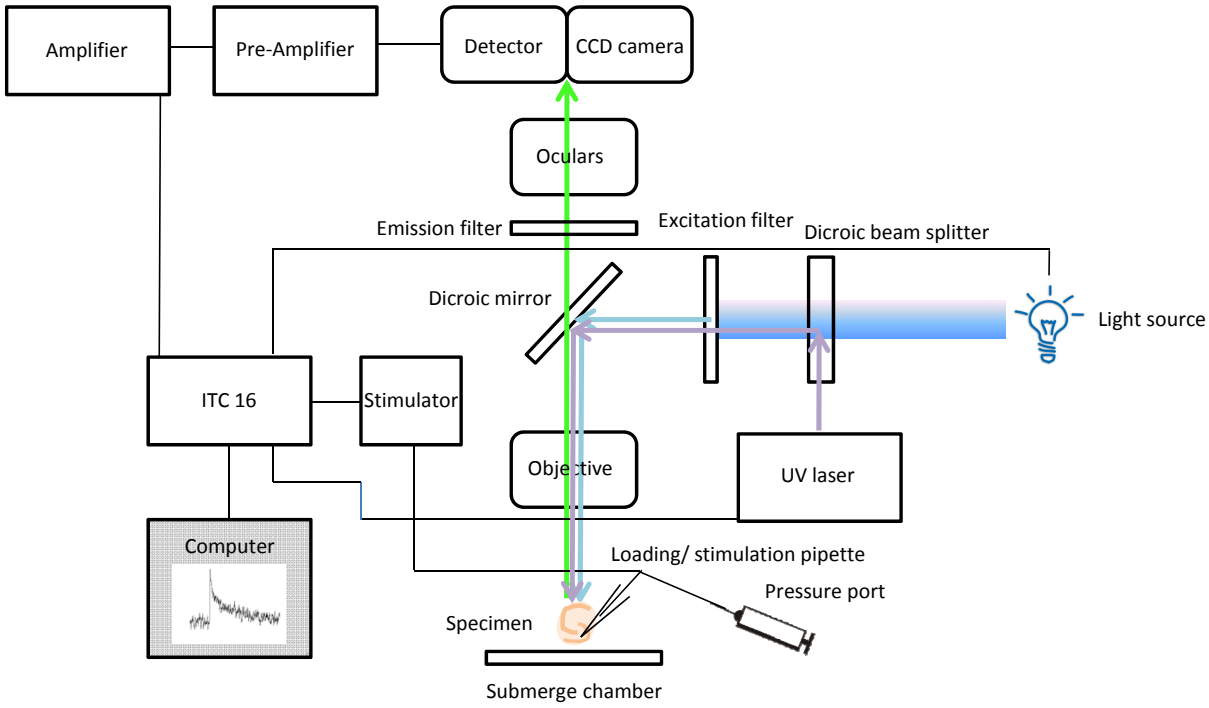

Figure 10. Imaging and recording setup

2.5.2 Loading of AM ester calcium indicator dye into the MPP fibre bundle

To prepare the labelling solution, 50µg of the AM-ester indicator (here: Magnesium Green AM or OGB1 AM) was dissolved in 30µl solution of 25% pluronic acid (Pluronic F-127, Invitrogen, Molecular Probes, Darmstadt, Germany) and 75% dimethyl sulfoxide (DMSO, Sigma-Aldrich, St. Louis, MO, USA) in a vial. The solution was vortexed for 30 seconds and sonificated for 3 minutes. Then 200µl artificial cerebrospinal fluid (ACSF for 35°C) was added and the solution was vortexed and sonificated again. The prepared mixture was filtered (Syringe Filter, 4mm, No. 171/cellulose acetate membrane, Nalgene, Thermo Fisher Scientific, Rochester, NY, USA) and kept on ice.

To load the indicator dye into rat brain slices the following protocol was used. The indicator dye solution was loaded into a pulled glass pipette via a spinal needle. Before the pipette entered the bath solution, slight positive pressure (0.5 units of a 1ml syringe, Becton Dickingson, Madrid, Spain) was applied to prevent it from blocking. Then, the loading pipette was lowered carefully near the surface of the slice. Step by step, the distance between the tissue and the pipette tip was minimized. The pipette was

positioned parallel within the medial perforant path fibre tract that was to be loaded. Additional positive pressure was applied, if the stream out of the pipette tip became weaker on the way to the slice surface.

Next, the pipette was positioned in the ideal loading plane. If a slight movement of the tissue surrounding the tip could be observed, the condition was optimal, if not, more pressure was applied. After 20 to 40 minutes of loading, the pipette was removed and the bath heater (temperature controller V, Luigs & Neumann, Ratingen, Germany) was switched on to increase the temperature in the bath to 35°C in order to perform experiments at physiological conditions approximately 20 minutes subsequently.

2.5.3 Electrodes

For the loading, a 5 to 6MΩ pipette was used to keep the spot at the injection site small and the loading as specific as possible. For stimulation a 3 to 4MΩ pipette was used to elicit presynaptic action potentials in many axons of the medial perforant path fibre bundle (stimulus length 0.2-0.4ms, stimulus strength 40-50V). The tip of the loading pipette was filled with approximately 3 to 4µl labelling solution and the stimulation pipette contained the ACSF for physiological temperatures.

2.5.4 Positioning of electrodes

Loading or stimulation pipette were positioned approximately 10 to 15 µm deep within the Ca^{2+} indicator dye loaded medial perforant path fibre tract, depending on the optimally loaded plane. Generally the best suited region for electrode positioning was distal to the dye injection site which was mostly close to the site where the perforant path projections from the entorhinal cortex enter the dentate gyrus.

2.5.5 Aperture

The aperture defined the fluorescence detection area. The aperture stop was adjusted in size to get an approximately 20µm x 20µm wide imaging field. For Ca^{2+} imaging the aperture was positioned in front of the stimulation pipette (distance ~5µm), slightly under the tip. For Ca^{2+} signal improvement, aperture and stimulation pipette position was carefully adjusted.

2.5.6 Analysis of MPP loading intensity and specificity

The MPP loading quality was assessed by visual judgment and Ca^{2+} signal quality.

2.6 Caged glutamate

The caged amino acid neurotransmitter glutamic acid (L-glutamic acid, γ-(α-carboxy-2-nitrobenzyl) ester, trifluoroacetic acid salt (γ-CNB-caged L-glutamic acid)) is biologically inactive before photolysis. Flash photolysis of the caging group with UV illumination at 355 nm results in a rapid and highly localized release of the free neurotransmitter at the site of illumination. γ-CNB-caged L-glutamic acid has the caging position at the carboxy end. This form of caged glutamate was chosen, because it combines rapid photolysis with high quantum efficiency.

2.7 Uncaging light source

γ-CNB-caged L-glutamic acid was dissolved in ACSF for physiological temperatures and added to the bath solution via perfusion. To obtain the best conditions for flash photolysis, the uncaging plane had to be adjusted to the imaging plane. Therefore, I performed tests with caged FITC (CMNB-caged fluorescein, Invitrogen, Eugene, Oregon, USA) while changing the coupling of the light fibre. CMNB-caged fluorescein is colourless and non-fluorescent before photolysis. Flash photolysis of the caging group with UV illumination at 355 nm results in fluorescein.

For tests, a drop (~5µl) CMNB-caged fluorescein was put on a slide. After the drop was dry, a coverslip was fixed with nail polish on the slide to protect the substance from water. Then I proceeded as follows: a short UV laser pulse was applied to excite the caged fluorescein. The fluorescent spot was set in focus and defined as the optimal imaging place. Next, the coupling of the UV laser light fibre was changed systematically until the best uncaging plane matched the best imaging plane (Figure 11A, right panel). This procedure was repeated with three light fibres of different diameter: 200µm (Figure 11), 400µm (not shown) and 1mm (not shown).

In addition to this adjustment, the intensity of the UV light for each light fibre was tested in bleaching experiments (Figure 11B) and the effectiveness of glutamate

uncaging was assessed by the strength of group II mGluR activation induced decrease in Ca^{2+} signal size.

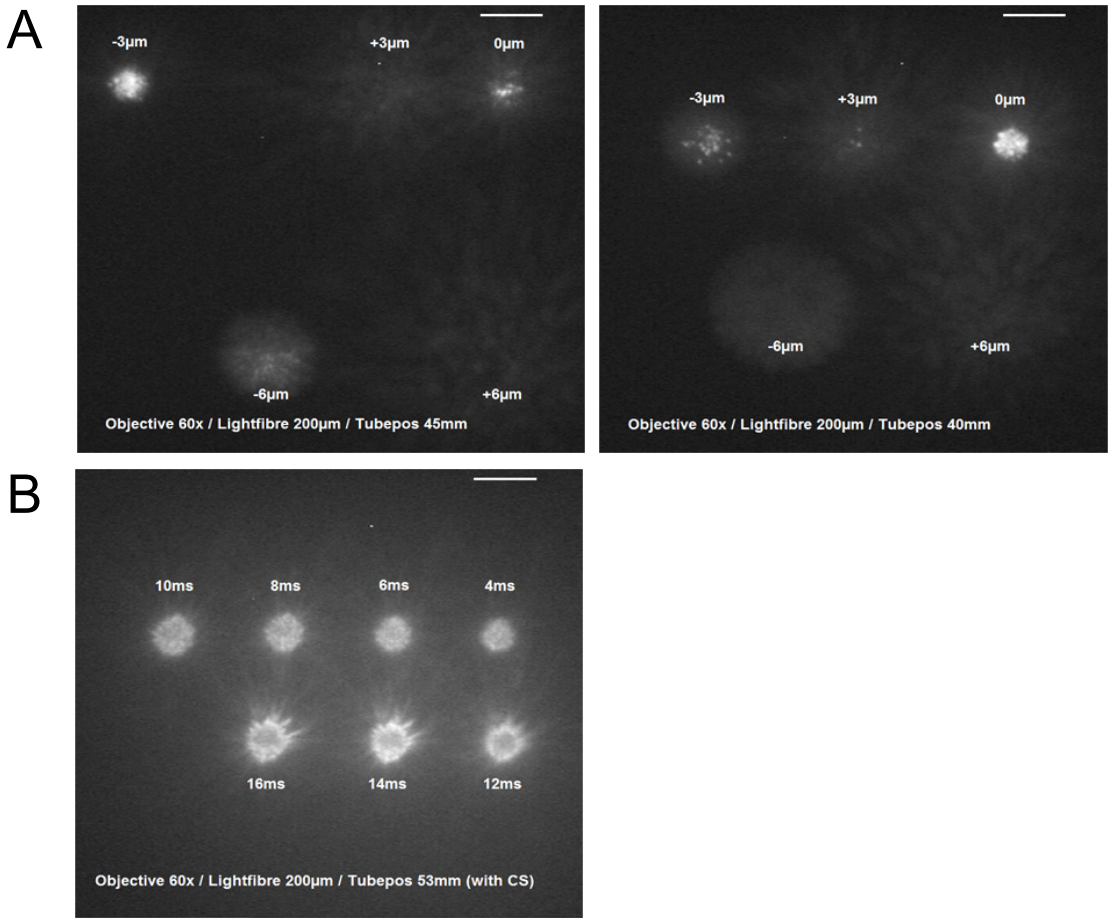

Figure 11. UV laser flash photolysed CMNB-caged fluorescein – adjustment of imaging and uncaging plane. (A) The optimal imaging plane is at 0µm. In order to find the uncaging plane, the focus was set to different planes with reference to plane zero (down +, up -) and the uncaged spot was assessed after flash photolysis. Whereas the best uncaging plane did not match the optimal imaging plane on the right panel, it is well adjusted on the left. **(B)** UV laser pulses of different length were applied in order to evaluate the power of the laser while using a 200µm thick light fibre. After 6ms of uncaging first bleaching effects were detectable, indicated by the black dot in the middle of the spot (scaling: 10µm).

2.8 Uncaging protocol design – Method 1: Voltage sensitive dye imaging with RH155

To examine astrocyte transporter activity during flash photolysis of glutamate, I planned to optically monitor astrocyte membrane potential changes during transporter currents by using the voltage sensitive dye RH155 which labels astrocyte membranes and changes its absorption properties with membrane potential changes (Figure 12).

For experiments, hippocampal slices (300µm) prepared from 20 to 40 day old Wistar rats were stained with the voltage sensitive dye RH155 (AnaSpec, San Jose, CA). This dye was reported to preferentially stain glial cells over neuronal cells (Konnerth et al., 1987). Based on the publication from Chang and Jackson (2003) the concentration and incubation time for RH155 was adjusted to attain an optimal optical density value (absorbance) during absorption measurements which is 2 at best and calculated with the following formula:

$A_\lambda = - \log_n I_{RH155} / I$

We ended up with an incubation of 0.2mg RH155/ ml for 30min (A_λ ~2.2). The stained slice was placed in the submerged chamber, mounted on an upright fluorescent microscope, perfused with ACSF (for RT) and equilibrated with 95% O_2/5% CO_2 mixture. The slice was illuminated with visible light of high power from the bottom side, dampened with neutral density filters (ND 1.3, 2, 4 corresponded to 5, 1 and 0.01% transmission, AHF Analysetechnik AG, Tübingen, Germany) in order to keep the baseline signal around 6V. Additionally, a higher light intensity, together with a lower amplification factor (1x) improved the signal-to-noise ratio.

The light that passed the tissue was filtered at 700nm (VersaCrome HC 700 ±13nm, AHF Analysetechnik AG, Tübingen, Germany). A photo-detector system (photodiode detector, Till Photonics GmbH, Gräfelfing, Germany) monitored the decrease in light intensity during RH155 absorption increase due to astrocyte membrane potential changes and converted the photocurrent into a voltage signal which was in turn transformed into a digital output (ITC 16, Instrutech cooperation, Long Island, NY, USA). Traces were filtered at 1kHz and sampled with 20kHz.

In all experiments, a 60x objective (60x Fluor, DIC H, NA 1.00, WD 2.0, Nikon Instrutech cooperation, Long Island, NY, USA) was used and the aperture (approximately 30 x 30µM) positioned above the middle molecular layer of the dentate gyrus. To check for RH155 signal, synaptic responses were evoked by delivering short pulses (stimulus length 0.3ms, IPI 5ms) to the medial perforant path fibre tract with a 3-4MΩ glass electrode and optical signals were averaged over 10 trials.

In the final experimental series, glial responses, as measured by dye absorption changes, were intended to be evoked by flash photolysis of caged glutamate. To prevent interference by UV light, it should be blocked by a long pass filter (Brightline HC 409/LP, AHF Analysetechnik AG, Tübingen, Germany) which unfortunately did not work properly.

At the end, tests revealed that this method was not suited for my purpose (section 3.3.1) and I had to take another approach in order to design an uncaging protocol.

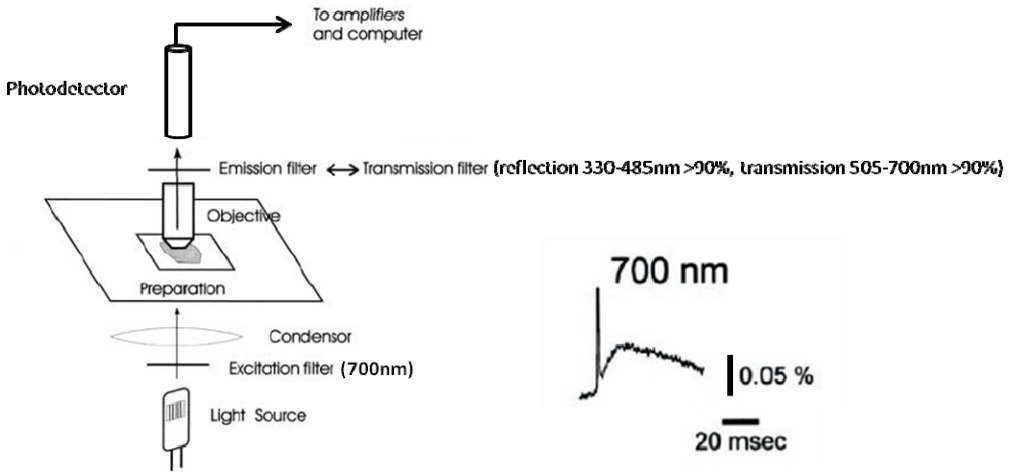

Figure 12. A schematic example of a voltage imaging system. The VSD stained slice is illuminated from the bottom. The light is filtered at 700nm, leading to an absorption increase of RH155 (see trace at the lower right corner), The picture is adapted from: Chang and Jackson, J. Membrane Biol., Vol. 196, pp. 105- 116, 2003

2.9 Uncaging protocol design – Method 2: Measuring astrocyte glutamate transporter currents

As already mentioned, the electrogenic glutamate uptake of astrocytes follows the time course of extra-synaptic glutamate. To measure the transporter current directly I patch clamped astrocytes. In the following section the experimental setup and procedure is described in detail.

2.9.1 Patch clamp setup and experimental procedure

Horizontal hippocampal slices were prepared according to the technique described in section 2.1.2. Thereafter, the slices (300µm) were transferred into 35°C warm, sucrose-ACSF for approximately 20-30 minutes and were subsequently incubated for 25 minutes in sucrose ACSF containing 1µM Sulforhodamine 101 (Invitrogen, Molecular Probes, Darmstadt, Germany), a fluorescent dye that preferentially stained astroglial cells. The solution was allowed to come to room temperature.

After staining, the slices were kept in RT-ACSF for at least 15 minutes before they were used for patch clamp recordings. For an experiment, slices were treated as described in the first part of section 2.5.1. The slice was perfused with 35°C-ACSF (rate: 1ml /minute) using a Minipuls 3 pump (Gilson, Middleton, WI) and bubbled with carbogen.

By illuminating the slice with 590nm LED light (OptoLED, Cairn, Faversham, Kent, UK) the fluorescent astrocyte indicator sulforhodamine 101 was excited and the emitted light was detected by a CCD camera (model FK 7512 IQ, Pieper GmbH, Schwerte, Germany), so that astrocytes could be pre-selected under magnification (60x objective, Fluor DIC H, 1.00W, WD 2.0, Nikon, Melville, NY, USA) for patch clamp experiments. The patch pipette was filled with 130 mM K-gluconate, 0.5mM $MgCl_2$, 4 mM NaCl, 5 mM KCl, 4 mM Na_2ATP, 10 mM HEPES and 0.1% Lucifer Yellow CH dipotassium salt (Sigma-Aldrich, St. Louis, MO, USA). The liquid junction potential of the gluconate based solution was -10mV with respect to the external solution.

In the whole cell mode, the fluorescent dye Lucifer Yellow (excitation wavelength 470nm) spread into the cell's fine processes and facilitated the assessment of the morphology. Whole cell patch clamp recordings of astrocytes were performed using a

patch clamp amplifier (EPC 7, HEKA Elektronik Dr. Schulze GmbH, Lambrecht, Germany). All recordings were acquired with an ITC16 (Instrutech cooperation, Long Island, NY, USA) and operated by IgorPRO (Wavemetrics Inc, Portland, OR, USA) and TIDA (HEKA Elektronik Dr. Schulze GmbH, Lambrecht, Germany) for Windows. IgorPro was used to monitor whole cell mode stability (filter 5kHz) whereas TIDA was used to measure compensatory currents arising during electrogenic uptake of glutamate by astrocytes (20mV/pA, filter 1kHz) elicited via UV laser uncaging (Rapp OptoElectronic GmbH, Hamburg, Germany) of γ-CNB-caged L-glutamic acid. Data were sampled at 20kHz and stored on a computer for further analysis. A schematic drawing of the patch clamp system is shown in the following graphic (Figure 13).

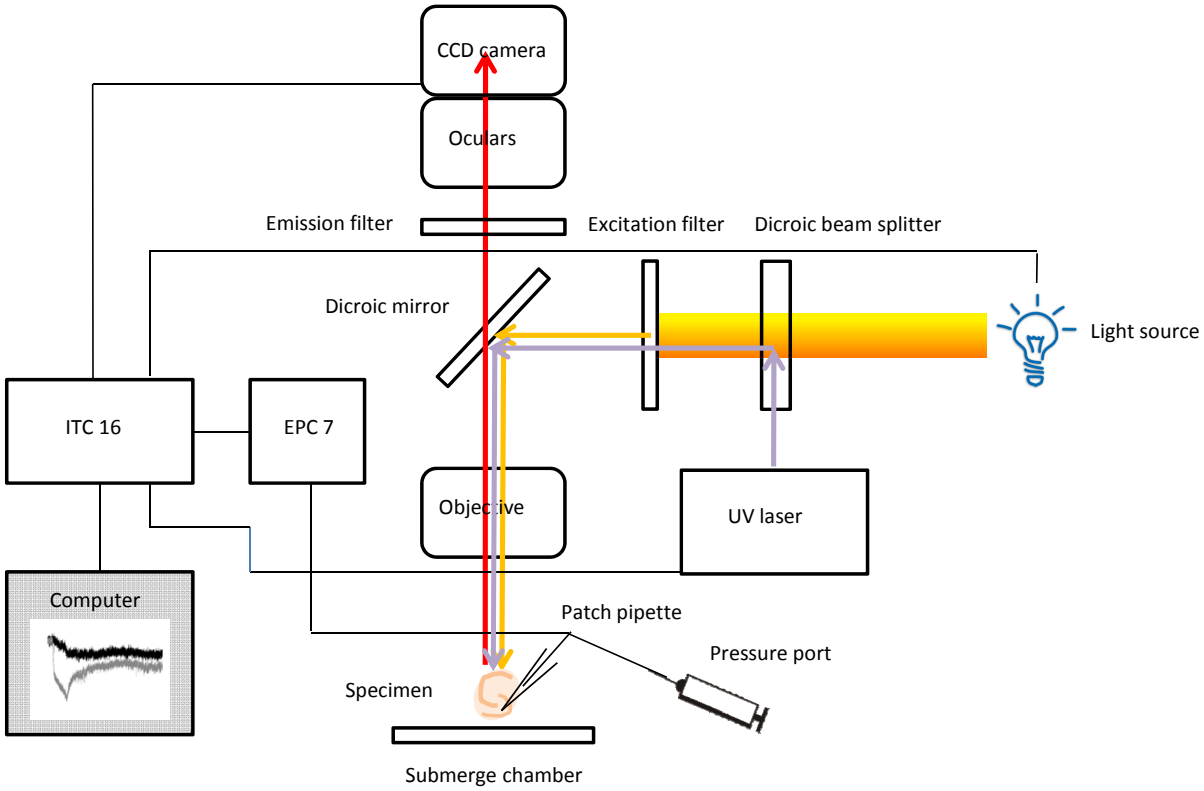

Figure 13. Imaging and patch clamp setup.

2.9.2 Astrocyte identification

First, astrocytes were identified by means of morphological features. As the name suggests, astrocytes are process-bearing stellate or star shaped cells distributed

throughout the brain and spinal cord and possess small cell bodies (~10µm). They are divided into protoplasmic and fibrous types.

The major identifying ultra-structural feature of astrocytes is the presence of intermediate filaments. These filaments are present in both types but much more prominent in fibrous astrocytes than in protoplasmic. In the dentate gyrus, protoplasmic astrocytes were predominantly found.

Second, astrocytes could be identified immunhistochemically. The major component of glial fibrils is the glial fibrillary acidic protein (GFAP) which is relatively specific for astrocytes in the CNS. Therefore, if a cell was positively stained for GFAP (Dako, Glostrup, Denmark) after patch clamp, the probability was high that this cell was an astrocyte. Astrocytes in acute brain slices could be labelled with the fluorescent dye sulforhodamine 101 (Sigma-Aldrich Chemie GmbH, Taufkirchen, Germany) to make a pre-selection for patch clamp experiments. Additionally, the patch clamp pipette was filled with the fluorescent dye Lucifer Yellow CH dipotassium salt (Sigma-Aldrich, St. Louis, MO, USA) to visualize the fine-architecture of the patched cell such as the intermediate filaments.

Third, astrocytes could be identified electrophysiologically. The cells were characterized by passive membrane properties, a low input resistance (≤ 30MΩ) and strongly negative resting potential (approximately -80 to -90mV).

2.9.3 Whole cell configuration

Astrocyte transporter currents were measure in the whole cell configuration during pharmacological isolation (10µM NBQX, 100µM DL-AP5, 50µM MK801, 10µM MPEP, 1µM TTX, 50µM LY367385, 40µM DL-TBOA (if required)). Strictly speaking, it was not the transporter current that was measured but rather the current injected to compensate the membrane potential changes during glutamate transporter activity elicited by glutamate uncaging.

Before a cell could be measured in the whole cell mode, the cell attached configuration had to be reached. This means the electrode (~4 to 5 MΩ) was sealed to the patch of membrane while the cell remained intact and capacitive currents occurring during the sealing process were compensated. To attain a whole cell configuration, the electrode was left in place on the cell and more suction was applied to rupture the membrane

patch, providing access to the intracellular space of the cell. Access resistance was monitored continuously during the experiment and was typically around 10MΩ.

2.9.4 Voltage clamp mode

In the voltage clamp configuration the cell was kept at a negative potential (-80mV), assumed to be the resting potential of the cell. This made it possible to measure ionic current crossing the cell's membrane at the given voltage during flash photolysis of glutamate and allowed a comparison between recorded astrocyte transporter currents. This technique is suited to analyze single currents but not really applicable to draw conclusions about the physiological excitation pattern of a cell.

2.9.5 UV laser uncaging protocol design

Whole-cell patch clamped astrocytes in voltage clamp configuration isolated from currents other than glutamate transporter currents were exposed to perfused γ-CNB-caged L-glutamic acid (250µM) at 35°C. The uncaging spot (200µm light fibre diameter) was centered on the astrocyte's soma and the astrocyte itself was in focus. UV laser flash pulses were applied in order to evoke a glutamate transporter current.
The aim was to quickly (or directly) reach a current which was relatively strong (time constant τ ~11ms; ~30pA) at the beginning, remained constant in a tenth to hundredth millisecond range and declined quickly after uncaging (the time constant τ describes the time an exponential rising or decaying process need to reach 63.2%, respectively 36.8% of its initial value). To achieve this, UV illumination time and inter-pulse interval were adjusted.

2.9.6 Application of drugs

Pharmacological substances were dissolved in ACSF for 35°C , kept in an extra beaker and applied either by perfusion or by adding them directly to the solution in the submerge chamber (true for caged glutamate and the mGluR antagonist LY341495). After caged glutamate was added and perfused once, the solution was recycled for the rest of the experiment. The perfusion rate was 1ml per min.

2.9.7 Analysis of glutamate transporter transients

Data acquired with the software TIDA (HEKA Elektronik Dr. Schulze GmbH, Lambrecht, Germany) were displayed and analyzed with IgorPRO (Wavemetrics Inc, Portland, OR, USA).

2.10 Combinatory Ca^{2+} imaging and uncaging protocol

For simultaneous Ca^{2+} imaging and glutamate uncaging the following stimulation protocol was designed (Figure 14, top). In the first part, a pre-stimulus pulse (P, 0.2-0.4ms, 40-50V) was applied followed by a series of UV laser flashlights (e.g. 1x50ms/ISI 6ms, 11x6ms/ISI 30ms, PUI 32ms) to uncage glutamate, and a test-stimulus (T, 0.2-0.4ms, 40-50V) was subsequently applied. During stimulation the corresponding Ca^{2+} transient was measured. In the second part, only a pre- and a test-stimulus were given. Next, the percentage inhibition of the presynaptic Ca^{2+} signal maximum mediated by uncaging evoked group II mGluR activation was calculated by using the following formula (L: UV laser, NL: no UV laser):

$$\frac{\Delta F/F_{\text{test\_L}} / \Delta F/F_{\text{pre\_L}}}{\Delta F/F_{\text{test\_NL}} / \Delta F/F_{\text{pre\_NL}}}$$

If Magnesium Green AM was used, the protocol was slightly changed. The protocol was repeated three times and an average value for each (response to pre- and test-stimulus) maximum Ca^{2+} signal was calculated.

In order to resolve the latency and activation kinetics of group II mGluRs, the duration of uncaged glutamate exposure time was varied, starting with one longer laser pulse. Then, the exposure to a constant uncaged glutamate concentration was prolonged step by step by adding further shorter stimuli to the laser protocol until the Ca^{2+} signal was maximally inhibited (Figure 14, middle). In a single experiment, only one data point per exposure time could be acquired.

In the next step, the time interval between the end of uncaging and the test-stimulus was increased to determine the time the Ca^{2+} signal needed to recover to its initial size

(before mGluR activation) (Figure 14, bottom). To assess the deactivation kinetics reliably, sufficient group II mGluR activation during uncaging was required, but the activation did not have to be maximal.

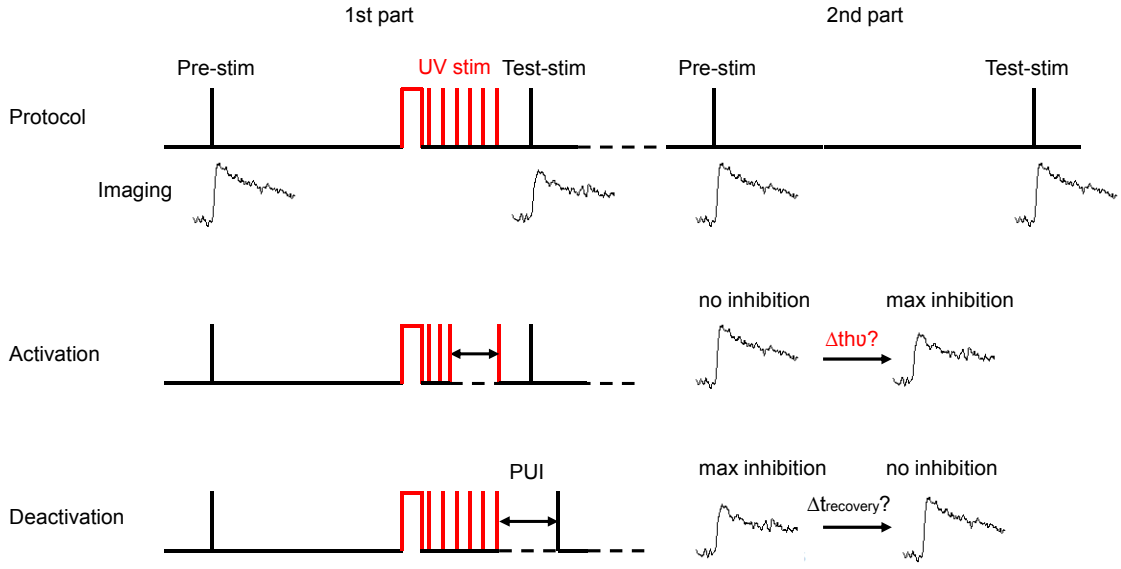

Figure 14. Combined stimulation, uncaging and imaging protocol. The protocol consists of two parts: in the first part, the Ca^{2+} response to a pre-stimulus (Pre-stim) and a test-stimulus (Test-stim) following flash photolysis of glutamate (UV stim) was imaged. In the second part only a pre- and a test-stimulus were applied. The mGluR mediated inhibition was assessed by comparing the Ca^{2+} transient depression after uncaging with the Ca^{2+} transient change without uncaging. The number of protocol repetitions and the order of uncaging (in the first or second part) varied depending on the Ca^{2+} indicator used. To resolve the latency and activation kinetics, the duration of flash photolysis was prolonged until maximum inhibition was reached and the PUI was kept constant. In contrast, to determine the deactivation kinetics, the uncaging time was kept constant and the post uncaging interval (PUI) increased until the Ca^{2+} transient recovered back to initial size.

2.11 GFAP Immunhistochemistry

After successful astrocyte patch clamp experiments, the horizontal hippocampal slices (300µm) were transferred into a minidish (TC-Plate 24 well, Greiner Bio-One GmbH, Frickenhausen, Germany) and incubated in PFA (8%) for 24 hours. Afterwards, they were washed with TRIS buffer (TBS, 0.1 M) three times for ten minutes. Following this procedure the slices were kept in TBS (0.1M) exclusively until they were fixed in agar and cut into thinner, 50µm thick slices for staining. By using an inverted microscope with Epi-fluorescence attachment (Eclipse TS100, Nikon, Melville, NY, USA), slices containing the Lucifer Yellow (excitation 470nm) loaded glia cell were pre-selected

(Filter F36-525, HC Set, EGFP, AHF Analysetechnik AG, Tübingen, Germany). These slices were again washed for ten minutes in TBS (0.1M).

In total, 8 slices were stained for GFAP (primary antibody: Polyclonal Rabbit Anti-Glial Fibrillary Acid Protein, Dako, Glostrup, Denmark; secondary antibody: Rhodamine Red –X conjugated AffiniPure Goat Anti-Rabbit lgG, Jacksonimmuno, Baltimore, USA). The first antibody anti-GFAP was diluted in 485µl TBS (0.1M) and 10µl Triton (10%). A maximal of 3 slices per microdish were incubated free-floating in this solution over night at 4°C. On day two, the slices were washed again (TBS three times for ten minutes) and stained with the second antibody gt anti-rb RRX (2.5µl) diluted in 485µl TBS (0.1M) and 10ml Triton (10%) for three hours. Finally, the washing procedure was performed a last time and the slices were mounted on a slide (Engelbrecht, Medizin- und Labortechnik GmbH, Edermünde, Germany) and covered with vectashield (Linaris, Dossenheim, Germany). To prepare the slices for scanning, they were covered (Coverslips, Labomedic, Bonn, Germany) and sealed 24 hours after with transparent nail polish. Astrocyte scans were performed with a confocal laser scanning microscope (Leica TCS NT, Leica Microsystems, Wetzlar Germany) and a 63x objective (Leica, 1.20 W Corr CS). The voxelsize was 0.04 (width) x 0.04 (height) x 1.5µm (depth) and the total area of every scanned plane was 39.7 (width) x 39.7µm (height). The number of sections was dependent on the size of the cell.

2.11.1 Analysis of immunhistochemical treated brain slices

Images were displayed and processed with the Leica confocal scanning software (LCS lite, Leica) and Zeissviewer 3.5 (Carl Zeiss AG, Oberkochen, Germany).

3 Results

3.1 Systematic analysis of presynaptic group II mGluR activation by synaptically released glutamate

To systematically analyse presynaptic group II mGluR activation by synaptically released glutamate, medial perforant path fibres in the dentate gyrus of hippocampal rat brain slices were stimulated and the corresponding field potential was measured.
A field potential (fEPSP) is an extracellular correlate to electrogenic processes within cells during potential changes and contains presynaptic (fibre volley) and postsynaptic (pspike) information. The presynaptic component reflects the temporal propagation of action potentials when passing the recording electrode. The postsynaptic component shows the summated response of dentate gyrus granule cells on presynaptic inputs. A positive fEPSP slope reflects a “source” (potential change to positive in the ECS and negative within the cell) and a negative slope a “sink” (positive potential in the cell and negative in the ECS).
If presynaptic inhibitory group II metabotropic glutamate receptors (located at medial perforant path fibres in the DG) get activated during presynaptic stimulation, they depressed further release of glutamate. As a consequence, the postsynaptic component of a measured fEPSP decreased. To investigate group II mGluR activation systematically we applied burst stimulation protocols specific to every mGluR activation limiting factor. Furthermore we assessed the mGluR mediated inhibition on the fEPSP via the antagonist induced abolishment of the fEPSP depression.

3.1.1 mGluR activation by spontaneous, stimulation independent glutamate release

Strikingly, baseline fEPSP recordings with 100µM DL-TBOA showed a decrease in the fEPSP amplitude after application of the substance alone, which could be reversed by applying 3µM of the group II mGluR antagonist LY341495 (Figure 15A). To verify the assumption that a high DL-TBOA concentration causes an accumulation of glutamate, which is probably stimulation independent and leads in turn to an activation of group II

mGluRs, we performed the following tests. We did paired pulse stimulation (stimulus length 0.1ms, inter-stimulus interval 40ms) and monitored the fEPSP response to the first pulse over time. After approximately 20 minutes of stable baseline we made a random decision between the conditions 1) stimulation break 2) stimulation break with 100µM DL-TBOA and 3) 100µM DL-TBOA alone. The obtained data supported the assumption of stimulation independent mGluR activation during strong blockade of glial glutamate uptake (Figure 15B). Tests under condition 2) as well as under condition 3) showed that during sustained 100µM DL-TBOA incubation, the fEPSP amplitude started to decline. Comparisons of averaged fEPSP amplitudes between time point "a" (before substance application and/or stimulation break, normalized to 100%) and time point "b" (after application and/or stimulation break) revealed a 19.9 ± 4.5% (n=5) decrease in fEPSP amplitude for condition 2) and a 16.3 ± 2.8% (n=5) decrease for condition 3) (Figure 15B). Experiments under condition 1) exhibited only normal fluctuations in baseline amplitude -0.1 ± 2.4% (n=5), except for the phase right after the stimulation break. The fEPSP amplitude was increased but declined relatively fast back to initial size. This effect can be explained by a refilling of the vesicle pool during the stimulation break. When stimulation continued, the amount of vesicles released was increased for a short period of time until the pool size restored to the level present during continuous paired pulse stimulation (Figure 15B). All in all the data showed that strong glutamate transporter blockade (100µM DL-TBOA) resulted most likely in an accumulation of spontaneously released glutamate. In order to avoid this effect, we had to lower the DL-TBOA concentration and repeated the experimental condition 3) with 40µM DL-TBOA. The comparison of averaged fEPSP amplitudes before ("a"=100%) and after application ("b") showed that the decline in fEPSP amplitude could be strongly reduced to a negligible degree (6.5 ± 41.7%, n=5, Figure 15C).

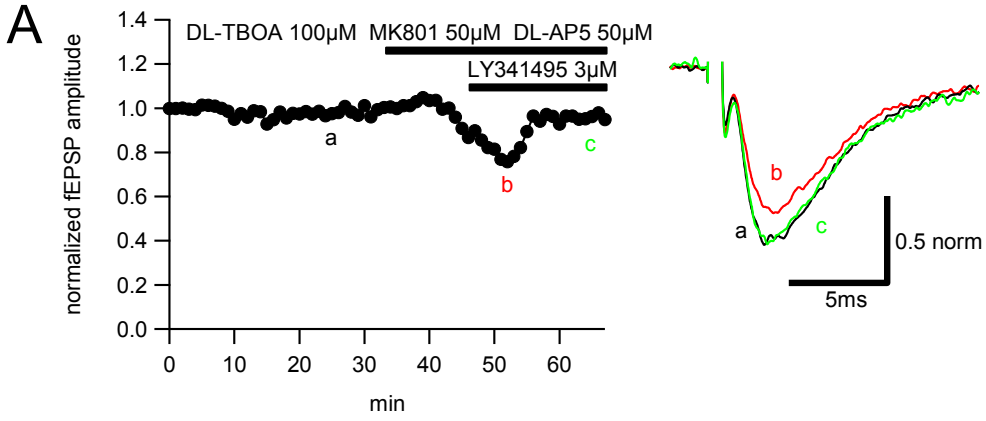

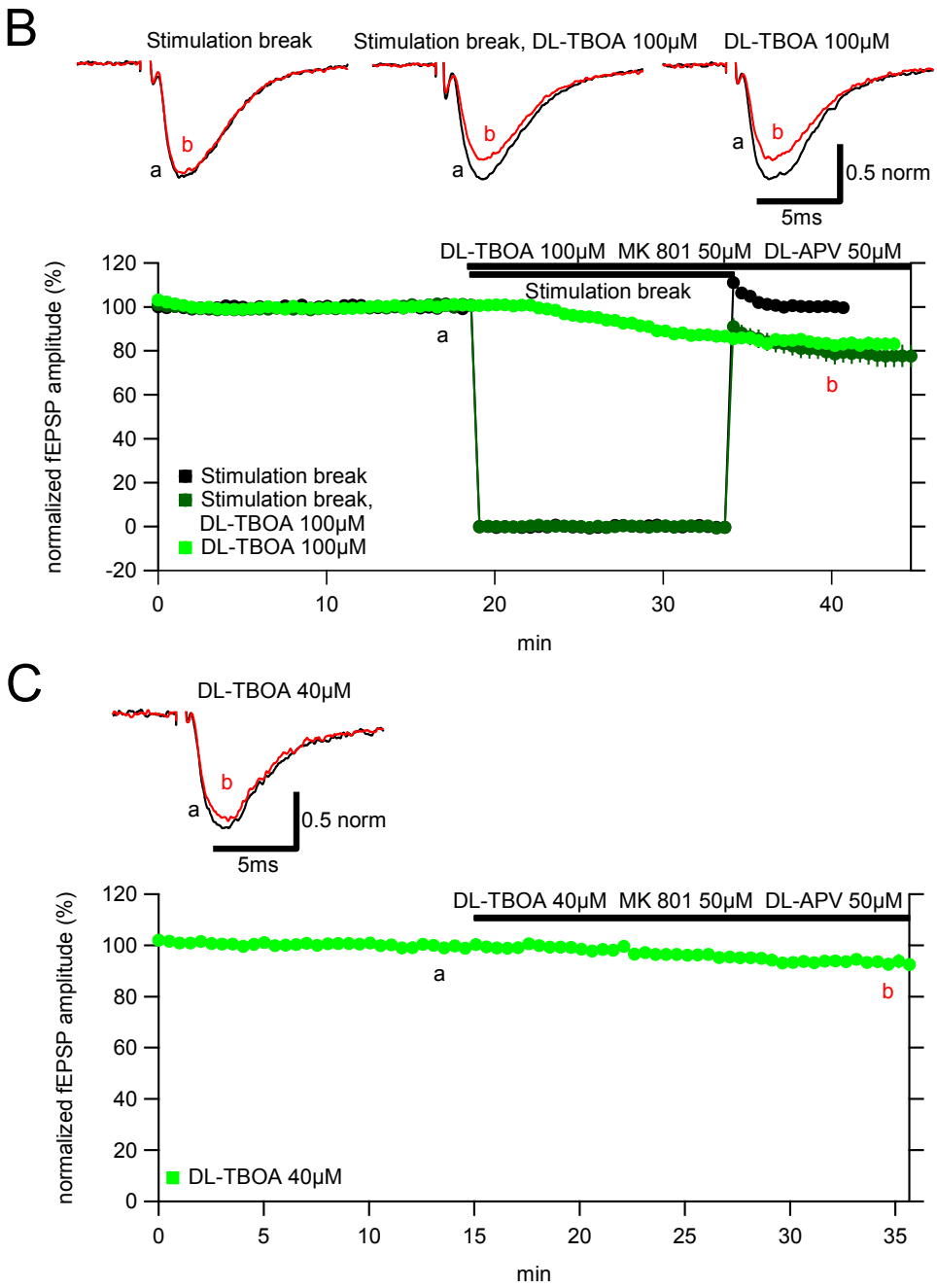

Figure 15. Glutamate transporter blockade with 100µM DL-TBOA leads to accumulation of spontaneously released glutamate. (A) Normalized fEPSP amplitudes of one single experiment recorded in the MML**.** Averaged (n=4) fEPSP responses for three different time points (a, b, c) are magnified. Traces are normalized on the average peak amplitude before drug application (black, scaling: 0.5 norm, 5ms). fEPSP responses declined after 100µM DL-TBOA application and recovered during mGluR blockade with 3µM LY341495. **(B)** Normalized fEPSP amplitudes of three different experimental conditions: stimulation break (black), stimulation break + 100µM DL-TBOA (dark green), continuous stimulation + 100µM DL-TBOA (light green). The upper part of the panel shows a comparison of single averaged fEPSP amplitudes (n=6): shortly before stimulation break (a, black), approximately 10 min after stimulation break respectively at the end of the experiment (b, red) (same scaling as in A). 100µM DL-TBOA caused stimulation independent group II mGluR activation by accumulated, spontaneously released glutamate. **(C)** Normalized fEPSP amplitudes of one experimental condition. Application of 40µM DL-TBOA caused only a negligible decrease in fEPSP amplitude (same scaling as in A and B).

3.1.2 mGluR activation by stimulation induced synaptic release of glutamate

3.1.2.1 Role of glutamate transporters

In every experiment the same burst protocol was applied (7stim at 100Hz). The average percentage inhibition under non-facilitating conditions was weak (5.5 ± 0.9%, n=8), whereas 40µM DL-TBOA strengthened mGluR mediated inhibition of synaptic transmission (12.6 ± 1.3%, n=32). An increase to 100µM DL-TBOA slightly raised the effect (17 ± 2.4%, n=13, Figure 16A, B).

Experiments performed with ACSF (-0.7 ± 1.2%, n=4) and 40µM DL-TBOA alone (-1.3 ± 1.7%, n=4) showed no significant difference in fEPSP response on the test-stimulus indicating that in both stimulation rounds the amplitude of the fEPSP was approximately inhibited to the same extent (Figure 16B).

A comparison between group II mGluR activation with the antagonist DCGIV (1µM) and stimulation induced mGluR activation under application of 100µM DL-TBOA illustrates the enormous discrepancy between a pharmacological and a synaptic mediated mGluR effect on synaptic transmission (Figure 16C). Whereas pharmacological activation leads to an approximately 80% depressed fEPSP amplitude (Figure 16C, left and upper right panel), activity induced mGluR activation causes a more than four times smaller depression of the fEPSP amplitude (Figure 16B, C lower right panel).

To sum up, the results show that mGluR activation increases the more the glutamate uptake by astrocytes is limited and that the depression on the test fEPSP amplitude during burst stimulation is not due to synaptic plasticity.

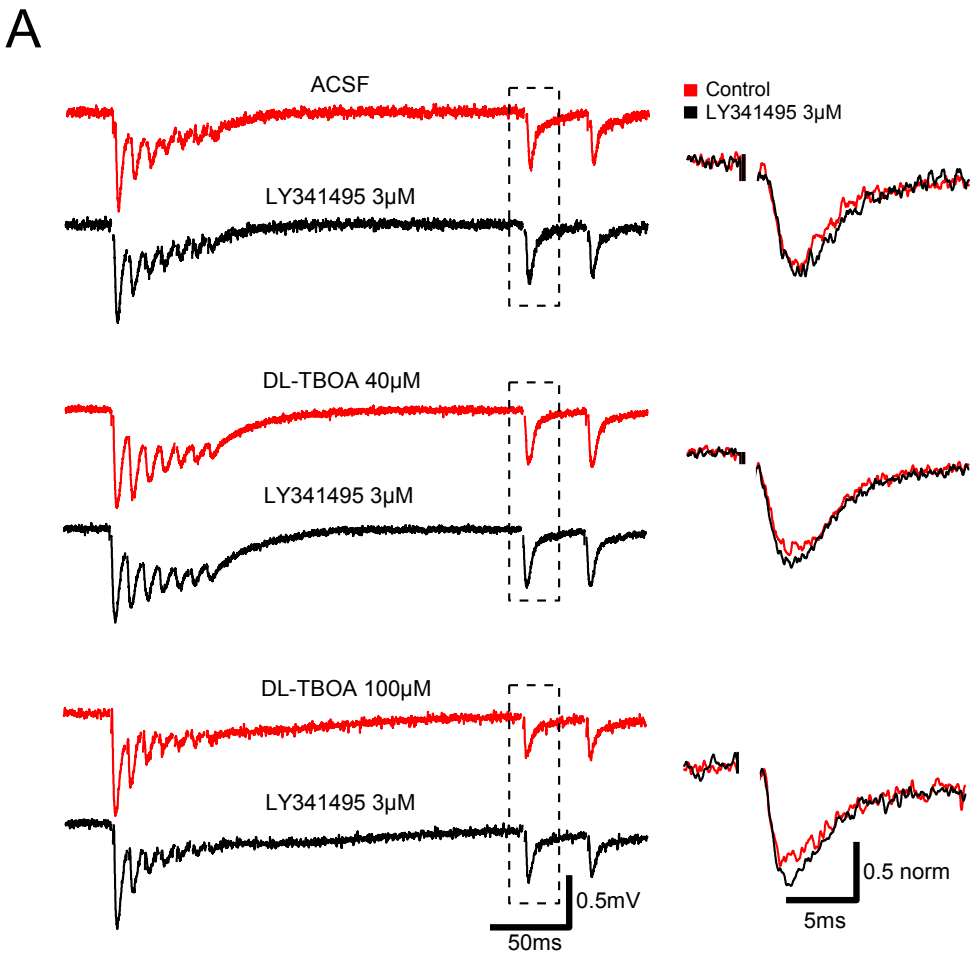
A
ACSF
LY341495 3µM
Control
LY341495 3µM
DL-TBOA 40µM
LY341495 3µM
DL-TBOA 100µM
LY341495 3µM
0.5mV
50ms
0.5 norm
5ms

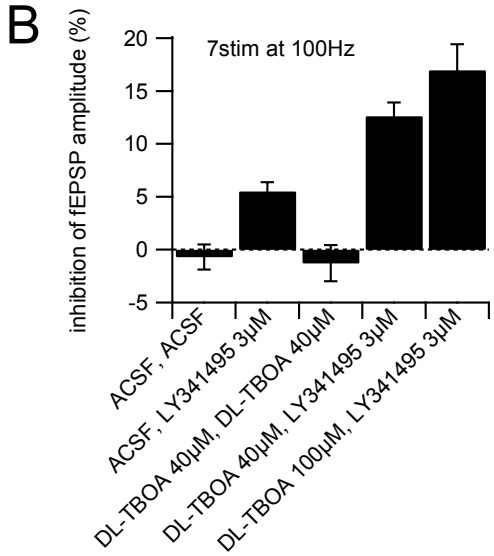
B
7stim at 100Hz
inhibition of fEPSP amplitude (%)
20
15
10
5
0
-5
ACSF, ACSF
ACSF, LY341495 3µM
DL-TBOA 40µM, DL-TBOA 40µM
DL-TBOA 40µM, LY341495 3µM
DL-TBOA 100µM, LY341495 3µM

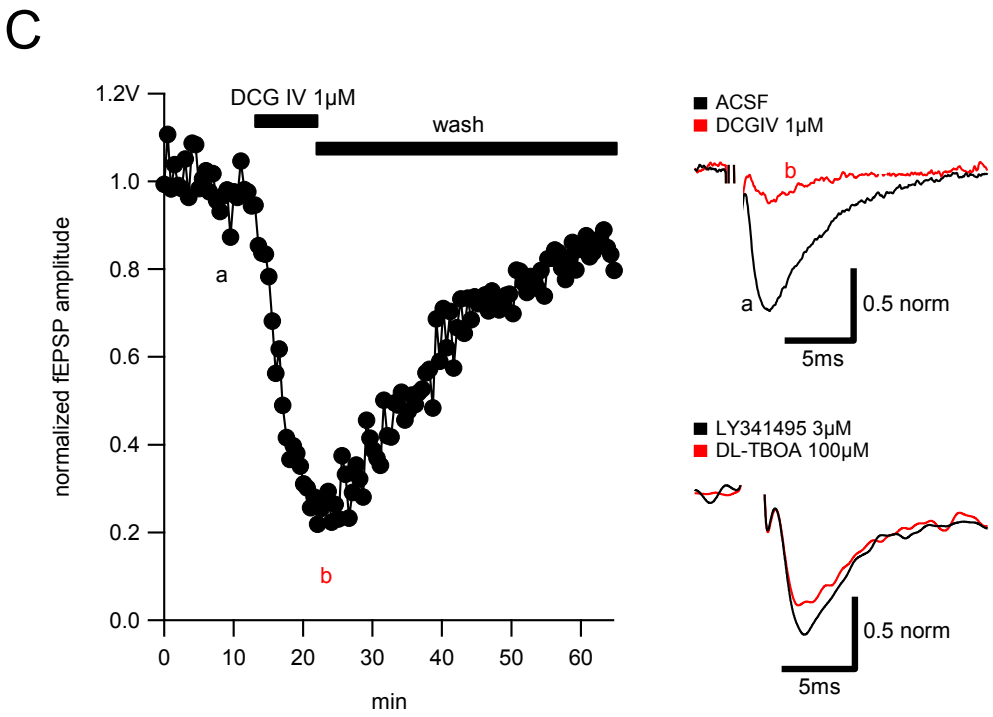

Figure 16. Glutamate transporter blockade by DL-TBOA facilitates mGluR mediated inhibition of synaptic transmission. (A) fEPSPs recorded and stimulated (7stim at 100Hz) in the middle molecular layer (MML) of the dentate gyrus (DG). Example traces are from three single experiments (scaling: 0.5mV, 50ms). In the upper trace of each example mGluRs were activated and in the lower trace blocked by the antagonist LY341495. The magnified illustrations (dashed rectangle) show peak comparisons between fEPSP responses on the first test-stimulus for both conditions. Traces are normalized on the peak amplitude under antagonism (black, scaling: 0.5 norm, 5ms). The more glutamate transporters were blocked by DL-TBOA, the stronger was the mGluR mediated inhibition. **(B)** Summary bar graph showing the percentage of mGluR mediated inhibition of single fEPSPs after burst stimulation under different mGluR activating conditions. The inhibition was low without DL-TBOA and highest with 100µM DL-TBOA. Tests with ACSF or 40µM DL-TBOA alone showed no significant difference in mGluR mediated inhibition between the first and second round of stimulation. **(C)** Single example of pharmacological mGluR activation by 1µM DCGIV. The fEPSP amplitude was strongly depressed to approximately 20% (b, red) of its initial size (a, black) (left graph and peak comparison in upper right panel). In contrast, synaptic activation (7stim at 100Hz, 100µM DL-TBOA) of mGluRs results in a much weaker inhibitory effect (to ~87% of initial size, lower right panel). Example traces are normalized on the peak amplitude before drug application (top) or on the peak amplitude under antagonism (bottom) (scaling: 0.5norm, 5ms).

3.1.2.2 Role of GABA receptors

To define the role of $GABA_A$ and $GABA_B$ receptors in feedback inhibition at medial perforant path synapses, the following experiments were performed.

At first, a burst protocol (28stim at 100Hz) was given in the presence of NMDA receptor blocker DL-AP5 (25µM) and glutamate transporter blocker DL-TBOA (40µM) to prevent plasticity and to facilitate mGluR activation. To assess the degree of fEPSP amplitude depression mediated by group II mGluRs, the stimulation protocol was repeated under group II mGluR blockade with LY341495 (3µM). The resulting inhibition of the fEPSP amplitude was 14 ± 2.2%, (n=13, Figure 17A upper traces).

Next, the experiment was performed as described before, but after stimulating (28stim at 100Hz) under 40µM DL-TBOA and 100µM DL-AP5 application, the slice was additionally incubated with the $GABA_A$ and $GABA_B$ receptor antagonists Bicucullin (10µM) and CGP (2µM) before repeating the stimulation protocol. Then, the group II mGluR blocker was added. The stimulation protocol was applied one last time and the resulting fEPSP amplitude depression measured via the LY341495 mediated increase in fEPSP amplitude. The inhibition with additional GABA receptor blockade was 7.4 ± 2.3% (n=4, Figure 17A lower traces).

Statistical analysis showed no significant difference in fEPSP amplitude depression between both groups ((1) additional $GABA_A$ and $GABA_B$ receptor blockade and (2) DL-TBOA alone, p= 0.097, Figure 17B). To sum up, GABA receptors are not significantly involved in feedback inhibition at medial perforant path fibre terminals.

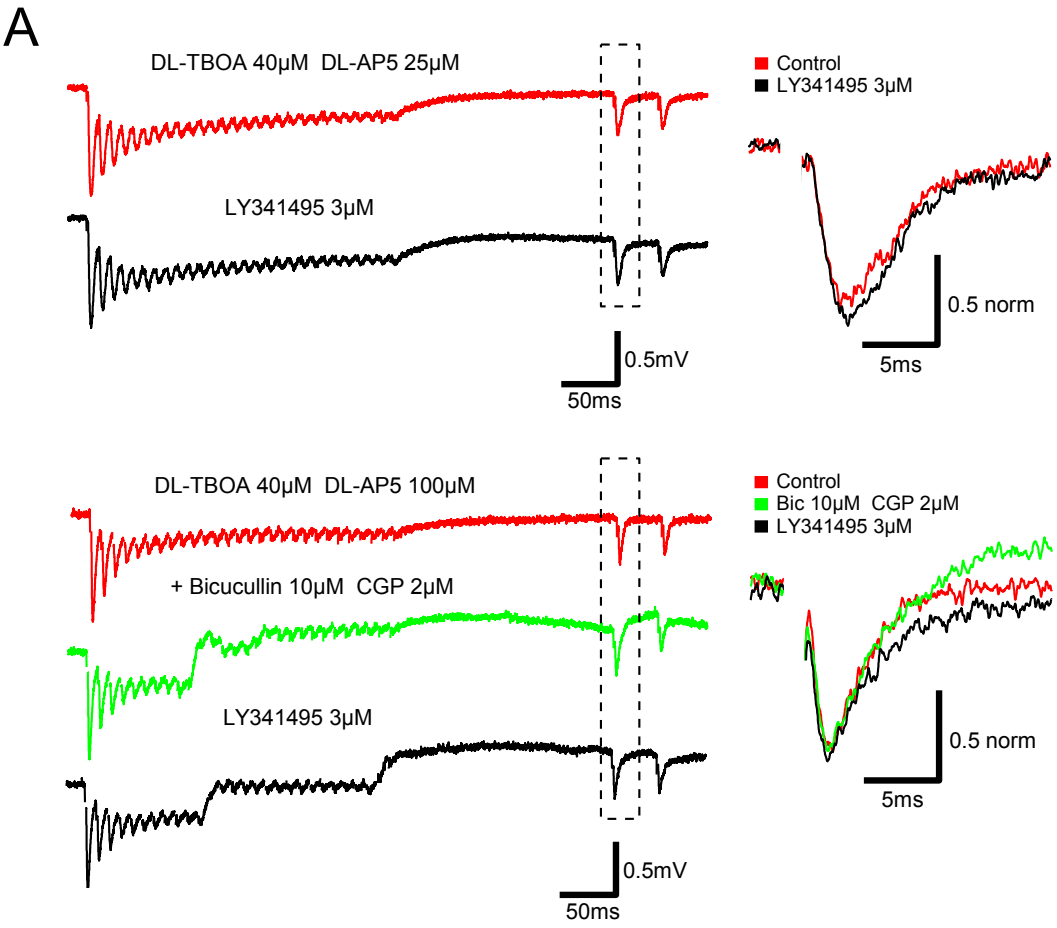
A
DL-TBOA 40µM DL-AP5 25µM
LY341495 3µM
0.5mV
50ms
Control
LY341495 3µM
0.5 norm
5ms
DL-TBOA 40µM DL-AP5 100µM
+ Bicucullin 10µM CGP 2µM
LY341495 3µM
0.5mV
50ms
Control
Bic 10µM CGP 2µM
LY341495 3µM
0.5 norm
5ms

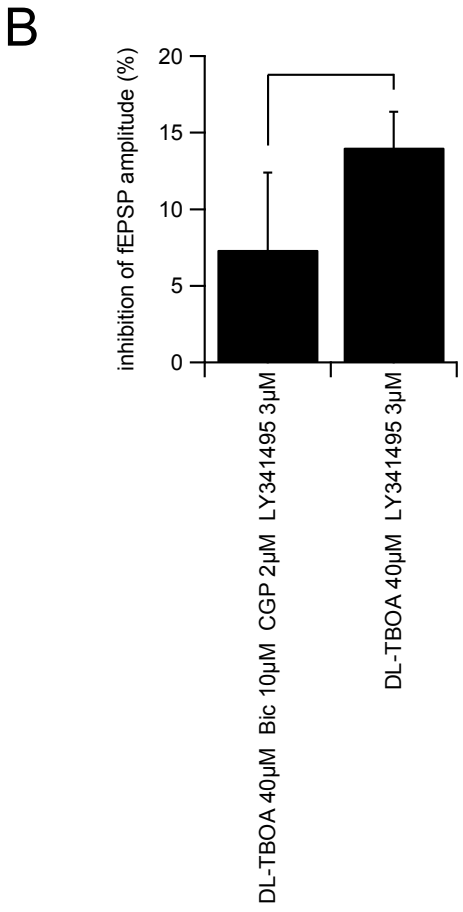
B
inhibition of fEPSP amplitude (%)
20
15
10
5
0
DL-TBOA 40µM Bic 10µM CGP 2µM LY341495 3µM
DL-TBOA 40µM LY341495 3µM

Figure 17. GABA receptors do not significantly contribute to LY341495 induced increase in fEPSP amplitude. (A) fEPSPs recorded and stimulated (28stim at 100Hz) in the MML. Example traces belong to two representative experiments (scaling: 0.5mV, 50ms). Group II mGluR activation is indicated in red, blockade with 3 µM LY341495 in black and in green $GABA_A$ and $GABA_B$ receptors were blocked additionally with 10µM bicucullin and 2µM CGP. On the right side, fEPSP responses on the first test-stimulus (dashed rectangle) are magnified and overlaid in each example experiment. Traces are normalized on the peak amplitude under antagonism (black, scaling: 0.5 norm, 5ms). The GABA receptor blockade did not attenuate the inhibition of synaptic transmission, indicating that the effect is predominantly mGluR mediated. **(B)** Summarized plot of the percentage mGluR of mediated inhibition on fEPSPs with and without GABA receptor blockade. The inhibition does not significantly differ between both groups (t-test, p= 0.097).

3.1.3 mGluR activation depending on stimulation frequency

To find out at which firing frequency of presynaptic perforant path neurons mGluR activation reached its maximum, stimulation protocols with varying stimulation frequency within a conditioning burst (5, 10, 20, 50, 100, 200Hz, Figure 18A, B) were designed. The length of the conditioning burst was 459 ± 26ms (n=5) and the time interval between conditioning burst and test-stimulus 200ms. mGluR activation was assessed as described in section 2.4.5.

Stimulation with 3stim at 5Hz led to a slight mGluR mediated inhibition (4.3 ± 2.9%, n=5, Figure 18A, B) which more than doubled in strength after stimulation with 5stim at 10Hz (10.2 ± 2.7%, n=3, Figure 18A, B). Applying the stimulation protocol 7stim or 10stim at 20Hz slightly increased the effect to 11.5 ± 2.0% (data sets of 7 and 10stim at 20Hz are averaged, n=7, Figure 18B). With the stimulation paradigms 25stim at 50Hz and 50stim, respectively 56stim at 100Hz the inhibition further increased to 16.6 ± 3.9% (n=3, Figure 18B) and 18.5 ± 4.3% (data sets of 50 and 56stim at 20Hz are averaged, n=11, Figure 18A, B) and reached a maximum with the 100stim at 200Hz (22.7 ± 3.3, n=10, Figure 18A, B).

To sum up, the data show that group II mGluR activation is strongly linked to the firing frequency of the presynaptic neurons.

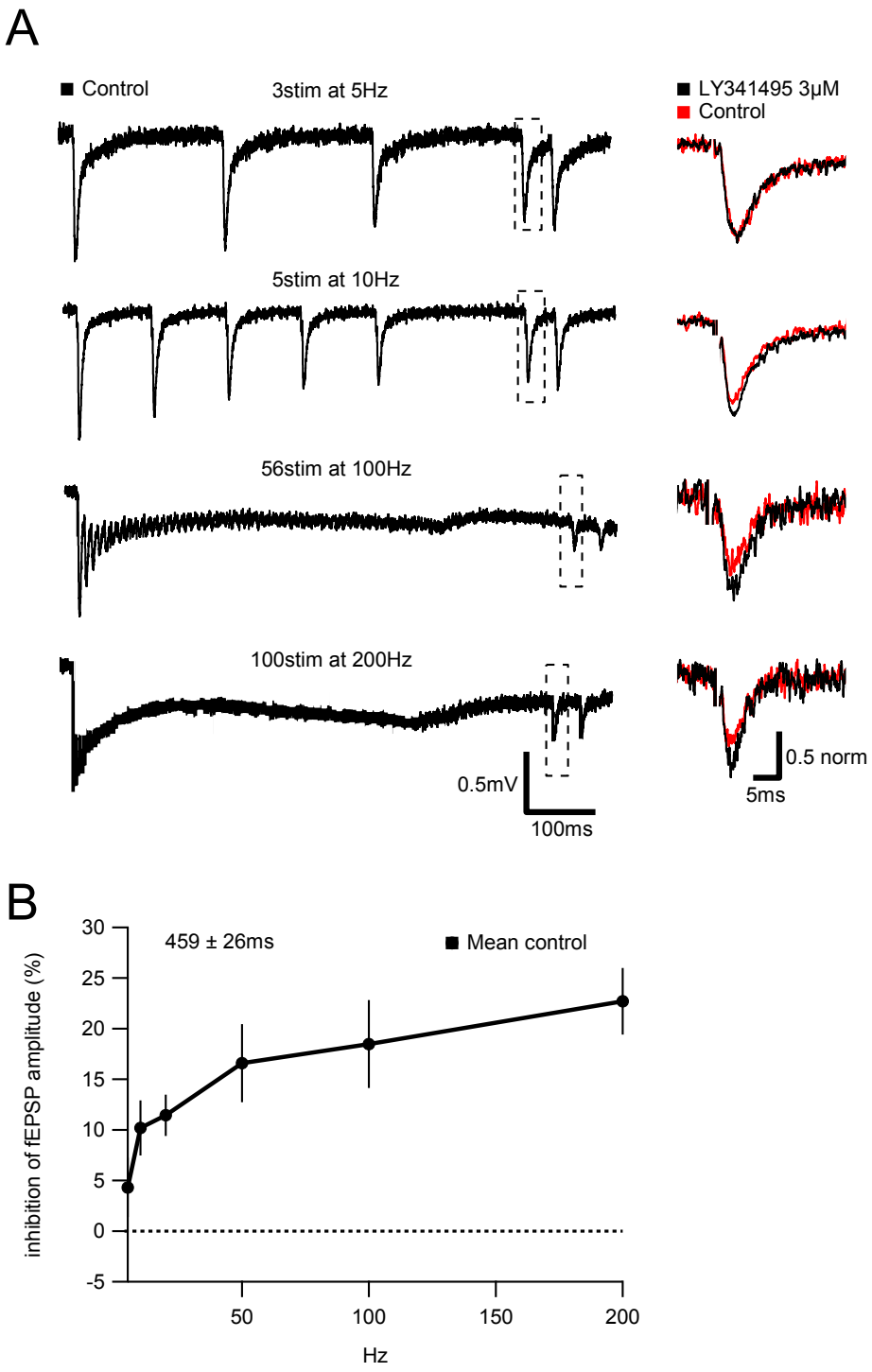

Figure 18. Group II mGluR activation increases with firing frequency of presynaptic neurons. (A) Representative fEPSP traces recorded in the MML with four different stimulation paradigms (frequency variation in a fixed time window of 459 ± 26ms, scaling: 0.5mV, 100ms). Highlighted are fEPSP responses on the first test-stimulus under group II mGluR activation (red) and blockade (black). Traces are normalized on the peak amplitude under antagonism (black, scaling: 0.5 norm, 5ms). The group II mGluR mediated inhibition increased with frequency. **(B)** Summarized percentage inhibition of the fEPSP amplitude mediated by group II mGluRs plotted against stimulation frequency. The inhibition reached a maximum at 100stim at 200Hz.

3.1.4 mGluR activation dependence on duration of stimulation

To unravel the meaning of the duration of medial perforant path fibre stimulation for group II mGluR activation, the following experiments were performed. The frequency of the applied conditioning burst was kept constant but the number of stimuli varied (1, 3, 7, 14, 25, 28, 50, 56, 100, 200 at 100Hz, 0.2sec PBI, Figure 19A, B). The stimulation protocol was applied under mGluR activating conditions (40µM DL-TBOA) and mGluR blocking conditions (3µM LY341495) (time in between: 10min). For each protocol cycle, ratios were calculated between the response on the test-stimulus and the first peak fEPSP response of the conditioning burst. The first ratio was divided by the second ratio to determine the degree of mGluR mediated inhibition. In order to check whether burst stimulation induced long term depression at some point, the stimulation protocol was applied exclusively with ACSF (Figure 19B, grey trace).

As expected, the stimulation protocol 1stim, 200ms post burst interval (PBI) was not sufficient to initiate mGluR activation (-0.3 ± 2.3%, n=7). Increasing the number of stimuli to 3 raised the mGluR mediated inhibition to 6.3 ± 3.3% (n=11, Figure 19B) and only a few stimuli more caused already a clearly detectable mGluR effect (14.1 ± 1.0%, n=29, 7stim at 100Hz, Figure 19A, B). Prolonging the burst to 14 stimuli caused a slight drop in the inhibition (11.5 ± 1.1%, n=12, Figure 19B) which was abolished again by giving the burst protocol 25stim or 28stim at 100Hz (14.0 ± 2.2%, data sets of 25 and 28stim at 100Hz are averaged, n=13, Figure 19B). Application of 50stim or 56stim at 100Hz led to an additional increase to 18.5 ± 4.3% (data sets of 50 and 56stim at 100Hz are averaged, n=11, Figure 19A, B) and the maximum activation was finally reached with 100stim at 100Hz (29.7 ± 5.8, n=9, Figure 19A, B). Prolonging the stimulation protocol to 200stim at 100Hz did not further raise the inhibition mediated by group II mGluRs (26.3 ± 4.2%, n=9, Figure 19B). Depending on the duration of stimulation the mGluR mediated inhibition on synaptic transmission increased with a time constant tau of 370 ± 190ms.

Experiments with ACSF alone were performed for three stimulation paradigms (50, 100 and 200stim at 100Hz) to test whether burst stimulation causes inhibition on synaptic transmission which is independent from group II mGluR activation. Stimulation with 50stim at 100Hz and 100stim at 100Hz under these conditions revealed no further increase in inhibition of the fEPSP amplitude when applying the stimulation protocol a second time (-2.2 ± 6.3%, n=6 and -6.0 ± 5.3%, n=6). However, giving the protocol

200stim at 100Hz resulted in a stronger inhibition 21.8 ± 8.4% (n=6) after the second application. This indicated that activity dependent plasticity effects occurred, which was most probably an AMPA receptor desensitization during this high frequent train of activity (Figure 19B).

To sum up, the data show that group II mGluR activation is strongly dependent on the number of stimuli and increases with sustained stimulation as long as vesicle supply is assured and no further plasticity initiated.

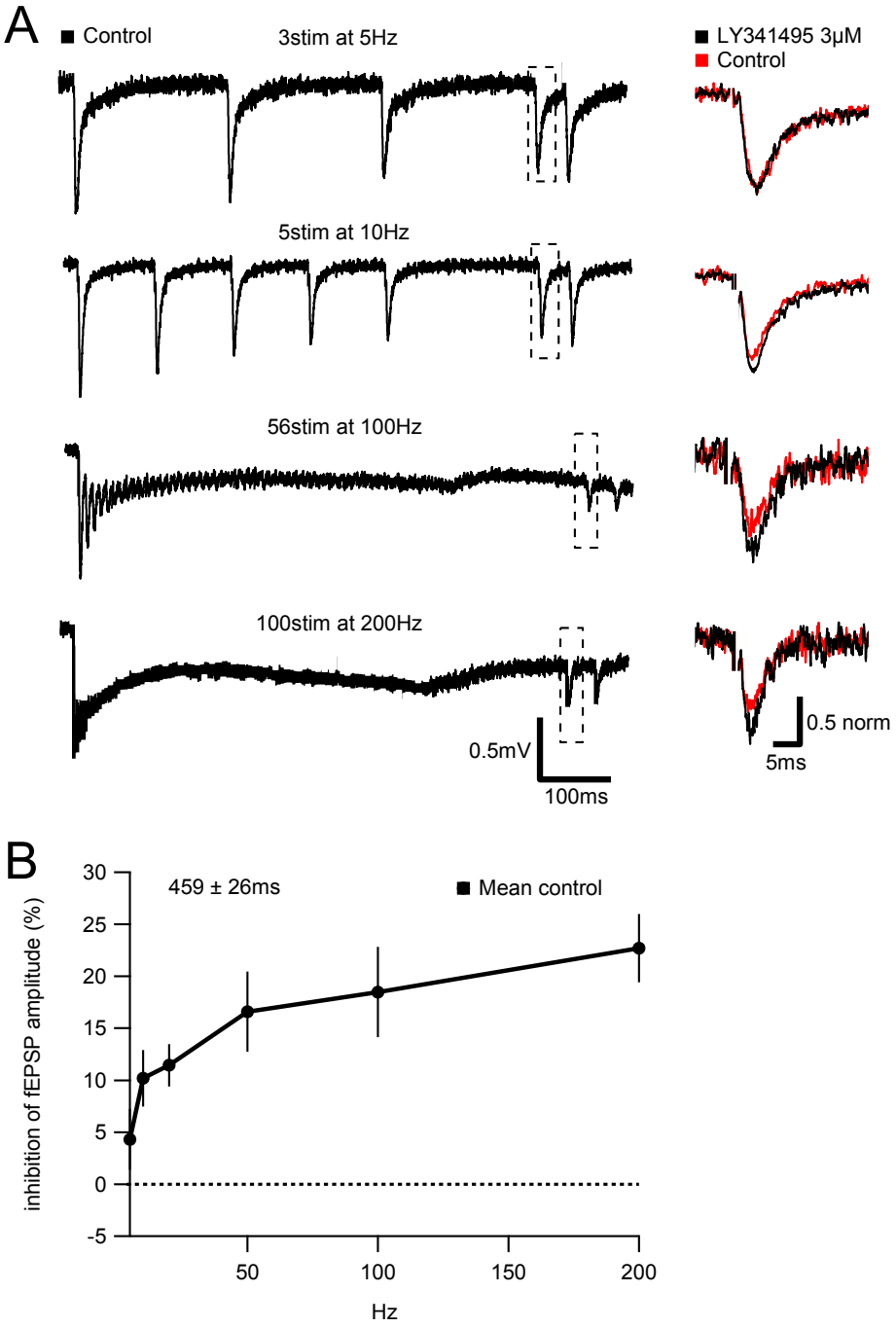

Figure 19. Prolonged presynaptic fibre activity strengthens group II mGluR activation. **(A)** Shown are four examples of fEPSP traces recorded in the MML (scaling: 0.5mV, 100ms). The stimulation frequency was kept constant and the number of stimuli varied. In each case the response on the first test-stimulus is enlarged. Compared are the fEPSP amplitudes under blockade of group II mGluRs (3µM LY341495, black) and facilitated mGluR activation (40µM DL-TBOA, red). Traces are normalized on the peak amplitude under antagonism (black, scaling: 0.5 norm, 5ms). **(B)** Summary plot of percentage inhibition mediated by group II mGluRs as a function of stimuli number (left side). mGluR activation raised with increasing number of stimuli and reached a plateau at 100stim at 100Hz (black). Test with ACSF alone did not show an inhibitory effect until a certain number of stimuli was reached (grey). On the right side, the mGluR mediated inhibition of fEPSP amplitude is plotted versus duration of stimulation (black). The curve fit (red) revealed a time constant tau of 370 ± 190ms.

3.1.5 Time course of mGluR mediated feedback inhibition of synaptic transmission

Next, it was important to look at the time course of group II mGluR activity and to answer the following questions: how long does it take to see a maximal mGluR effect and how long does it last? In order to describe it, mGluR activation was tested at different post burst intervals (PBI: 0.03, 0.05, 0.1, 0.2, 0.3, 0.5, 0.8, 1, 3, 6, 20s, Figure 20A, B).

At 0.03s PBI the mGluR mediated inhibitory effect on synaptic transmission was 2.4 ± 5.4% (n=4) and raised up to 7.4 ± 4.3% (n=6) at 0.05s PBI. The inhibition further increased after 0.1s PBI (9.9 ± 2.2%, n=9) and reached its maximum at 0.2s PBI (12.8 ± 1.2%, n=34). Prolonging the post burst interval further reversed the effect and the mGluR mediated inhibition on synaptic transmission started to decline (0.3s PBI, 10.5 ± 3.3%, n=8). After 0.5s PBI 8.9 ± 1.6% (n=6) of the inhibitory effect was present and it was even detectable after 0.8s PBI (8.2 ± 1.2%, n=7). At 1s PBI the degree of inhibition dropped to 4.0 ± 1.4% (n=14) and reached after 3s a value of 2.4 ± 1.6% (n=12). After 6s PBI the inhibitory effect on synaptic transmission did not significantly decrease anymore (2.0 ± 0.8%, n=17) and the last tested PBI (20s) revealed a residual inhibition of (0.0 ± 0.9%, n=8).

For two different PBIs, experiments were performed with ACSF alone to check whether there was no difference in the degree of mGluR mediated inhibition between responses on test stimuli after applying the burst protocol a first and a second time (Figure 20B). This was true for 0.2s PBI (-0.7 ± 01.2%, n=4) as well as for 20s PBI (1.9 ± 1.0%, n=5). Fitting the time course of mGluR mediated inhibition revealed faster mGluR activation kinetics (tau= 40 ± 20ms) and slower deactivation kinetics (tau= 840 ± 230ms).

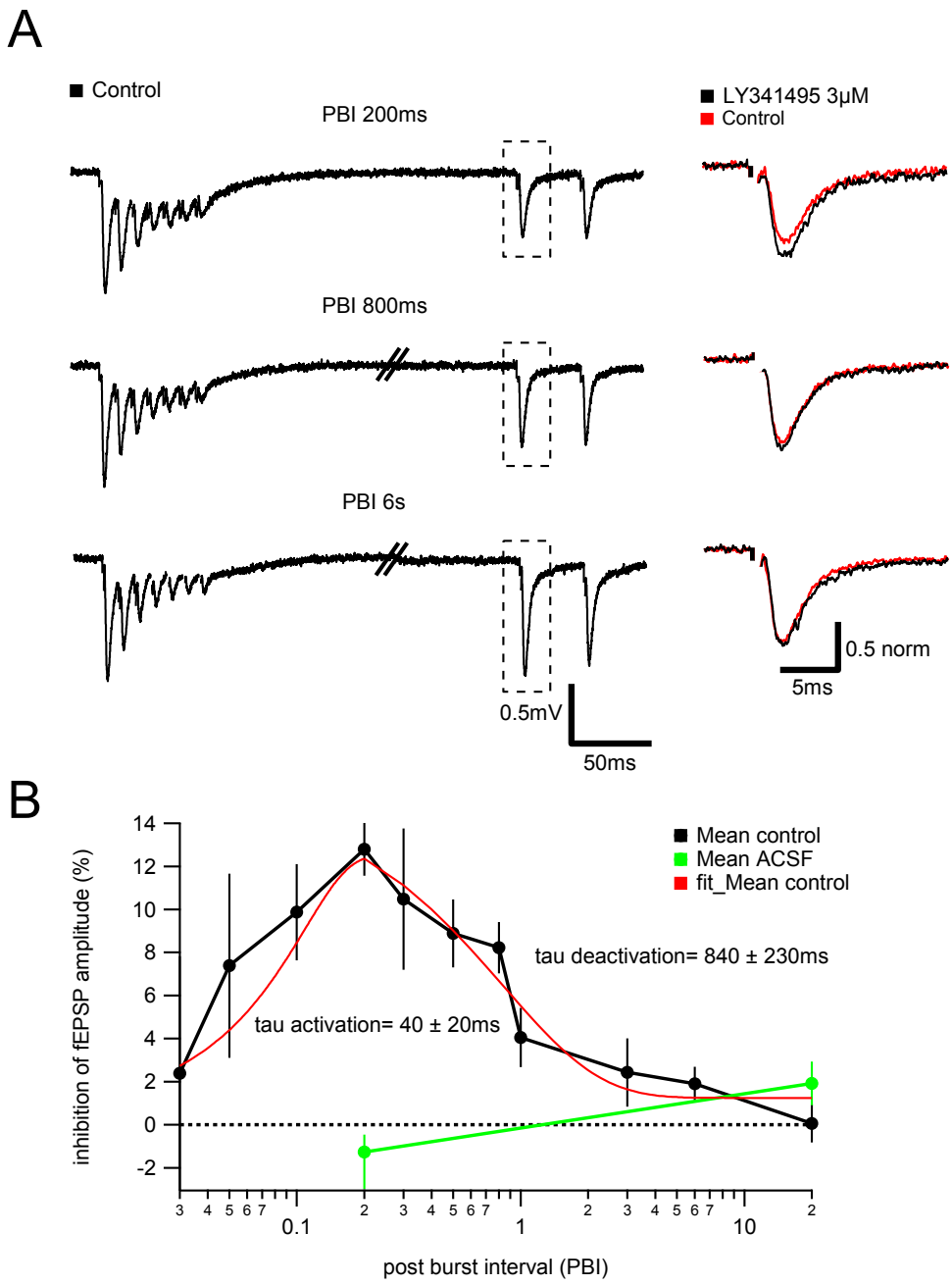

Figure 20. Group II mGluRs activate within 200ms and remain active for at least 800ms. **(A)** Illustrated are three fEPSP example traces recorded and stimulated (7stim at 100Hz) in the MML (scaling: 0.5mV, 50ms). The post burst interval (PBI) increases from top to bottom. The fEPSP response on the first test-stimulus under mGluR activation (red) and blockade (black) is magnified (right panel).). Traces are normalized on the peak amplitude under antagonism (black, scaling: 0.5 norm, 5ms). **(B)** Average plot of percentage inhibition on synaptic transmission mediated by group II mGluRs depending on PBI (black) with a curve fit displayed in red. The inhibition reached its maximum after 200ms PBI (tau activation= 40ms ± 20ms) and was still detectable after 800ms (tau deactivation= 840 ± 230ms). Experiments with ACSF alone showed no mGluR mediated inhibition (green).

3.1.6 Influence of repetitive burst stimulation on mGluR activation

The maximum mGluR mediated inhibition on synaptic transmission was reached during receptor activation by synaptically released glutamate after applying the conditioning burst protocol 100stim at 100Hz (29.7 ± 5.8%, n=9, Figure 19A, B) under mGluR activation facilitating conditions (40µM DL-TBOA). This degree of inhibition was still far away from the strength of depression induced by pharmacological mGluR activation (≥ 80%, Figure 16C).

We assumed that group II mGluRs started to deactivate before they fully activated. If the vesicle pool depleted during continuous burst stimulation, less glutamate was released. Potentially, a smaller amount of transmitter had a chance to overcome the homeostasis between release and removal to keep mGluRs activated or to further increase the degree of receptor activation, respectively.

To allow vesicle pool refilling, we started using a stimulation protocol composed of repetitive bursts with different inter burst intervals (IBI, 0.05s, 0.3s, 0.5s) and varying number of stimuli (2, 3, 7) and frequency (50Hz, 100Hz) within the burst. In every experiment the repetitive burst stimulation protocol was applied two times, under A) mGluR activating (DL-TBOA 40µM) and B) under mGluR blocking (LY341495 3µM) conditions.

For the analysis of each given protocol, the peak amplitude of the first fEPSP response to each burst and to the first test-stimulus subsequent to bursting was determined. Then, ratios were calculated by comparing these amplitudes with the response on the first stimulus in the very first burst. The ratios for condition A) were divided by the corresponding ratios for condition B) to calculate the degree of group II mGluR mediated inhibition on the fEPSP amplitudes.

In order to test whether group II mGluR activation increases with repetitive burst stimulation, we started with the protocol 4x7stim at 100Hz (0.5sec IBI, 0.2s PBI, Figure 21A). However, instead of increasing, the mGluR mediated inhibition declined after the second burst and reached only a maximum of 14.6 ± 2.7% (n=6, see asterisk in example one Figure 21A). Perhaps, the IBI was too long for cumulative mGluR activation and the receptors already reached a deactivated state between the bursts.

Next, we shortened the inter burst interval and adjusted the number of stimuli within a burst in order to optimize vesicle release and refilling during repetitive bursting. Moreover, the number of repetitions was increased (10x2stim at 100Hz, 0.05sec IBI,

0.2sec PBI, Figure 21A). This time the mGluR mediated inhibition raised while bursting but the maximum gained inhibitory effect was smaller than before (6.4 ± 5.0%, n=4, see asterisk in example two Figure 21A). We assumed, that the inter burst interval was perhaps too small as well as the stimulation frequency within a burst, still causing a strong depletion of the vesicle pool.

As a consequence, we lowered the frequency and increased the IBI again. To complete the design of the stimulation protocol, I added one more stimulus to a burst and increased the total number of bursts (15x3stim at 50Hz, 0.3sec IBI, Figure 21A). However, despite the changes, even this repetitive burst protocol did not generate any increase in mGluR mediated inhibition (14.6 ± 3.3%, n=4, see asterisk in example three Figure 21A).

To sum up, no cumulative effect on mGluR activation by repetitive burst stimulation could be shown.

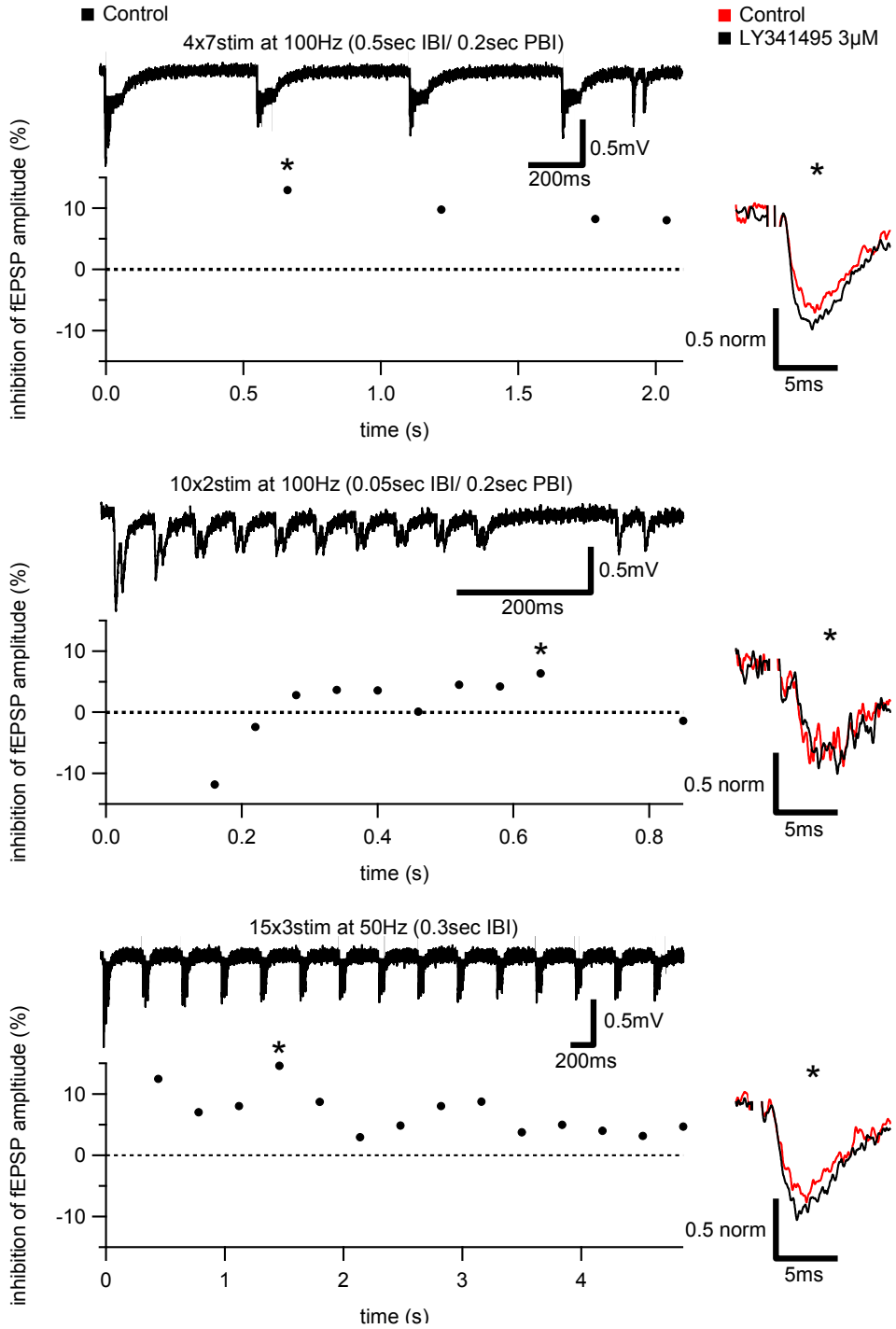

Figure 21. Repetitive burst stimulation does not potentiate mGluR mediated feedback inhibition. Example fEPSP traces from three different repetitive burst stimulation experiments in the MML associated with the percentage mGluR mediated inhibition on the first fEPSP response of every burst in the stimulation protocol (scaling: 0.5mV, 200ms). The maximum inhibited fEPSP amplitude is marked by an asterisk. Highlighted is the maximum inhibited field potential response (red) compared with the response on the very first stimulus (black). Traces are normalized on the peak amplitude under antagonism (black, scaling: 0.5 norm, 5ms). None of the tested stimulation protocols caused a summation of the group II mGluR mediated inhibitory effect that significantly differs in strength from values obtained in single burst experiments.

3.2 Presynaptic Ca^{2+} imaging as a tool to directly assess presynaptic inhibition

At this point, the most interesting findings on group II mGluRs were that the receptor mediated inhibitory effect on synaptic transmission developed with a time-constant tau between 40 ± 20ms (Figure 20B) and 370 ± 190ms (Figure 19B), disappeared slower with a time constant of 840 ± 230ms (Figure 20B) and reached a lower maximum (29.7 ± 5.8%, n=9, Figure 19A, B) compared to pharmacological conditions (~80%, Figure 16C), even under glutamate transporter blockade (40µM DL-TBOA).

We decided to investigate the kinetics of group II mGluR mediated inhibitory action on synaptic transmission in more detail in order to find out at which time point 1) the group II mGluR activation causes first inhibitory effects (latency) 2) synaptic transmission is maximally depressed by mGluR activity and 3) the mGlu receptor deactivation ends and the strength of synaptic transmission is back at initial level before mGluR action.

The presynaptic Ca^{2+} signal was the best readout for this purpose because mGluR activation causes a signal cascade that leads to an inhibition of presynaptic N- or P/Q-type voltage-gated Ca^{2+}channels (Chavis et al., 1994, McCool et al., 1996, Takahashi et al., 1996, Robbe et al., 2002), which is in turn directly coupled to the neurotransmitter release machinery (Spafford and Zamponi, 2003), meaning that the depression of the presynaptic Ca^{2+} signal reflected a nearly simultaneous depression of glutamate release.

3.2.1 Loading of MPP fibres with an AM ester Ca^{2+} indicator dye

As described in section 2.5.2, I selectively loaded medial perforant path fibres with an acetoxy-methyl (AM) ester form of a membrane-permeable fluorescent Ca^{2+} indicator (either Magnesium Green AM or Oregon Green Bapta-1 AM) via positive pressure injection (Figure 22A, top) and waited 20 to 40 minutes until the fibre tract was sufficiently loaded. The fluorescence F was detected by illuminating the slice with 470nm light. After 20 minutes of heating the bath up to 35°C to measure at physiological temperature (in the meantime the fluorescence F further intensified and stabilized at the end) the stimulation pipette was placed distal to the injection site and the pinhole (defines the region of interest (ROI)) distal to the tip of the stimulation

pipette (Figure 22A, middle). During stimulation of the MPP the fluorescence increased by ΔF (Figure 22A, bottom).

First of all, I had to check, whether the Ca^{2+} signal monitored in the MML was of presynaptic origin. Therefore I performed calcium imaging experiments during wash-in of the AMPA receptor blocker CNQX (30µM). Postsynaptic AMPA receptors predominantly mediate fast synaptic transmission which is also Ca^{2+} dependent. If the Ca^{2+} signal contained a postsynaptic component, the ΔF peak amplitude would have become smaller in the presence of CNQX. In the first ten minutes after application there was no change in amplitude detectable compared to the Ca^{2+} signal under ACSF alone (ACSF: 1.4 ± 0.1%, n_{points}=6, CNQX: 1.4 ± 0.0%, n_{points}=6; Figure 22B, black and grey trace). The slight decrease was due to a continuous run-down of the signal during the experiments (see comparison between the black and grey trace, Figure 22B, left panel and Ca^{2+} peak comparison between "a" (black) and "b" (red), Figure 22B, right panel). When the sodium channel blocker TTX (1µM) was added, action potential generation during presynaptic stimulation was prevented and the calcium signal started to disappear, and it was finally gone after a few minutes (0.0 ± 0.1%, n_{points}=6, Figure 22B, green trace). This additionally supports the previous result, meaning that a Ca^{2+} signal detected was mostly presynaptic in origin. However, a certain fraction of postsynaptic involvement can never be excluded completely.

To sum up, our experiments provided evidence that specifically the medial perforant path fibre tract with its presynaptic terminals was loaded and not its postsynaptic counterparts (dendritic spines of granule cells).

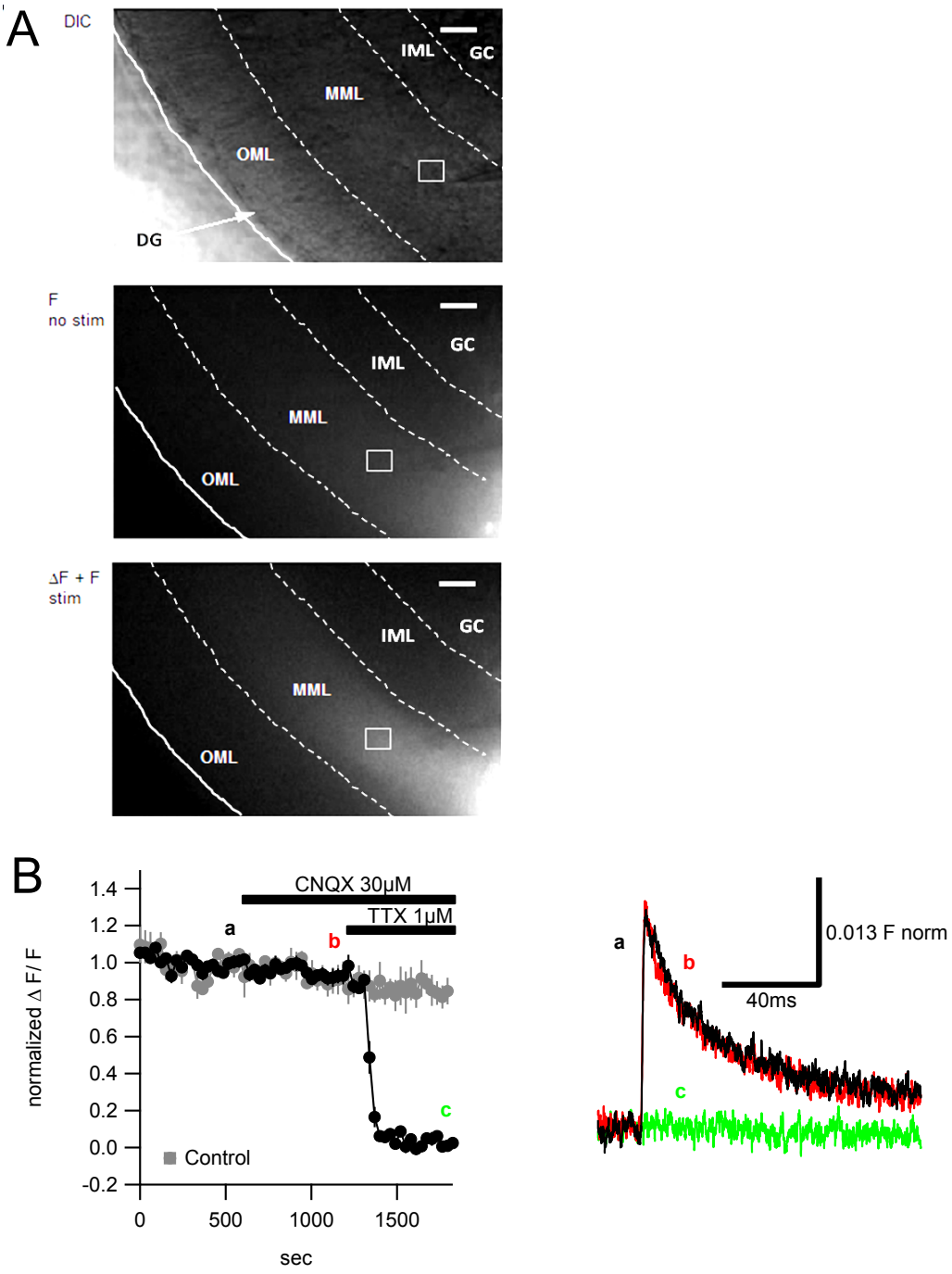

Figure 22. The Ca^{2+} signal is of presynaptic origin. (A) Section of the hippocampal dentate gyrus (top) shown in the differential interference contrast (DIC) mode. The border between granule cell, inner-, middle- and outer molecular layer is indicated by a dashed line. The border of the dentate gyrus is marked by a continous line. Medial perforant path fibres are loaded with a fluorescent calcium indicator (here: Oregon Green 488 BAPTA-1 AM, middle). Illuminating the slice with 470 (bandwidth ±30nm) light results in fluorescence F. Stimulation of the MPP fibre tract leads to a calcium influx causing a fluorescence increase by ΔF (bottom) (scaling: 30µm). Changes in fluorescence were detected within a defined region (square) of the MPP fibre tract. **(B)** The inset shows a normalized, averaged calcium signal over time. Whereas the calcium signal amplitude was unaffected by CNQX (30µM), the application of TTX (1µM) caused a tremendous decrease. Illustrated on the right side is an overlay of calcium signal averages from three different time points (a, b, c; n= 6, scaling: 0.013 F norm, 40ms).

3.2.2 Pharmacological group II mGluR activation depresses the Ca^{2+} signal amplitude

Next, it was important to test if presynaptic group II mGluR activation really affects the presynaptic Ca^{2+} signal. Again, I recorded Ca^{2+} signals induced by MPP stimulation and used the low affinity Ca^{2+} indicator Magnesium green AM.

After 10 minutes of baseline recoding in the presence of CNQX (30µM) and DL-AP5 (30µM), I added the selective group II mGluR orthosteric agonist DCGIV (1µM), which binds on the active site of the receptor. As a result, the presynaptic Ca^{2+} signal decreased to 63.4 ± 5.0% ("b", average of n_{points}=4) compared to the amplitude ("a", average of n_{points}=4) before application of DCGIV (Figure 23A).

In contrast, the group II mGluR antagonist LY341495 abolished the effect of DCGIV and the Ca^{2+} signal recovered back to baseline (Figure 23A). Slight deviations from the initial size are due to a run-down during the experiments.

In summary, the tests showed that pharmacological group II mGluR activation negatively affected the size of the presynaptic Ca^{2+} signal.

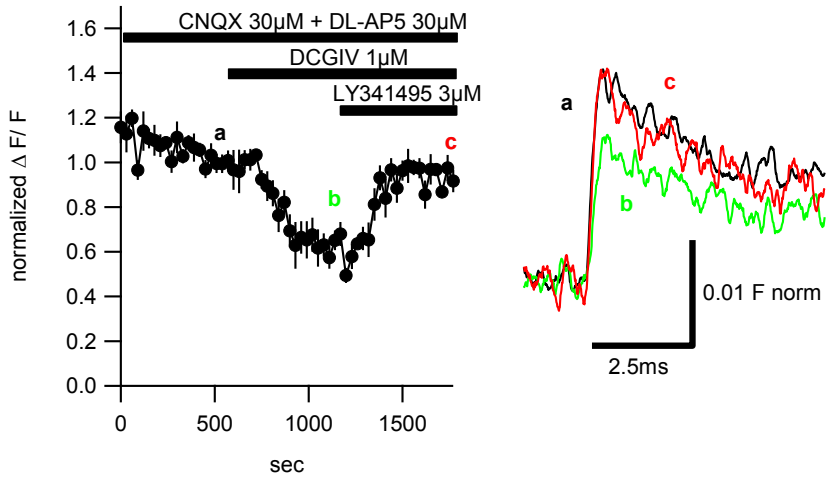

Figure 23. Activation of group II mGluRs by DCGIV causes a decrease in calcium signal amplitude. Shown is the temporal change of normalized, averaged calcium signal amplitudes depending on group II mGluR activation (DCGIV 1µM) respectively blockade (LY341495 3µM). MPP fibres were loaded with the low affinity calcium indicator Magnesium Green AM. Pharmacological activation by DCGIV almost caused a bisection of the calcium signal size which could be completely reversed by LY341495 mediated antagonism. The right side of the inset shows averaged Ca^{2+} signals (n= 6) of three different time points (a, b, c, scaling: 0.01 F norm, 2.5ms).

3.2.3 Influence of glutamate uncaging induced mGluR activation on Ca^{2+} signal amplitude

So far, the experiments affirmed that the presynaptic Ca^{2+} readout seemed to be an appropriate way to assess the activation and deactivation kinetics of the presynaptic inhibitory feedback process. The last step to clarify was, whether exposing the metabotropic glutamate receptors to the endogenous ligand glutamate causes activation as well.

We decided to perform glutamate uncaging instead of synaptic stimulation because the essential advantage of this technique is a direct and constant exposure of the freed ligand to the receptor. In contrast, synaptically released glutamate can underlie plasticity and varies in concentration. However, before we finally used this method, we had to find out whether uncaged glutamate effectively activated presynaptic group II mGluRs and caused a depression of the presynaptic Ca^{2+} signal of assessable size.

In principle, the experimental procedure could be described as follows (see also section 2.10). First, a calcium indicator loaded MPP fibre tract was stimulated with a pre-stimulus, followed by UV laser uncaging and a test-stimulus (inter stimulus interval (ISI) ~ 1s) and the corresponding Ca^{2+} signal response on the pre- and test-stimulus was monitored (Pinhole, Figure 24A). A pre-stimulus was applied to get a reference Ca^{2+} signal reflecting the unaffected state before mGluR activation. The Ca^{2+} response on the test-stimulus after uncaging of glutamate displayed the state after mGluR activation. If group II mGluRs activated, the response on the test-stimulus should have been depressed. However, a part of the depression might not only be due to mGluR activation but also arising from plasticity at the synapses. Therefore, in the second part of the protocol, only a pre- and test-stimulus were applied (Figure 24A) and ratios were calculated between the peak amplitude on the test-stimulus and pre-stimulus for the first as well as the second part of the protocol. Then the ratio for the first part (with uncaging) was divided by the ratio for the second part (without uncaging) to extract the quotient of inhibition of the calcium transient.

To provide evidence, that the inhibition is due to group II mGluR activation, the previous experimental series was also performed under wash-in of group II mGluR antagonist LY341495 (3μM).

The data showed that mGluR activation via uncaging caused an integral depression of the calcium signal by 11.5 ± 0.0% (n=4) Figure 24B), however less pronounced as

under pharmacological activation (36.6 ± 5.0%, average of n_{points}=4, Figure 23A, "b" left panel).

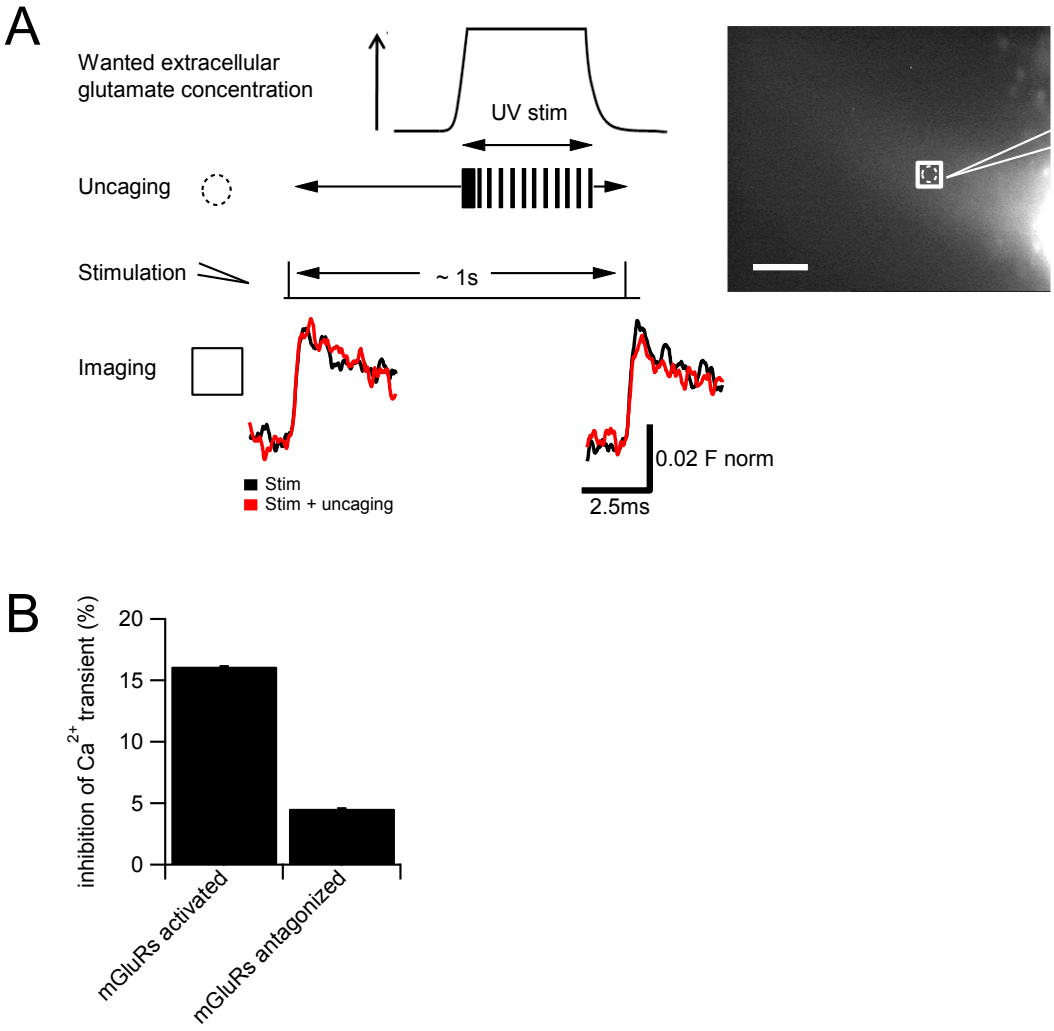

Figure 24. Glutamate uncaging induced group II mGluR activation in the MML causes presynaptic calcium signal depression. (A) Schematic illustration of a combined imaging and uncaging protocol (scaling: 40µm). The upper right snapshot shows a calcium indicator dye (Magnesium Green AM) loaded MPP fibre tract exited with 470nm (bandwidth ±30nm) light. The aperture (area of calcium signal detection) is positioned close to the tip of the stimulation pipette. The uncaging spot is centered to the middle of the pinhole. The following experimental procedure is described by an alternating protocol starting with a combination of pre-stimulus, UV laser mediated uncaging and test-stimulus followed by a pre- and test-stimulus alone. During stimulation, calcium signals were measured and peak ratios were calculated and compared (($Teststim_{uncaging}$/ $Prestim_{uncaging}$)/ (Teststim/ Prestim)) (scaling: 0.02 F norm, 2.5ms). **(B)** Comparison of averaged percentage inhibition of calcium signal amplitudes between: mGluRs activated by caged glutamate and mGluRs blocked by LY341495 (3µM). Similar to pharmacological activation but less pronounced, activation of group II mGluRs by uncaged glutamate (250µM) caused a reduction in calcium signal size which could be inverted by 3µM LY341495.

3.3 Assessing the time course of extracellular glutamate during uncaging

In order to describe the kinetics of group II metabotropic glutamate receptors as exactly as possible, conditions that disturbed the activation and deactivation process, e.g. a fluctuating glutamate concentration, had to be avoided. The aim was to create a UV laser protocol that produces a nearly rectangular glutamate concentration in the extracellular space, in other words, a fast increase of free glutamate, followed by a maintaining of the prevailing concentration and a fast drop after uncaging. In order to determine how the glutamate concentration varied during uncaging, we made use of processes directly coupled to glutamate uptake by astrocytes. The uptake rate is proportional to the change in extracellular glutamate.

3.3.1 Method 1: Voltage sensitive dye imaging with RH155

The first method tested was voltage sensitive dye (VSD) imaging. VSDs bind to the external surface of cell membranes without interrupting their normal function and act as molecular transducers that transform changes in membrane potential in an optical signal with a high temporal resolution. The VSD we used was RH155 which preferentially stains glia cells over neurons. Medial perforant path fibres in a RH155 stained slice were stimulated with the protocol 5stim at100Hz to cause synaptic glutamate release. The optical VSD signal arising from astrocyte membrane potential changes during electrogenic glutamate uptake was monitored. Tests were performed in the presence of the AMPA receptor blocker CNQX (30µM) because in addition to glutamate transporters also AMPA receptors are expressed in astrocytes (Seifert et al., 1997) and glutamate induced AMPA receptor currents were not in the focus of interest.

After CNQX application the VSD signal amplitude decreased to 76.4% of its initial size (Figure 25A). In order to check whether the VSD signal seen was due to glutamate transporter current induced changes in astrocyte membrane potential, we performed the synaptic stimulation experiment under wash-in of 40µM DL-TBOA to block glutamate transporters. As a result of this, the VSD signal strongly suppressed to 16.8% (Figure 25A).

In general, the size of the observed VSD signal during stimulation was smaller than expected from literature (Kojima et al., 1999). We assumed that light absorption of the tissue could be a limiting factor for voltage sensitive dye imaging with RH155. In order to shed light on this, I determined the spectral values for unstained and stained slices between approximately 400 and 700nm wavelength (Figure 25B).

We measure the intensity of visible light passing stained and unstained tissue with and without band-pass filter between 400 and 700nm and divided the value obtained with a filter (Figure 25B, right, red trace) by the value gained without the band-pass filter (Figure 25B, right, red trace). The relative absorption intensity exhibited two peaks for the unstained as well as the stained slice, one around 530nm and the second one around 700nm (Figure 25B, left graph). The latter turned out to be very problematic, because in the VSD imaging experiments the light absorption changes caused by RH155 were also detected at 700nm (filter: F35-700 Versa Chrome HC 700/ 13).

Another problem occurred, when we tried to uncage glutamate and image the RH155 signal at the same time. We used a beam splitter (reflection 330-485nm >90%, transmission 505-700nm >90%) together with a second filter (F39-409 Brightline HC 409/ LP) to exclude the UV light from the optical signal. However, we could detect an optical signal during uncaging, reflecting rather the time course of uncaging (Figure 25C, left, black trace) instead of a VSD signal time course corresponding to astrocyte membrane potential changes during glutamate uptake (Figure 25C, left, red trace: synaptic stimulation induce VSD signal). An explanation might be, that the UV light excited the voltage sensitive dye RH155, leading to a strong fluorescence detected at 700nm (bandwidth ±13nm).

Summarized, the optical properties of the slice and the voltage sensitive dye RH155 under UV illumination made the combinatory approach (glutamate uncaging and VSD imaging) impossible to use for our purpose.

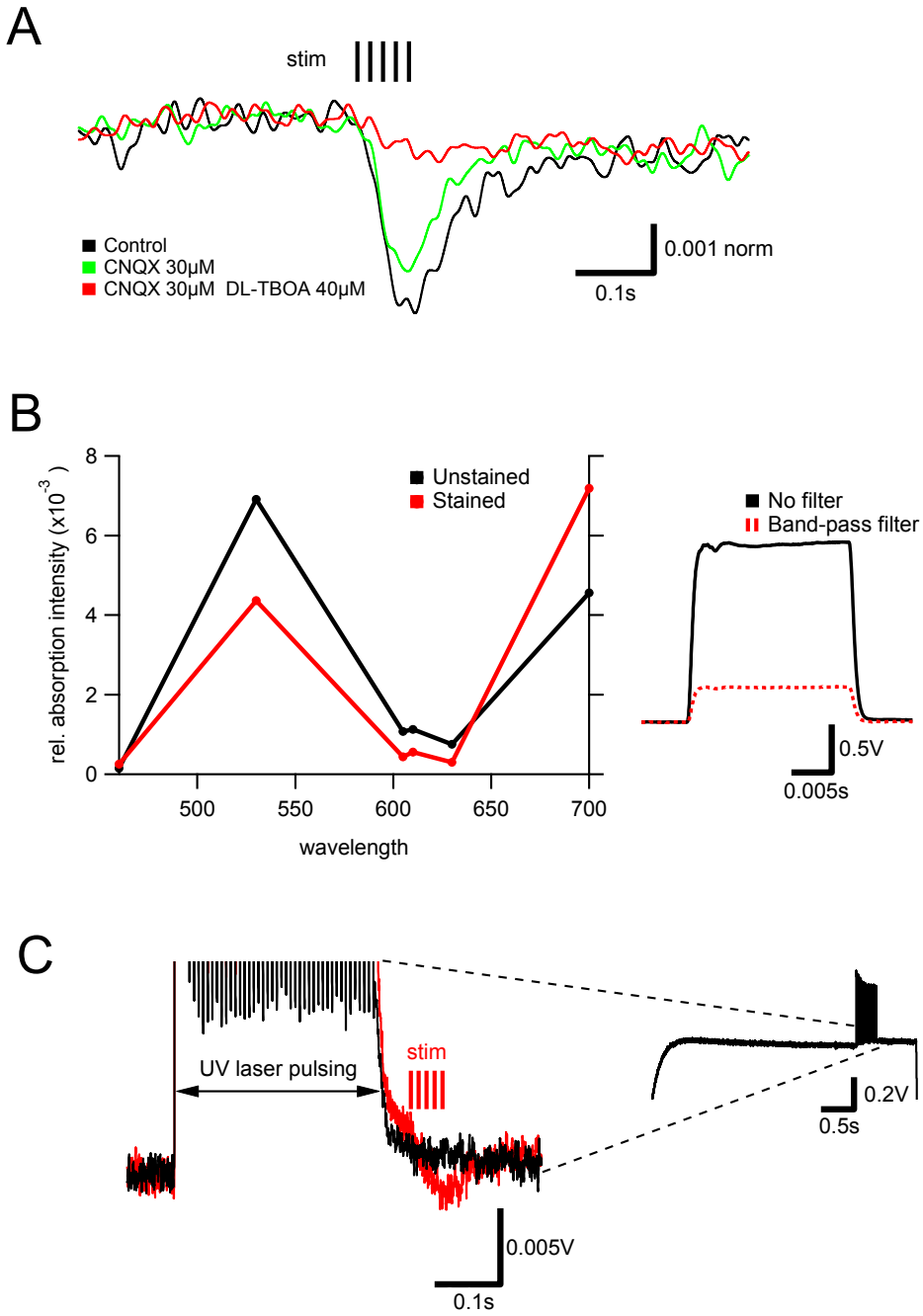

Figure 25. Voltage sensitive dye imaging with RH155 is not suited to detect astrocyte membrane potential changes during glutamate uncaging. (A) VSD imaging in the MML of the dentate gyrus during synaptic stimulation of the MPP fibre tract. Slices were loaded with RH155, preferentially staining glial cells, and illuminated with visible light. Optical signals were detected at 700nm (bandwidth ±13nm). Changes in glial membrane potential are indicated by an absorption increase. Whereas 30µM CNQX hardly affected the VSD signal, 40µM DL-TBOA almost completely abolished it. The baseline (before stimulation) is normalized to 1 (scaling: 0.001 norm, 0.1s). **(B)** Summary plot of absorption values for different wavelength in a stained and unstained slice. The relative absorption intensity was calculated as follows: optical $signal_{band\ pass\ filter}$ / optical $signal_{\ no\ filter}$. The relative absorption intensity exhibited two peaks within the tested wavelength range. The first peak value approximately at 530nm was higher for the unstained slice and the second peak at 700nm for the stained slice (scaling: 0.5V, 0.005s). **(C)** Optical signal of RH155 stained slice during UV stimulation (black) and during synaptic stimulation (red).

3.3.2 Method 2: Measuring astrocyte glutamate transporter currents

The second technique I applied was the measurement of astrocyte glutamate transporter currents directly during glutamate uncaging while whole cell patch clamping the astroglial cell (Figure 26A, filled with lucifer yellow).

Sodium dependent glutamate transporters are responsible for removing released glutamate from the extracellular space (Anderson and Swanson, 2000, Danbolt, 2001, Gadea and Lopez-Colome, 2001) and the transporter current displays a linearly filtered representation of glutamate clearance (Bergles et al., 1997, Diamond, 2005). Due to the translocation of net positive charge during each transport cycle, it was possible to monitor the transport electrophysiologically. Measuring glutamate uptake during flash photolysis of caged glutamate did not display a problem because it has been shown that stimulation as well as uncaging induced glutamate transporter transients exhibited similar kinetics (Diamond, 2005).

In general, astroglial glutamate transporters exhibits rapid kinetics and are capable of binding glutamate on a sub-millisecond timescale (Figure 26B), similar to the binding rates estimated for ionotropic glutamate receptors (Bergles et al., 1997). Immuncytochemical studies demonstrated that GLAST and GLT-1 are glutamate transporter types mainly expressed in astrocytes. GLAST predominates in the cerebellum and GLT-1 in the cerebral cortex and hippocampus (Lehre et al., 1995, Lehre and Danbolt, 1998). Astrocytes were identified by sulforhodamine 101 labelling (see section 2.9.2) (Nimmerjahn et al., 2004) and GFAP staining (Figure 26C) (Eng, 1985) as well as by their passive membrane properties (Figure 26D) (Bergles and Jahr, 1997).

When we started to perform glutamate uncaging and glutamate transporter current measurements simultaneously, the experiments showed, that the time course of glutamate transporter transients was strongly dependent on the laser pulse length and frequency and on pharmacology, especially DL-TBOA (Figure 26E, F). It was important to find the right interplay between laser pulse length and frequency under a certain DL-TBOA exposure to create a nearly rectangular glutamate transporter current and extracellular glutamate concentration gradient, respectively. Figure 14E displays two examples of transporter currents exhibiting suboptimal time courses during uncaging. In contrast, the last example (Figure 26F) shows the most suited, nearly

rectangular looking glutamate transporter current obtained by eliciting a long followed by a series of shorter UV laser flashlights in the presence of 40µM DL-TBOA.

We continued to use the latter UV stimulation protocol for combinatory Ca^{2+} imaging and glutamate uncaging experiments in order to investigate the kinetics of the presynaptic group II mGluR mediated inhibitory process in detail.

However, the slowed transporter current decay (tau= 440ms) was unavoidable after uncaging. It took approximately 800ms until the transient recovered to the resting level before uncaging. None of the changes we tried to prevent this worked out well. Testing the involvement of other receptor types revealed neither NMDA receptor blockers (100µM DL-AP5, MK 801 50µM), AMPA receptor blockers (CNQX 30µM or NBQX 10µM) nor mGluR1 (LY367385 50µM) and mGluR5 blockers (MPEP 10µM) had a fastening effect on the decay. Also an increase in laser spot size did not cause any change. The only parameters affecting the kinetics of the decay were the duration of UV laser pulsing and the DL-TBOA concentration. The longer the UV stimulation and the higher the DL-TBOA concentration the more prominent the decay was slowed. However, we had to activate group II mGluRs to an assessable extent, meaning that we needed a certain minimum duration of uncaging as well as DL-TBOA to facilitate mGluR activation. All in all, the range of possibilities was small to circumvent our problem.

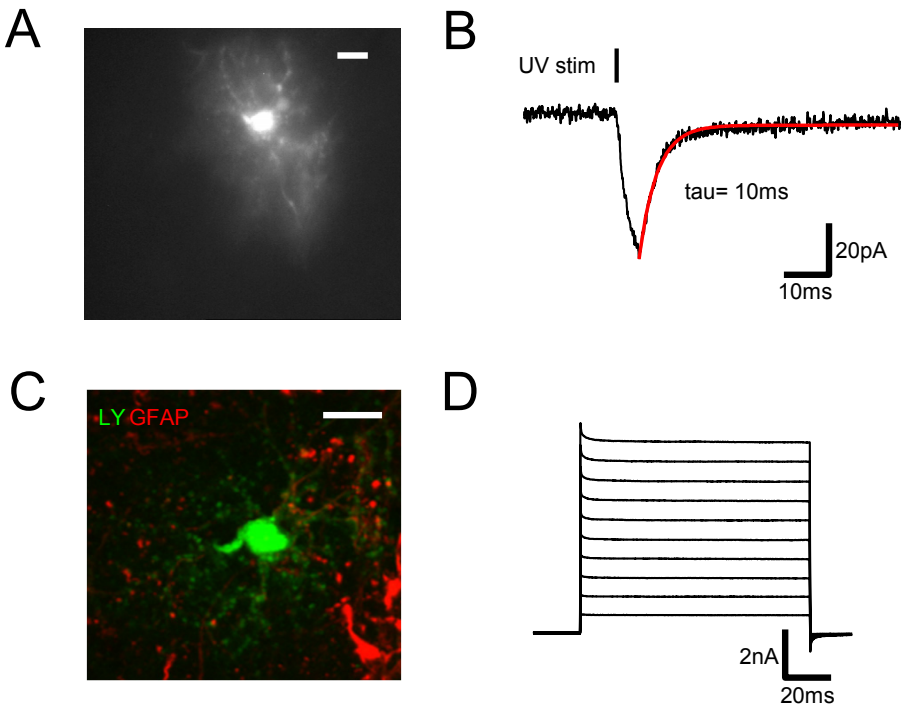

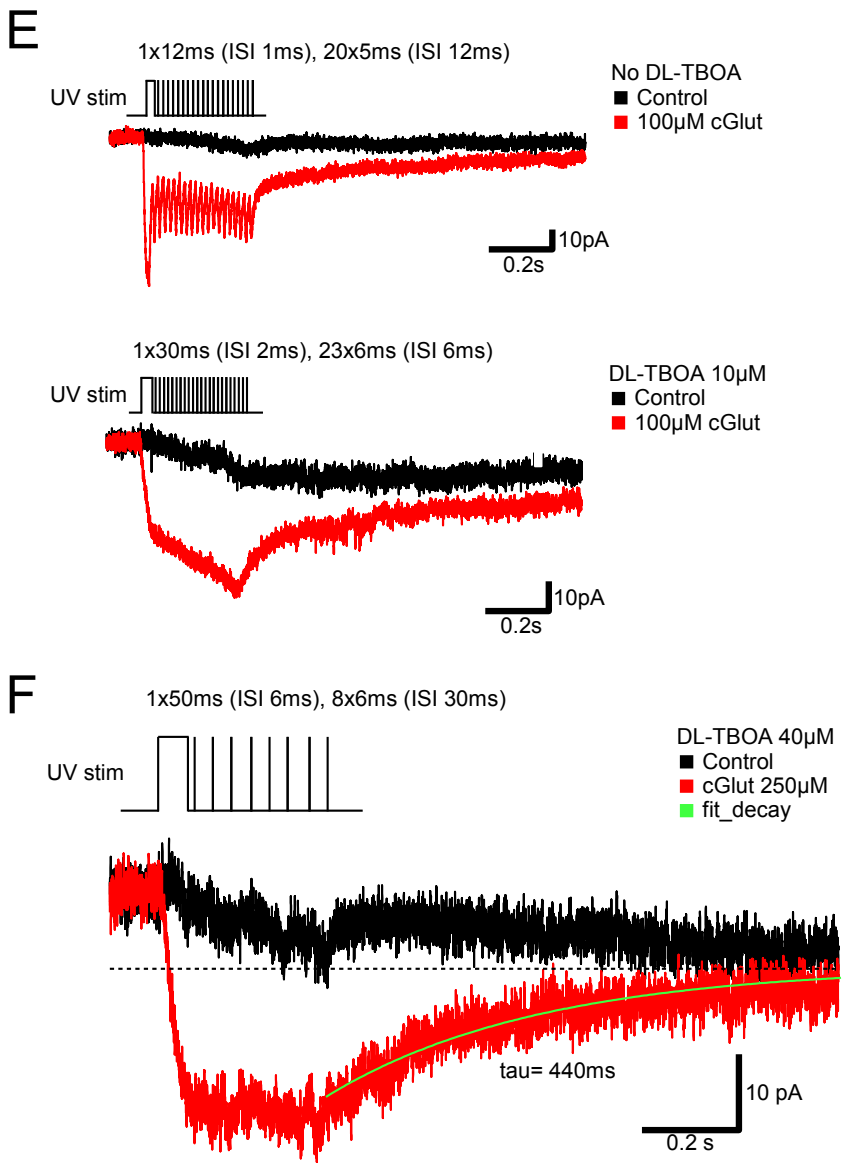

Figure 26. Astrocyte glutamate transporter current profile is strongly dependent on pharmacology and the UV laser uncaging protocol. (A) Patch clamped astrocyte (scaling 10µm) in whole cell mode filled with Lucifer yellow (1%). **(B)** Example of an astroglial transporter current caused by 10ms uncaging of glutamate (vertical bar; scaling: 20pA, 10ms). **(C)** Lucifer yellow labelled astrocyte which is GFAP+ (scaling 20µm). **(D)** Whole cell current pattern of an astrocyte (scaling: 2nA, 20ms). From a holding potential between -80 and -90mV cells were depolarized in steps of 10mV up to +20mV. **(E)** Glutamate transporter current pattern depending on the glutamate uncaging protocol and the used DL-TBOA concentrations (red, scaling: 10pA, 50ms). Control traces without caged glutamate are labelled in black. Particularly the glutamate transporter blocker DL-TBOA strongly slowed the current and the onset of the current was faster than the decay after uncaging. **(F)** The ideal glutamate transporter current during uncaging was more or less "step-like" to reach a constant glutamate concentration in the extracellular space while uncaging. The time constant (tau) for the decay after uncaging was 440ms. The decay (red) was fitted (green) to the mean baseline current between the black and the red trace after uncaging (dashed line).

3.4 Receptor kinetics of presynaptic group II mGluRs

In the following experimental series we investigated the kinetics of presynaptic group II mGluRs in detail. For this purpose we performed glutamate uncaging together with presynaptic Ca^{2+} imaging and assessed group II mGluR activation via uncaging-induced inhibition of presynaptic Ca^{2+} transients.

3.4.1 Latency and activation kinetics

For the assessment of latency and activation kinetics we exposed group II mGluRs to uncaged glutamate (γ-CNB-caged L-glutamic acid 250µM) for varying duration in the presence of following drugs: DL-TBOA 40µM, NBQX 10µM and DL-APV 100µM (Figure 16A). The glutamate transporter blocker DL-TBOA was used to facilitate group II mGluR activation and the AMPA receptor blocker NBQX as well as the NMDA receptor blocker DL-AP5 were applied to prevent postsynaptic Ca^{2+} signals and influences on the presynaptic Ca^{2+} transient.

For the experimental series, the combinatory Ca^{2+} imaging and uncaging protocol described in section 2.10 was used. The uncaging protocol was based on the protocol shown in Figure 26F. The degree of uncaging induced Ca^{2+} transient inhibition was obtained by calculating ratios between the Ca^{2+} signal response on the test-stimulus and the Ca^{2+} signal response on the pre-stimulus and dividing the ratio for the first part (with uncaging) of the combinatory protocol by the ratio for the second part (without uncaging). The same experiments were performed under wash-in of the group II mGluR antagonist LY341495 (3µM) and the resulting inhibition on the presynaptic Ca^{2+} transient mediated by group II mGluRs was determined via the antagonist mediated increase in the Ca^{2+} signal amplitude.

To resolve the onset of mGluR mediated presynaptic Ca^{2+} transient inhibition, we started with a short uncaging protocol (1x20ms UVstim; Figure 27A, upper left UV stimulation protocol) and imaged the calcium signal after 32ms post uncaging interval (PUI). The resulting inhibition was 4.0 ± 1.1% (n=4, Figure 27A). Next, we prolonged the UV laser protocol by increasing the duration of the first long laser pulse and added a series of shorter laser pulses with a defined inter stimulus interval (ISI) (1x50ms UVstim (ISI 6ms), 2x6ms UVstim (ISI 30ms), PUI 32ms; Figure 27A, upper right UV

stimulation protocol). As a result, we monitored an increase in presynaptic Ca^{2+} transient inhibition (9.3 ± 3.5%, n=3, Figure 27A). The inhibition further rose with increasing duration of uncaging (15.8 ± 2.7%, n=3; 1x50ms UVstim (ISI 6ms), 7x6ms UVstim (ISI 30ms), PUI 32ms) and reached its maximum after approximately 450ms of uncaging (16.7 ± 2.5%, n=3, 1x50ms UVstim (ISI 6ms), 11x6ms UVstim (ISI 30ms), PUI 32ms, Figure 27A). The time constant (tau) for the activation kinetics was 150 ± 30ms (Figure 27A). Experiments with the antagonist LY341495 were performed using the shortest (1x20ms UVstim, PUI 32ms) and the longest laser protocol (1x50ms UVstim (ISI 6ms), 11x6ms (ISI 30ms), PUI 32ms) resulting in 3.5 ± 0.6% (n=3) and 2.8 ± 0.6% (n=2) inhibition (Figure 27A).

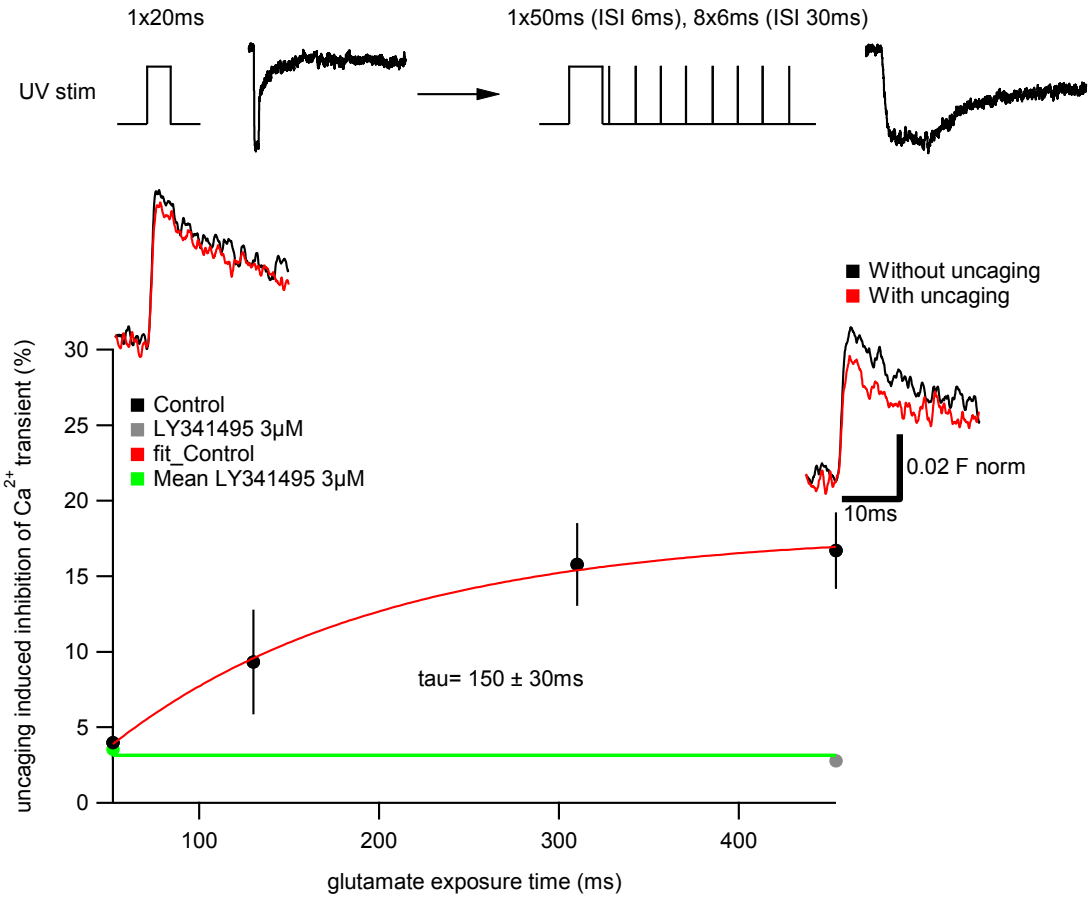

Figure 27. Activation kinetics of presynaptic group II mGluRs. Summary plot of percentage inhibition of the Ca^{2+} signal amplitude depending on glutamate exposure time (black). The curve fit is displayed in red. Within 450ms of glutamate uncaging, group II mGluRs fully activated (tau= 150 ± 30ms). Under blockade with 3µM LY341495 inhibition of the Ca^{2+} transient was missing (grey, average: green). On top of the graph, representative examples of Ca^{2+} peak comparisons (black: without uncaging, no mGluR activation; red: with uncaging, mGlurs activated) for the first and last exposure time are shown (scaling: 0.02 F norm, 10ms).

3.4.2 Deactivation kinetics

To determine the deactivation kinetics of group II mGluRs we monitored the recovery of the presynaptic Ca^{2+} transient after glutamate uncaging induced depression. During the experiments, the slices were exposed to 40µM DL-TBOA to block partially glutamate uptake in order to facilitate group II mGluR activation and additionally to 30µM CNQX and 30µM DL-APV to block AMPA as well as NMDA receptors and prevent postsynaptic Ca^{2+} signals. For the experimental series we used again the combinatory Ca2+ imaging (dye: Magnesium Green AM) and uncaging protocol described in detail in section 2.10.

First, we applied an uncaging protocol (1x20ms UVstim (ISI 3ms), 40x4ms UVstim (ISI 3ms); Figure 28A, upper UV stimulation protocol) to maximally activate group II mGluRs by freed glutamate (100µM γ-CNB-caged L-glutamic acid). Right after uncaging (post uncaging interval 60ms) the inhibition of the Ca^{2+} signal was strong (16.5 ± 9.0%, n=4, Figure 28A). Then, we prolonged the post uncaging interval (PUI) but kept the duration of uncaging constant. The inhibition of the Ca^{2+} signal declined after 600ms PUI to 10.8 ± 4.2% (n=5), and after 2000ms PUI 2.7 ± 4.4% (n=3) inhibition was detected (Figure 28A). The time constant (tau) for this decay was 1870 ± 60ms.

Experiments with the antagonist LY341495 (3µM) confirmed that the resulting Ca^{2+} transient inhibition was mGluR mediated. The inhibition could be completely blocked after 60ms PUI (-4.2 ± 1.7%, n=3) and 2000ms PUI (-5.0± 13.7%, n=2, Figure 28A).

As described in section 3.3.2, the decline of the transporter current after glutamate uncaging was slow (tau= 440ms, Figure 26F). A consequence of this slowed astrocyte glutamate reuptake was a persistently elevated glutamate concentration in the extracellular space. This was not a problem when resolving the activation kinetics of group II mGluRs because only the constant exposure to glutamate during uncaging was important. However, for the deactivation kinetics a persistently elevated glutamate concentration turned out to be critical. It was important to clarify to which extent this slowed reuptake influences the real group II mGluR receptors kinetics.

We developed an uncaging protocol causing a glutamate transporter current that matched the course of the slowed glutamate transporter transient, which occurred after applying the laser protocol which was described first in this section (Figure 28A, lower UV stimulation protocol). We tested, whether the amount of freed glutamate during this

protocol was enough to activate group II mGluRs. The experiments were performed under application of AMPA receptor (10µM NBQX) and NMDA receptor blockers (100µM DL-AP5, 50µM MK801), glutamate transporter blocker DL-TBOA (40µM), as well as with mGluR5 and mGluR1 (group I) antagonists (10µM MPEP, 50µM LY367385) and the sodium channel blocker TTX (1µM). The γ-CNB-caged L-glutamic acid concentration used was 250µM.

The resulting inhibition was 4.3 ± 0.5% (n=2), which could be blocked by LY341495 3µM (1.0 ± 0.0%, n=2, Figure 28A). Consequently, we assumed that the prevailing glutamate concentration during the slowed reuptake was enough to keep some mGluRs activated, which probably explains approximately 3.3% of the inhibition after 540ms PUI (Figure 28A). We also assumed, that the decay of the inhibition is mainly a representation of group II mGluR deactivation but partially also of mGluR activation. Insofar, the first experimental series provides rather a rough upper estimation on group II mGluR receptors kinetics.

The next step was to design a UV laser protocol that sufficiently activates mGluRs but does not cause a slow glutamate concentration time course after uncaging in order to make a lower estimation about the deactivation kinetics of group II mGluRs.

In combined astrocyte patch clamp and glutamate uncaging experiments we could observe that a relative short laser protocol (< 50ms UVstim) elicited no slowed decay. Moreover, we decided to abstain from DL-TBOA which additionally slowed the decay of the transporter transient and we used the high affinity Ca^{2+} indicator OGB1 AM because the bigger Ca^{2+} signal size and the better signal to noise ratio made it easier to detect small differences in Ca^{2+} signal amplitude. γ-CNB-caged L-glutamic acid was used in a concentration of 250µM. The uncaging protocol (20ms UVstim (ISI 6ms), 2x6ms UVstim (ISI 6ms)) was applied in the presence of the AMPA and NMDA receptor blocker NBQX (10µM) and DL-AP5 (100µM) (Figure 28B).

The inhibition monitored 109ms after uncaging, was small (7.3 ± 0.6%, n=4, Figure 28B). After 259ms PUI the inhibition decreased to 4.9 ± 0.7% (n=4) and dropped to 1.7 ± 0.4% (n=6) after 409ms PUI (Figure 28B). However, after 559ms PUI the inhibition increased again (2.3 ± 0.7%, n=6, Figure 28B).

We fitted the data to the average inhibition (2.3 ± 0.7%, n=4) obtained in the group II mGluR antagonization series with LY341495 (3µM) and calculated 150 ± 110ms for the time constant tau (Figure 28B). The big error was due to the high variability in the

data set, certainly arising to a great extent by activating group II mGluRs at a very low level. Because the weaker the mGluR mediated inhibition of the Ca^{2+} transient, the more difficult is it to determine the exact size if the inhibitory effect.

To sum up, the described two experimental series provide an upper and a lower estimation for the group II mGluR deactivation kinetics to contain the temporal range of receptor deactivation.

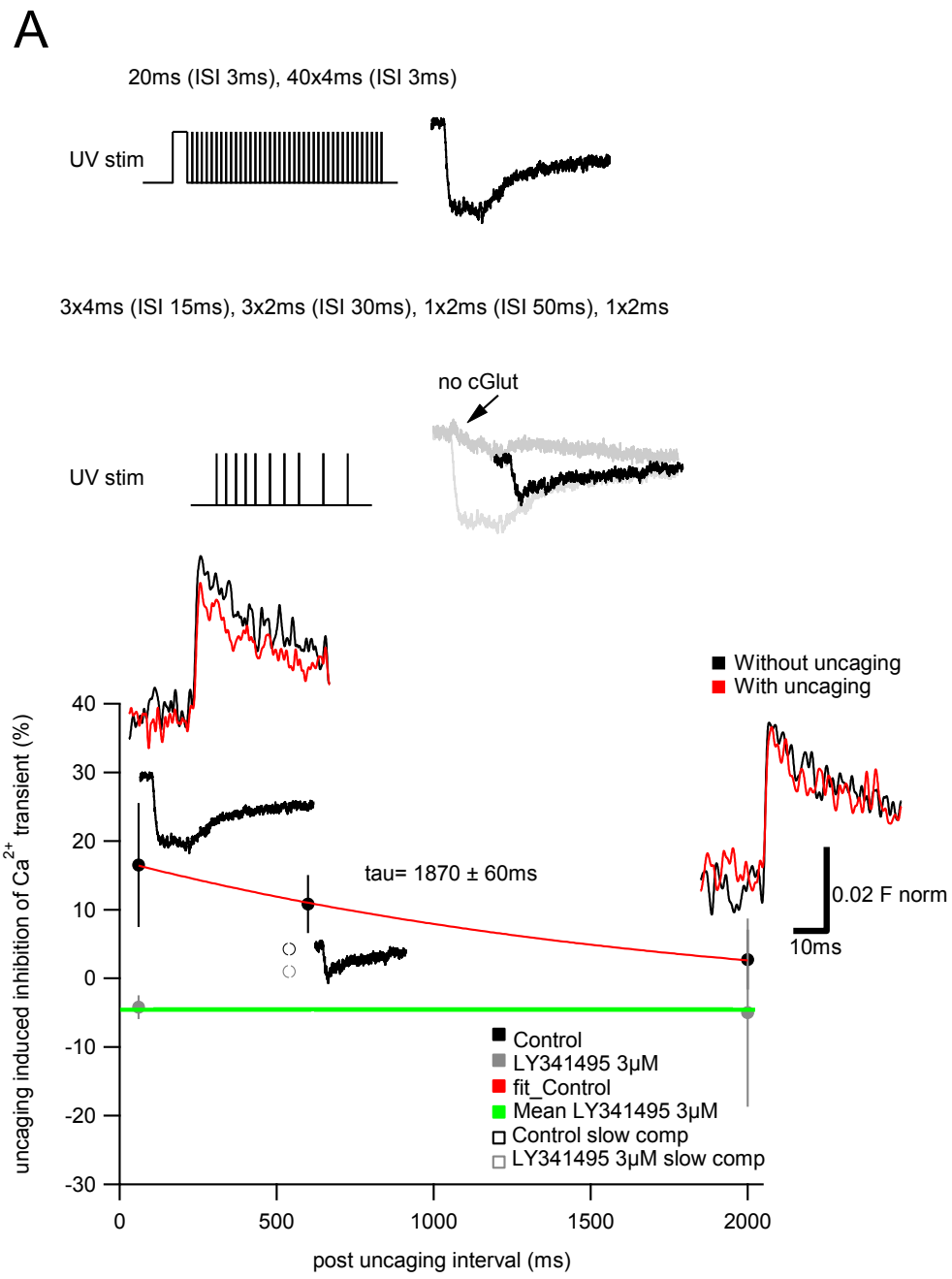

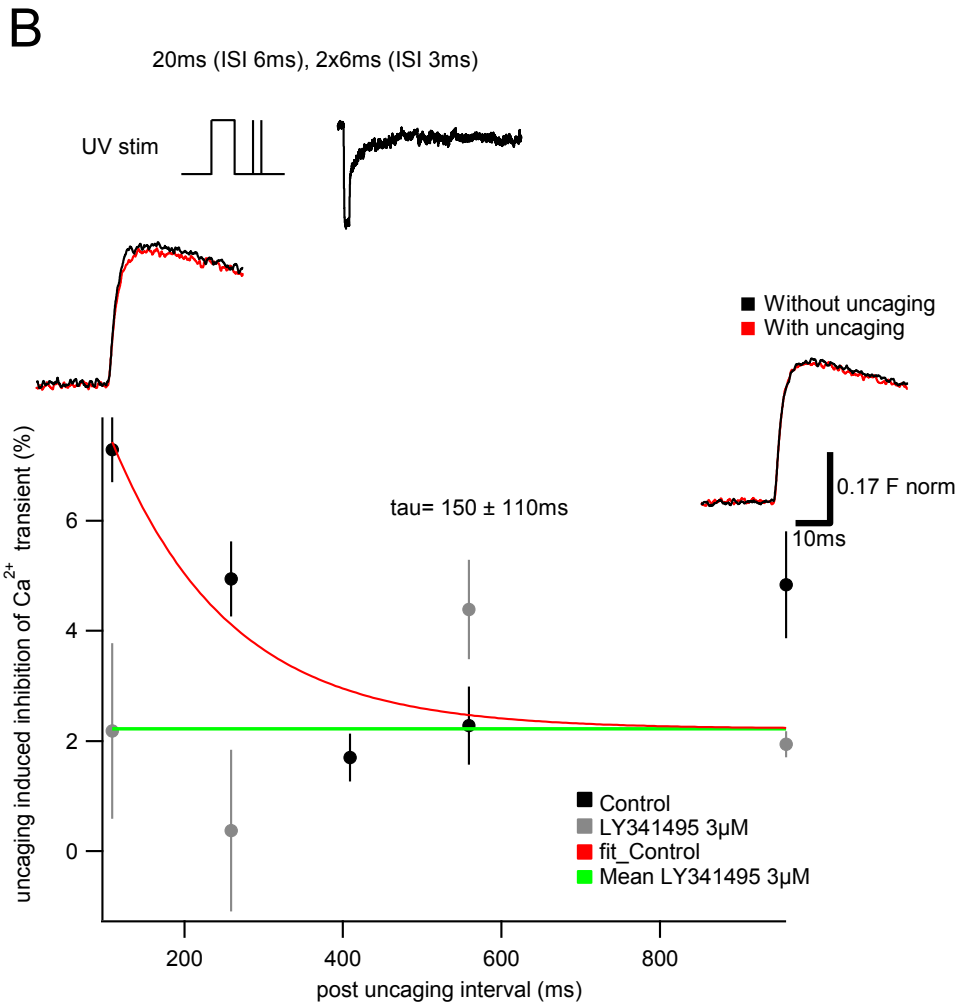

Figure 28. Persistent glutamate due to slow glutamate reuptake after uncaging possibly interferes with mGluR deactivation. (A) Summarized graph of percentage inhibition of the Ca^{2+} signal amplitude depending on post uncaging time. On top of the panel, schematic drawings and example traces of used UV laser uncaging protocols are illustrated (upper: "step-like" with slow decay component, lower: only slow component).When testing different post uncaging intervals after applying the "step-like" uncaging protocol with the slow decay component after uncaging, the ΔF peak amplitude slowly recovered back to its initial size before mGluR activation (red: curve fit, tau= 1870 ± 60ms). Testing the slow component-protocol to mimic the slow decay after uncaging, revealed presence of mGlu receptor activation, indicating a delayed deactivation of group II mGluRs when applying the "step-like"-protocol. Grey indicates averaged values of experiments performed under blockade of group II mGluRs with 3µM LY341495 to set the threshold for mGluR activation (green). Representative Ca^{2+} peak (Magnesium Green AM) comparisons (black: without uncaging, no mGluR activation; red: with uncaging, mGlurs activated) at two different post uncaging intervals are shown (scaling: 0.02 F norm, 10ms) **(B)** Summarized graph illustrating the recovery of inhibited Ca^{2+} signal amplitude after group II mGluR activation with a short glutamate uncaging protocol (top). Here, in contrast to (A), the decay of the mGluR effect was much faster (red: curve fit, tau 150 ± 110ms). Two Ca^{2+} peak (OGB1 AM) comparisons for two representative time points were selected (scaling: 0.17 F norm, 10ms).

3.5 Collaborative work

3.5.1 Does mGluR8 activation affect vesicle refilling in lateral perforant path terminals?

In general, presynaptic metabotropic glutamate receptors are believed and have been shown to inhibit synaptic transmission via blockade of presynaptic Ca^{2+} influx (Yoshino and Kamiya, 1995, Takahashi et al., 1996, Pinheiro and Mulle, 2008). However, there are many ways of modulating glutamate release. Apart from the reduction of Ca^{2+} entry by inhibition of calcium channels or activation of K^+ channels, different parts of the release machinery could be directly influenced through presynaptic mGluR activity.

So far, evidence was provided that certain mGluR subtypes mediate such a secondary effect downstream of Ca^{2+} entry (Scanziani et al., 1995, Tyler and Lovinger, 1995). In this study, the transduction target of mGluR8 was analyzed and it could be shown that this receptor inhibits transmitter release without affecting Ca^{2+} entry. Moreover, suggestions about the functional properties were made which could be affected by modulatory mGluR8 activity.

The field potential experiments we performed for this study concentrated on answering the following question: is the synaptic transmission during sustained trains of activity higher during mGluR8 activation than during inhibition of voltage-gated calcium channels? For this purpose, we compared repetitive synaptic responses when transmission was depressed to the same degree either by the mGluR8 agonist PPG (3µM) or by the low affinity Ca^{2+} channel antagonist Co^{2+} (600µM). Co^{2+} blocked but did not permeate Ca^{2+} channels and depressed fEPSPs to 56.0 ± 1.0% (n=11) similar to PPG (58.5 ± 2.0%, n=9, Figure 29A-C). When a steady depression of the fEPSP was reached, we stimulated lateral perforant path fibres with the protocol 35stim at 25Hz. In both cases, a pronounced transient facilitation of synaptic transmission due to a decreased release probability initially occurred (Figure 29A-C, third pulse; PPG: 159.2 ± 3.9%, n= 9; Co^{2+}: 155.3 ± 4.3%, n=11). The facilitation declined fast, probably, because the vesicle supply became a limiting factor. Conspicuously, after approximately 250ms (first 5 – 7 stimuli), the fEPSP responses under Co^{2+} became clearly smaller whereas in the presence of PPG larger amplitudes were maintained. At the end of the

train the amplitudes reached 84.9 ± 5.5% and 67.3 ± 4.1% under PPG and Co^{2+}. These results supported the assumption that mGluR8 activity does not affect Ca^{2+} entry.

The conclusion of the whole study was that mGluR8 mediated inhibition might be explained by a decrease in the apparent Ca^{2+} affinity of the release sensor and, to a smaller extent, by a reduction of the maximal release rate.

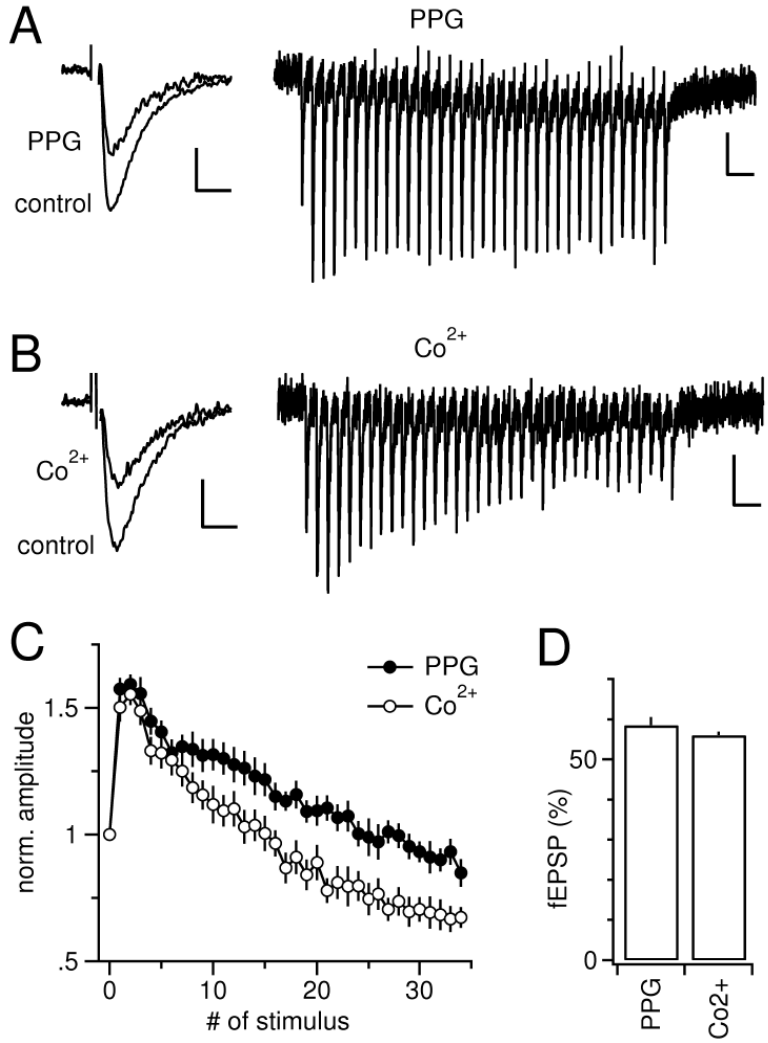

Figure 29. Inhibition of release by mGluR8 allows for a higher potency of transmission during sustained trains of activity. This figure is reproduced from Erdmann et al. (2011). **(A)** Reduction of the first fEPSP in the train of stimulations by 3 µM PPG (left panel) (scaling: 0.2mV, 5ms). Response to a train of action potentials evoked by 35 stim at 25Hz (right panel). After the initial facilitation there was only a slight decline of the amplitudes roughly back the amplitude of the first fEPSP (scaling: 0.1mV, 0.1s). **(B)** Same experiment as in A but performed with Co^{2+} instead of PPG. Co^{2+} concentration was adjusted to achieve an identical inhibition of synaptic transmission when compared to PPG (600µM, see left panel). After the initial facilitation of transmission amplitudes of fEPSPs strongly declined to a value substantially below the one of the first pulse (Right panel). Scaling as in A. **(C)** Summary of experiments performed as shown in A and B. Under activation of mGluR8 there was a stronger synaptic potency during the late phase of the train. **(D)** Summary of percentage inhibition of single fEPSPs caused by PPG and Co^{2+} in the experiments shown in A to C.

3.5.2 Does frequency facilitation at mossy fibres synchronously go along with an increase in Ca^{2+} influx?

Frequency facilitation, elicited by low-frequency stimulation (LFS) is a specific property of mossy fiber–CA3 synapses. The CA3 region responds to LFS with potent enhancement of evoked responses (Salin et al., 1996, Toth et al., 2000, Nicoll and Schmitz, 2005).

So far, it is still unclear how this phenomenon is generated, which factors are involved and how these factors act together. For a study dealing with potential mechanisms controlling frequency facilitation, we performed presynaptic Ca^{2+} imaging experiments on hippocampal mossy fibres.

In principle, the augmentation of transmitter release during frequency facilitation could be due to an increase in local free Ca^{2+} concentration at the Ca^{2+} sensor for vesicle fusion via an increased Ca^{2+} influx. In order to test this assumption, we loaded mossy fibres in acute mouse brain slices with the low affinity Ca^{2+} indicator Magnesium green AM and imaged presynaptic intra-terminal Ca^{2+} transients during LFS (6x10stim at 1Hz, Δ t between stimulation protocol application= 9s, Figure 30A-D). However, we could not detect any increase in Ca^{2+} influx (Figure 30C, D) during stimulation (all Ca^{2+} signals are normalized on the first of the train, 1st: 1 ± 0.0ΔF norm; 10th: 0.97 ± 0.0ΔF norm, n=5, Figure 30D).

All in all, the data show that the presynaptic Ca^{2+}entry is not affected during low frequency stimulation. Therefore, it can be excluded as possible mechanism controlling frequency facilitation.

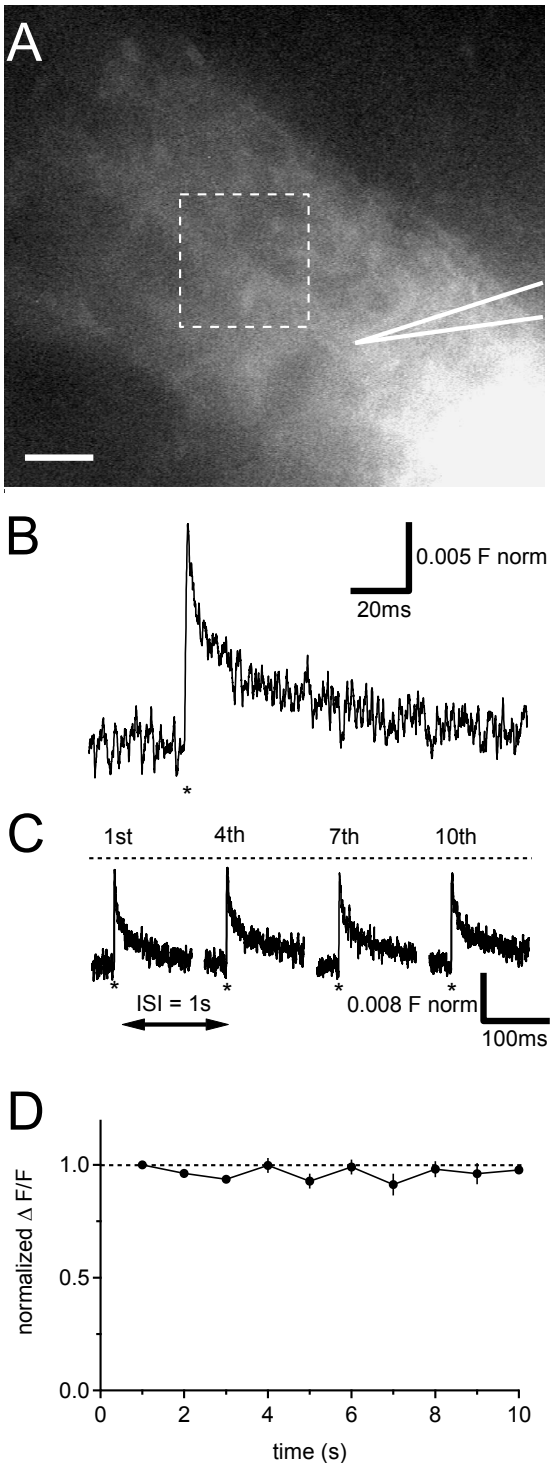

Figure 30. The peak intra-terminal Ca^{2+} level within mossy fibres does not increase during 1Hz facilitation. (A) Mossy fibres loaded with the fluorescent Ca^{2+} indicator Magnesium Green AM (scaling: 20µm). Optical signals were detected within a pinhole (dashed square) which was positioned in front of the pipette tip distal to the injection site. **(B)** Representative example of peak fluorescence (ΔF) during MF stimulation (asterisk) (scaling: 0.005 norm F, 20ms). **(C)** Averaged Ca^{2+} signals normalized on the first peak of ten in total. The graph shows every third peak beginning with the first. Stimulation is indicated by an asterisk and the time interval between two peaks is 1s (scaling: 0.008 norm F, 100ms). **(D)** The inset shows normalized Ca^{2+} signal amplitudes plotted versus stimulus number. The peak fluorescence underlay slight fluctuations but did not increase with sustained stimulation.

4 Discussion

4.1 Limiting factors of presynaptic inhibitory group II mGluR activation

To date, very few studies have dealt with the activation or presynaptic inhibitory group II mGluRs by synaptically released glutamate (Scanziani et al., 1997, Dube and Marshall, 2000, Awatramani and Slaughter, 2001, Kew et al., 2001). In this studies, we tied in with these findings and continued testing the synaptic recruitment of presynaptic inhibitory group II mGluR by performing field potential recordings in the middle molecular layer of the rat hippocampal dentate gyrus. The reason why we have chosen this region is mainly explained by two important facts. The terminal field of the perforant path in the middle molecular layer of the dentate gyrus exhibits a high expression level of group II mGluRs as revealed by immunhistochemistry (Neki et al., 1996, Petralia et al., 1996, Shigemoto et al., 1997, Ohishi et al., 1998) and autoradiographic studies (Mutel et al., 1998, Schaffhauser et al., 1998). Apart from that, medial perforant path fibres are highly laminar organized (McNaughton, 1980, Witter, 2007) which made them very well suited for field potential recordings as well as presynaptic Ca^{2+} imaging.

In agreement with the above mentioned studies, moderate burst stimulation of medial perforant path fibres caused a relatively weak group II mGluR mediated inhibition of synaptic transmission. To facilitate mGluR activation and to make it more assessable, we used a glutamate transporter blocker DL-TBOA causing a stronger accumulation of glutamate in the extracellular space (Takayasu et al., 2004). The use of 40µM DL-TBOA more than doubled the mGluR mediated inhibitory effect which further increased with the application of 100µM DL-TBOA. This huge potentiating effect on group II mGluRs activation made clear that glial glutamate uptake is an important limiting factor in this respect.

In addition to strengthening mGlu receptor activation during burst stimulation, 100µM DL-TBOA caused an inhibition of baseline transmission independent from stimulation. We suggest an activation of pre-terminal group II mGluRs by spontaneously released

glutamate during strong transporter blockade indicating that the receptor activation by the endogenous ligand is not necessarily coupled to firing of the presynaptic neurons they are located on. To allow controlled group II mGluR activation via burst stimulation, the side-effect had to be reduced to a negligible degree by lowering the DL-TBOA concentration ending up with 40µM.

In the past it has been indicated, that presynaptic group II mGluR activation increases with the frequency of synaptic stimulation (Scanziani et al., 1997). We systematically tested this at medial perforant path fibres and confirmed an mGluR effect clearly integrating the firing frequency of the presynaptic neuron. This was also true for the duration of stimulation. The mGluR mediated inhibitory effect on transmitter release became stronger until a plateau was reached after a few hundred milliseconds of stimulation. Circumstances that might have led to this limitation were, for example, a limited vesicle supply during high frequent synaptic stimulation (Model et al., 1975, Fernandez-Alfonso and Ryan, 2004). The exocytosis rate was higher than the endocytosis rate, leading to a continuous depletion of the vesicle pool. Probably at some point, the amount of vesicles released was too small to increase the degree of mGluR activation. Another factor that might have limited mGluR activation is AMPA receptor desensitization. It is known that high frequent activity can cause an AMPA receptor state in which the ligand no longer causes the receptor channel to open (Arai and Lynch, 1998). The inhibitory modulatory effect of presynaptic group II mGluRs might have got restricted by the capacity of ionotropic AMPA receptors on the postsynaptic site. NMDA receptors did not need to be taken into account because all experiments were performed under blockade of these receptors. As another factor, one cannot rule out that maximum possible group II mGlu receptor occupation had already been reached. Glutamate clearance mechanisms like uptake and diffusion always keep the amount of available glutamate in the extracellular limited (Min et al., 1998, Huang and Bergles, 2004), restricting group II mGlu receptor activation as well.

Subsequently, we determined the time course of action on synaptic transmission. The onset of the effect was relatively fast and the maximum inhibition was reached after a few hundred milliseconds (100-300ms). In contrast, the decline was slow and lasted hundreds to thousands of milliseconds before the inhibition finally disappeared. This is consistent with findings about the kinetics of class C G-protein coupled $GABA_B$ receptors at parallel fibre to Purkinje cell synapse in cerebellar slices (Dittman and

Regehr, 1997). Whereas activation of presynaptic group II mGluRs is tightly controlled by the spatiotemporal profile of glutamate diffusion following exocytosis, the deactivation process is indicated to be driven by intrinsic receptor and signal cascade kinetics.

So far, the maximum endogenous inhibition achieved had been still far beyond the inhibition reached by pharmacological activation of mGluRs by DCG IV (Yoshino et al., 1996). Possibly, the amount of released glutamate was not sufficient enough to fully activate presynaptic group II mGluRs or to keep the receptors activated, respectively. We hypothesized, repetitive burst firing (Larson and Lynch, 1988) mimics to a certain extent oscillatory firing pattern in the entorhinal cortex (Bragin et al., 1995, Paulsen and Sejnowski, 2000, Buzsaki, 2002) and that it potentially causes a temporal summation of released glutamate and potentiates receptor activation. For this purpose, an alternating protocol was designed that was composed of bursts to release transmitter and a break between each burst, only long enough to get the vesicle pool refilled before the transmitter (released before) completely diffused away. However, we could not observe any cumulative mGluR effect on synaptic transmission during repeated burst application.

To summarise, none of the tested stimulation protocols caused an effect comparable in size to pharmacological induced inhibition, suggesting that the functional significance might not be determined by the degree of inhibition but rather by the long persistence of inhibition on synaptic transmission consistent with the finding about $GABA_B$ receptors (Pfrieger et al., 1994, Dittman and Regehr, 1997) and feedback inhibition in general (Kupchik et al., 2011).

4.1.1 Performing field potential recordings to systematically investigate group II mGluR activation

The performance of field potential recordings displayed the most simple and most effective way to study group II mGluR activation direct and systematically. Group II mGluRs are distinctively and numerously distributed at the terminals of highly dense and parallel medial perforant path fibres (Hjorth-Simonsen and Jeune, 1972, Shigemoto et al., 1997). Due to a specific paired pulse plasticity (paired pulse depression) (McNaughton, 1980) and the nearly perfect laminar arrangement of the MPP fibre tract which forms excitatory synaptic contacts with granule cell dendrites it was possible to

selectively stimulate the MPP fibre tract and record the corresponding postsynaptic response of granule cell dendritic spines with less experimental effort. mGluR activation during MPP burst stimulation was indicated by a decrease of the postsynaptic response and could be directly assessed after the experiment. Each presynaptic limiting factor (duration of activity, frequency of activity, pattern of activity) and other group II mGluR activation influencing factors (glutamate uptake by astrocytes, GABAergic inhibition of synaptic transmission), as well as the time course of mGluR action on synaptic transmission could be determined separately via applying appropriate stimulation protocols. To not run the risk of causing long term plasticity during high frequent stimulation, NMDA receptor blockers were used and a restriction of mGluR activation due to fast glutamate removal was avoided by lowering the glutamate uptake by astrocytes with the glutamate transporter blocker DL-TBOA.

It was disadvantageous, that these manipulations created an environment less physiological in favour of an inhibitory mGluR effect of assessable size. Another critical factor to be taken into account is that field potentials can only be used to get rough approximations about intracellular events. Especially peak measures of field EPSPs at high stimulation intensity can be contaminated with pspikes (potentials corresponding to the action potential), pIPSPs (or population IPSPs) and polysynaptic events. Moreover, one could argue that in vitro experiments in general have less physiological validity. However, investigations have to start at some point and experiments, e.g. on brain slices often provide important insights, helpful for future experimental series in vivo.

Despite critical points, this technique permitted a robust screening of mGluR activation in order to make progress in finding out how and when these receptors activate and which mechanism might significantly control this process.

4.2 Kinetics of presynaptic group II mGluR mediated inhibition

Activation of presynaptic voltage gated calcium channels results in a rapid triggering of vesicle fusion and release (Sabatini and Regehr, 1996). Consequently, an inhibition of presynaptic Ca^{2+} influx, for example by a metabotropic glutamate receptor induced

signal cascade (Takahashi et al., 1996), results in a direct depression of transmitter release. The activation of presynaptic group II mGluRs induces a $G_{i/o}$ dependent internal signal cascade which in turn negatively affects the presynaptic, action potential dependent Ca^{2+} signal of P/Q-type voltage gated calcium channels (Chavis et al., 1994, Pin and Duvoisin, 1995). The time course, starting with receptor activation and ending with the calcium influx directly acting on the release machinery reflects the onset of mGluR mediated inhibition of synaptic transmission. To resolve the temporal dynamics of presynaptic group II mGluR induced depression and to shed light on the question whether the temporal dynamics of the inhibitory effect is shaped predominantly by the uptake and diffusion of glutamate or rather by the intrinsic kinetics of the mGlu receptor mediated signalling process within the presynaptic terminal, we performed Ca^{2+} imaging at presynaptic medial perforant path terminals and measured the action potential triggered Ca^{2+} influx via the transient increase in indicator fluorescence (Sabatini and Regehr, 1995). In combination with Ca^{2+} imaging, UV laser uncaging of glutamate was performed to selectively activate or deactivate group II mGluRs, respectively.

The onset of the mGluR effect and the time to reach maximum inhibition (200-300ms) were comparable to the results obtained when group II mGluRs were activated synaptically (see Figure 20). The determination of group II mGluR deactivation kinetics turned out to be problematic. As mentioned later on (section 4.2.4), the glutamate uptake by astrocytes was delayed after uncaging with a UV laser stimulation protocol, originally designed to cause a nearly rectangular glutamate concentration in the extracellular space during uncaging.

In general, glutamate is cleared away very fast after synaptic release by diffusion (~1ms) (Clements et al., 1992, Clements, 1996, Wahl et al., 1996, Diamond, 2005), through binding by glutamate transporters on a sub-millisecond time scale (Diamond and Jahr, 1997) and by glutamate uptake (>10ms) (Bergles et al., 1997, Bergles and Jahr, 1997).

Strikingly, in our experiments we observed that longer exposure of a patched astrocyte to uncaged glutamate slowed the decay of the glutamate transporter current. This suggest that glutamate transporters close to the uncaging spot were saturated by the endogenous ligand, forcing glutamate to diffuse a longer distance to find farther available sites. Potentially, cell damage caused by the UV laser or the activation of other

channels could also account for this slow decay. But, none of the changes like increasing the size of the uncaging spot, dampening the UV laser with neutral density filters, lowering the caged glutamate concentration, nor the blockade of several types of receptors and channels (AMPAR, NMDAR, group I mGluRs, sodium channels) potentially affecting the current, led to a significant change. Tests with a "slow-component" UV laser protocol, mimicking the time course of the transporter current occurring after uncaging with the previous describe protocol, confirmed that the amount of glutamate present after applying a "step-like" protocol is still potent enough to keep at least a few mGluRs active. Thus, the rapid removal of glutamate from the extracellular space after flash photolysis was an essential condition for a reliable conclusion concerning the time course of deactivation we were not able to manage. One could argue, that the slowed reuptake is an effect which also appears under physiological conditions when presynaptic neurons are highly active, causing a saturation of glutamate transporters which in turn supports ongoing mGluR receptor occupancy. But, this is speculative and not yet shown. Unfortunately, the suboptimal conditions only allowed making an upper and a lower estimation about the deactivation kinetics.

For the upper estimation a long-lasting uncaging protocol and DL-TBOA (40µM) was used to activate group II mGluRs maximally, but we had to take into account that the time course of inhibition after uncaging reflects interplay between deactivation and activation, the former to a greater extent than the latter. Interestingly, the upper estimation (tau ~1800ms) revealed a timescale well fitting the duration of fEPSP recovery after synaptically activated mGluRs (see Figure 20). In both cases the inhibition lasted up to a few seconds (~2s) before it became un-assessable.

The lower estimation was made using a short uncaging protocol and no DL-TBOA to prevent interference by a slowed reuptake. In contrast to the previous result, the inhibitory effect declined much faster (tau ~150ms) and was already gone after approximately 400ms. However, the total inhibition was weak and the assessibility limited due to the high variability in the data set.

If we suggest, that the real duration of group II mGluR deactivation is somewhere in between lower and upper estimation, the process is indicated to be rather long lasting. This in turn strongly supports the assumption, that the deactivation is controlled by intrinsic slow receptor kinetics rather that extracellular glutamate dynamics. If the

deactivation was be dependent on receptor occupation with the ligand glutamate and follow its temporal decline in concentration during diffusion and glial uptake, the process would be much faster.

Although we were restricted to approximations, the data strongly support the suggestion that presynaptic group II mGluRs rather mediate a weak and persistent inhibition as it was shown for another metabotropic (class C) G-protein coupled receptor (Dittman and Regehr, 1997) and indicated for the mGluR1 subtype in cultured PC12 cells (Marcaggi et al., 2009).

4.2.1 Using Ca^{2+} imaging as a tool to assess the dynamics of mGluR mediated inhibition

To resolve the kinetics of presynaptic group II mGluR mediated inhibition, we had to measure the presynaptic Ca^{2+} transient peak amplitude at different mGluR activity states. It would have been complicated to measure presynaptic Ca^{2+} currents in patch clamp experiments because medial perforant path terminals are very small. An easier way to measure Ca^{2+} transients was the usage of a fluorescent indicator specific for Ca^{2+} (Sabatini and Regehr, 1998). In our imaging experiments, we used acetoxy-methyl (AM) ester derivates of fluorescent indicators (Magnesium green AM, OGB-1 AM). Fluorescent indicators are derivatives of the Ca^{2+} chelators EGTA, APTRA and BAPTA. Masking carboxylic acids of the chelator with AM ester groups results in an uncharged lipophilic molecule that can permeate cell membranes. Within the cell, the lipophilic blocking AM esters groups get cleaved by intracellular esterases resulting in a charged form that leaks out of the cell whereas the impermeable polycarboxylate stays in the cell. The hydrolysis of the esterified groups is essential for binding the target. The fluorescent Ca^{2+} indicators described here operate at visible wavelength and binding of Ca^{2+} leads to a change in fluorescence emission intensity. An advantage of AM-linked Ca^{2+} indicator dyes is that, for example, cellular compartments can be selectively labelled. It was challenging to find out, if medial perforant path fibres could really be loaded with a fluorescent Ca^{2+} indicator via pressure injection because these fibres are myelinated and it was not clear whether the loading would be selective enough. Fortunately, it turned out to work and we started optically monitoring stimulation induced presynaptic Ca^{2+} transients before and after presynaptic group II mGluR activation.

Ca^{2+} indicators are characterized by their binding affinity reflected in the dissociation constant K_d. Most experiments were performed with the low affinity Ca^{2+} indicator Magnesium green AM. Lower affinity indicators are suited for measuring Ca^{2+} in cellular compartments with higher concentrations (like presynaptic terminals during action potential triggered Ca^{2+} influx) and these indicators can also be used to measure rapid changes in Ca^{2+}. Due to their low affinity for Ca^{2+}, the kinetics of the reactions are rapid enough to analyze Ca^{2+} alterations with high temporal resolution. For our purpose, this was advantageous because we wanted to resolve fine changes in Ca^{2+} signal size at certain time points after glutamate uncaging induced mGluR activation. However, the relatively small Ca^{2+} signal size (approximately 2-4%) was disadvantageous, causing suboptimal signal to noise ratios. In a single experiment, stimulation paradigms had to be repeated and the corresponding data points averaged to prevent high variability. In contrast, high affinity indicators like OGB-1 AM produced a much bigger Ca^{2+} signal and showed a better signal to noise ratio but these dyes may also buffer intracellular Ca^{2+}. Moreover, due to their high-affinity, they saturate at relatively low levels and errors in the Ca^{2+}estimation can occur.
In the end, it had to be pondered which Ca^{2+} indicator suited best for the corresponding experimental series to create most optimal conditions.

4.2.2 Using flash photolysis to expose mGluRs to glutamate

For the temporal resolution of the dynamic inhibitory process mediated by presynaptic group II mGluRs *in situ* it was important to bring glutamate directly to the receptor and to create constant conditions during activation. Flash photolysis of caged glutamate provided several advantages compared to synaptically released glutamate and this method has been already successfully tested, for example in a study about $GABA_B$ receptor kinetics (Dittman and Regehr, 1997) and in a variety of cellular and circuit level processes in the last decades (Callaway and Katz, 1993, Nikolenko et al., 2007). Whereas burst stimulation of presynaptic fibres causes an indefinite glutamate concentration due to a spatial gradient of glutamate after release and a naturally occurring depletion of the vesicle pool, light activation of glutamate allows a controlled delivery of glutamate with temporal and spatial precision. Moreover, synaptic release underlies a certain plasticity which does not occur during uncaging. Another important advantage of glutamate uncaging is that the concentration of the caged ligand is known

before flash photolysis and conclusions about the temporal changes in the amount of glutamate in the extracellular space during uncaging can be made by detecting astrocyte glutamate transporter currents. In this study, γ-CNB-caged L-glutamic acid was chosen because an illumination of this photo-activatable derivate with 355nm light resulted in a rapid, highly localized release of the freed neurotransmitter glutamate at the site of illumination. However, there are limitations to the caged compound that can be used. Typically 1- 2% gets spontaneously uncaged and if high concentrations are used it is likely that high affinity receptors get activated before UV laser uncaging (Dittman and Regehr, 1997, Ellis-Davies, 2007). Despite this restriction, it can be concluded that uncaging of glutamate was best suited to expose presynaptic group II mGluRs directly to the endogenous ligand with a constant concentration over a definite time. This allowed resolving the activation and deactivation kinetics of the mGluR mediated inhibitory process in detail because diffusion times and changing glutamate levels could be prevented.

4.2.3 Applying voltage sensitive dye imaging to assess extracellular glutamate levels during uncaging

To verify the temporal course of freed glutamate during uncaging, we first came up with the idea to optically monitor uncaging induced glutamate transport. The advantage was that it did not require a reconstruction of the setup and the technique of voltage sensitive imaging was relatively easy to apply. The plan was to stain preferentially astrocytes with the voltage-sensitive dye RH155. When glutamate transporters activated, the glial membrane potential changed and the VSD responded with a change in absorption. In preliminary work we could show a stimulation induced VSD signal which was of glial origin because a blockade of glutamate transporters (40 or 100µM DL-TBOA) abolished it. Next we wanted to uncage glutamate and monitor the corresponding VSD signal simultaneously. However, this did not work out well. We observed an increase in optical signal intensity following the time course of uncaging instead of a decrease which was expected as a result of RH155 absorption increase during glutamate uncaging induced astrocyte membrane potential changes. An explanation would be that UV light excited the voltage sensitive dye RH155, leading to an emission at the wavelength range (~700nm) where originally the VSD signal itself should have been detected. Besides, the calculation of absorption values for a defined wavelength range

under stained and unstained conditions revealed tissue absorption intensity peaking at two different wavelengths, approximately at 530nm and at 700nm additionally disturbing the detection of an absolute RH155 signal. All in all, this combinatory approach turned out to be impracticable.

4.2.4 Performing glutamate transporter current measurements on astrocytes during flash photolysis to evaluate extracellular glutamate levels

The measurement of astrocyte glutamate transporter currents is a successfully tested way to estimate the concentration time course of extracellular glutamate (Bergles et al., 1997, Bergles and Jahr, 1997). Moreover, it could be shown that synaptically released glutamate is taken up at the same rate as glutamate released via flash photolysis, indicating that the time course of clearance is not affected by the spatial location of transporters to the site of glutamate release (Diamond, 2005). In order to verify the temporal change of glutamate during uncaging at physiological temperature (35°C), we patch clamped astrocytes. Successfully patched astrocytes were kept in whole cell configuration and the current was monitored in voltage clamp mode. A disadvantage was that the relative expensive caged glutamate had to be added by perfusion because in preliminary tests it turned out that local bath application accompanied by a perfusion stop led to drastically temperature changes affecting the glial glutamate uptake which is highly temperature dependent (Asztely et al., 1997).

Apart from the lastly mentioned disadvantage, measuring glutamate transporter currents is an absolute useful way to get information about the temporal course of freed glutamate during uncaging which was mandatory for us in order to design usable UV laser protocols.

4.3 Pharmacological activation of mGluRs versus endogenous activation by glutamate

Pharmacological activation of presynaptic inhibitory group II mGluRs has been extensively tested in the past decades (Dietrich et al., 1997, Kilbride et al., 1998, Bradley et al., 2000, Capogna, 2004, Doherty et al., 2004). The strong inhibition of

synaptic transmission induced by agonist binding together with the high affinity of these extra-synaptically located receptors (Pin and Duvoisin, 1995) let many to suggest an auto-regulatory role for presynaptic group II mGluRs (Macek et al., 1996, Conn and Pin, 1997, Cochilla and Alford, 1998) and an important functional role in many neuronal processes (Nakanishi, 1992, Conn and Pin, 1997, Niswender and Conn, 2010). Although a few studies already identified an obvious discrepancy between pharmacological and synaptic activation by released glutamate (Scanziani et al., 1997, Kew et al., 2001, Kilbride et al., 2001, Price et al., 2005), it has never been focused on it in detail. Our systematic analysis aimed to shed light on this antilogy. In fact, our results provide evidence for a real difference between pharmacological mGluR activation and activation by the endogenous ligand glutamate. Using the potent agonist DCGIV (affinity at mGluR 2/3 200 - 300nM (Conn and Pin, 1997)) resulted in a strong inhibition of synaptic transmission (~80%, Figure 16C). In contrast, the maximum inhibition reached by glutamate (affinity at mGluR in the micro molar range 4 – 20µM (Conn and Pin, 1997)) was only about 30% (Figure 19B) despite extensive testing of a variety of stimulation paradigms within the physiological range (Paulsen and Sejnowski, 2000) and beyond.

The molecular basis for the high affinity and selectivity of DCGIV is mediated in part by an interaction between a third carboxylic acid group on DCGIV not present in the glutamate molecule and a tyrosine and arginine present in the binding pocket of group II mGlu receptors (Yao et al., 2003). An assumption explaining the different effect on synaptic transmission after pharmacological agonist binding and glutamate binding to group II mGluRs could be that the ligand binding domains (LBD) in the dimeric mGlu receptor show allosteric properties, however, only in the case of glutamate binding. As it has been shown for mGluR 1 (Suzuki et al., 2004) it could be that in terms of subunit-subunit communication it comes to a negative cooperativity, meaning that binding of glutamate to one LBD weakens the binding of a second glutamate molecule to the other LBD. Contrary to glutamate, the strong affinity of DCGIV may overcome the weak binding conformation and achieves also to bind on the second LBD or binding of DCGIV to a LBD in general does not cause allosteric effects. A possible role for negative cooperativity in receptor function is to extend the glutamate concentration range to which the receptor can respond which would be useful for example in situations where continuous activity at synapses takes place. The receptor would be able

to respond because the ligand binding sites are not completely saturated. Another advantage would be a greater sensitivity for a lower ligand concentration.
Despite this obvious discrepancy in inhibitory strength during pharmacological and synaptic or uncaging induced group II mGluR activation by glutamate, the integral inhibition on network activity mediated by group II mGluRs could be the same compared to a receptor mediating a direct and strong effect on synaptic transmission, because evidence is provided that the inhibitory group II mGluR effect is long lasting. In other words, the total inhibition does not necessarily differ between a fast and strong and a weak and continuing inhibition, meaning that the latter could be as effective as the first.

4.4 How and when could presynaptic inhibitory group II mGluRs activate under physiological conditions?

To understand glutamatergic modulation by presynaptic inhibitory group II mGluRs at medial perforant path terminals, morphological determinants as well as extrinsic and intrinsic factors have to be considered. The complexity of this scenario is immense, however it is worthwhile consider it to find potential answers on unsolved secrets. Medial perforant path fibre terminals form axo-spinous asymmetric synapses at granule cell dendrites (Frotscher et al., 2000). Asymmetric synapses are surrounded by astrocytes (Theodosis et al., 2008), amongst others responsible for glutamate clearance after release. Group II mGluRs are located peri-synaptically nearer the axonal part of the neuron facing away the synaptic cleft (Lujan et al., 1997) on MPP terminals and show a high glutamate affinity (Pin and Duvoisin, 1995). Immediately after presynaptic release glutamate can reach millimolar concentrations at least in the synaptic cleft (Barbour, 2001), but diffusion restricts the spatial range of released glutamate enormously (Min et al., 1998), and also astrocyte glutamate transporters can eliminate glutamate within milliseconds after release (Diamond, 2005). As we have shown in our experiments, astroglial glutamate uptake is one of the limiting factors tightly controlling the degree of mGluR activation. The high receptor affinity for glutamate implies activation even at very low concentration. However, the literature (Scanziani et al.,

1997) and our systematic analysis of group II mGluR activation confirm that they do not activate during normal level of glutamate release during low-frequent activity.

Obviously the interplay between the anatomical arrangement of involved neurons and glia, the sub-cellular location of presynaptic group II mGluRs and the competitions brought to the synapse by glutamate transporters makes receptor activation highly specific to certain presynaptic inputs which cause a spread of neurotransmitter that overcomes the strong homeostasis between release and removal. This suggests a group II mGluR activation by at least a homo-synaptic mechanism, meaning that glutamate spills over from the same synapses in the stimulated fibre tract to bind to the metabotropic receptors (Cosgrove et al., 2011). How strong this input must be, illustrates for example a study from Diamond and Jahr (2000). High frequent stimulation (3, 4, 9, 10stimuli at 100Hz) did not overwhelm astrocyte glutamate transporter, giving rise to the assumption that group II mGluR activation needs a much stronger presynaptic activity. In accordance with studies, for example from Kew (2001) and Scanziani (1997), our systematic analysis of group II mGluR supports this assumption.

If we think about the naturally occurring firing pattern in this range, the possibilities are restricted. Medial perforant path fibres are projections mainly from layer II of the entorhinal cortex (Segal and Landis, 1974, Steward and Scoville, 1976, Ruth et al., 1982, Tamamaki and Nojyo, 1993, Witter, 2007). Depending on the behavioural state of the rat, for example REM sleep phase (Jouvet, 1969) or voluntary, preparatory, orienting or exploratory activities (Vanderwolf, 1969), layer II and III entorhinal cortex neurons can fire in a theta (5-10Hz) (Buzsaki, 2002, Shao and Dudek, 2011) and/or gamma (40-100Hz) frequency pattern (Bragin et al., 1995). The latter is modulated by theta cycles. Layer II and III entorhinal cortex neurons convey these collective signals to their targets within the hippocampus, for example to the dentate gyrus. The neurons there are also entrained into theta-gamma activity in conjunction with their entorhinal input (Bragin et al., 1995, Chrobak et al., 2000).

These finding suggest that the information flow from the entorhinal cortex to the hippocampus is regulated in a frequency dependent manner (Gloveli et al., 1997). Potentially, group II mGluRs could activate during those high frequent firing pattern and regulate the incoming information.

Apart from this, high frequent activity in the dentate gyrus occurs also, if this region undergoes multiple and consistent pathological changes (Dudek et al., 2002). It has been shown that the "gate"- function of the dentate gyrus is disturbed, which normally limits the incoming activity from the entorhinal cortex. In rats with kindling induced epilepsy, theta rhythms cause epileptiform discharges in the DG (Shao and Dudek, 2011) which give rise to the idea, that presynaptic group II mGluRs play also a modulatory role in this context.

Another possibility is that, group II mGluR could activate during high pathological levels of glutamate arising through disturbed glutamate uptake, maybe arising by a reduced or missing glial glutamate transporter expression (Tanaka et al., 1997, Rao et al., 1998)

4.5 Potential significance of group II mGluR mediated inhibitory modulation of presynaptic glutamate release in the hippocampus

Activation of mGluRs has different outcomes depending on the location of the receptor, the source of glutamate and the frequency of the input. We suggest that presynaptic inhibitory group II mGluRs at medial perforant path terminals activate cooperatively, presumably by a homo-synaptic mechanism, implemented by high frequent entorhinal activity entering the dentate gyrus which causes a high ambient glutamate concentration in the ECS. "Cooperatively" means convergence of released glutamate from many synapses might be necessary to activate group II mGluRs effectively. The opposite would be an autarkic activation via the glutamate released from the synapse where the mGlu receptors are located. It is known that in the DG, high frequent firing occurs during behaviour like sleep and exploration, strongly linked to memory formation and consolidation.

We suggest, that group II mGluRs might act as fine-tuners of synaptic communication (Cosgrove et al., 2011) within learning and memory consolidation processes by acting persistently but weak over a hundreds to a thousands of millisecond time scale on the synaptic strength of a connection. Besides, the highly frequency dependent activation of

mGluRs gives rise to the assumption that these receptors might have evolved to keep glutamate transmission within the physiological range to prevent hyper-excitability or, for example, epileptic discharges from interfering with normal brain functions (Schoepp, 2001).

4.5.1 mGluR mediated inhibition of glutamate release versus GABAergic inhibition

Apart from inhibition on synaptic transmission via mGluRs, GABAergic inhibition is also evident in the hippocampus. GABAergic inhibition is mediated via ionotropic $GABA_A$ or metabotropic $GABA_B$ receptors which can both be presynaptically or postsynaptically, as well as extra-synaptically located. Fast $GABA_A$ receptor activation controls action potential firing in a point-to-point manner and inhibits dendritic Ca^{2+} spikes. Slower inhibitory responses ("tonic inhibition"), lasting 500 to 2000ms, are caused by $GABA_B$ or extra-synaptic $GABA_A$ receptor activation. Extra-synaptic $GABA_A$ and $GABA_B$ receptors are substantially activated by GABA spillover arising during repetitive stimulation or oscillatory activity of the neuronal network, respectively.

$GABA_B$ receptors show similarities to metabotropic glutamate receptors (Kaupmann et al., 1997). They are also coupled with $G_{i/o}$ proteins, either to inhibit neurotransmission presynaptically (Thompson et al., 1993, Wu and Saggau, 1997) or to decrease postsynaptic excitability by opening G-protein coupled inwardly rectifying K+ (GIRK) channels (Sodickson and Bean, 1996, Luscher et al., 1997). The $GABA_BR$ mediated $G_{i/o}$ protein activation can also depress adenylyl cyclase and reduce Ca^{2+} channel currents (Mintz and Bean, 1993, Kerr and Ong, 1995). In addition, our study provided evidence that presynaptic inhibitory group II mGluRs show very similar activation kinetics compared to $GABA_B$ receptors (Dittman and Regehr, 1997). One can get the impression, that mGluRs and $GABA_B$ receptors fulfil the same function. However, there are differences between inhibition at excitatory synapses mediated by mGluRs and $GABA_B$ receptors. Whereas the activation of presynaptic mGluRs is coupled to the synaptic release of glutamate during high frequent activity, causing feedback inhibition, activation of $GABA_B$ receptors is in contrast dependent on transients of ambient GABA and potentially serve to detect enhanced and/or simultaneous activity of GABAergic

interneurons, for example when many interneurons fire synchronously in population oscillations (Bragin et al., 1995, Ylinen et al., 1995).

It is interesting that these two mechanism of inhibition on synaptic transmission can act together, which is described as hetero-synaptic crosstalk (Fernandes et al., 2011). mGluRs can control GABA release and/or GABA receptor activity (Chen and Bonham, 2005, Lu, 2007, Errington et al., 2011) and GABA receptors can in turn control glutamate release and/or mGlu receptor activity (Hirono et al., 2001, Ladera et al., 2008). The integrated combination of these influences determines their functional contributions to information processing.

5 Summary

Whereas pharmacological evidence suggests that presynaptic group II mGluRs function as autoreceptors and predominantly mediate a strong negative feedback regulation on synaptic transmission (Ugolini and Bordi, 1995, Macek et al., 1996, Dietrich et al., 1997, Kilbride et al., 1998), the little knowledge about endogenous activation created reasonable doubts on this theory, because the synaptic activation caused a much weaker inhibitory effect on transmitter release compared to the agonist induced depression (Scanziani et al., 1997, Kew et al., 2001). However, nobody had tried yet to shed light on this discrepancy finding out whether there is some truth in it or not. If so, it could drastically change the view about potential functional roles (Conn and Pin, 1997, Schoepp, 2001, Pinheiro and Mulle, 2008, Byrnes et al., 2009, Niswender and Conn, 2010) presynaptic inhibitory group II mGluRs might play in neuronal processes or disorders. In my thesis, I attended to this matter and performed a systematic analysis of group II mGluR activation by synaptically released glutamate in order to find the presynaptic factors controlling mGluR activation, the maximum mGluR induced inhibition and to define the time course of action on synaptic transmission. Apart from presynaptic firing pattern, mGluR activation is also controlled by glutamate uptake mechanism (Huang and Bergles, 2004), diffusion (Asztely et al., 1997, Kullmann and Asztely, 1998, Min et al., 1998), sub-cellular location (Lujan et al., 1997, Muly et al., 2007), receptor affinity (Conn and Pin, 1997) and receptors kinetics (Parnas and Parnas, 2007). The interplay of all these factors account for the presynaptic mGluR effect on glutamate release. In general, at excitatory synapses, fast chemical synaptic transmission occurs in a point to point fashion. Glutamate binds to ionotropic glutamate receptors in the active zone of presynapses and gets simultaneously cleared from the synaptic cleft via diffusion and astrocyte transporter mediated uptake within milliseconds (Scanziani et al., 1997). Extra-synaptically located receptors at presynapses like group II mGluRs can only activate, if released glutamate overcomes the homeostasis between release and removal and gets the chance to diffuse to the receptor. First, I performed fEPSP recordings and tested mGluR activation with a stimulation protocol that has already been tested successfully (Kew et al., 2001), checked the influence of slowed glutamate reuptake on mGluR activation and could

show that the mGluR mediated inhibition on synaptic transmission is strongly dependent on glial glutamate uptake. Raising the number of stimuli within the activating burst led to an increase in inhibition until a plateau was reached, mainly due to presynaptic fatigue during sustained stimulation. Changing the inter pulse interval within a burst of constant duration revealed that mGluRs also integrate the firing frequency of the presynaptic neurons. Surprisingly, repetitive burst application did not cause a temporal summation of mGluR activity. When the time course of mGluR action on synaptic communication was determined, a faster activation and a slower deactivation component could be identified. However, none of the stimulation protocols used turned out to cause an mGluR effect as drastic as a pharmacological effect, raising the question whether the functional significance of the receptor might rather be the duration of inhibition and not the strength. I focused on the kinetics in detail and determined the activation- and deactivation kinetics of the mGluR mediated inhibitory process by a combined Ca^{2+} imaging and glutamate uncaging method. For the activation kinetics the time constant could be clearly identified (τ = 150 ms), whereas in contrast, an upper and a lower estimation had to be made for the deactivation kinetics (τ ~ 150 – 1870 ms), arising from limitations of the used technique. Apart from that, these data strongly supported the assumption that presynaptic inhibitory group II mGluRs act as modulators, generating a sustained effect on synaptic communication within the MML of the DG whose integral inhibition might be comparable to a receptor which mediated a direct and strong effect. Concerning the functionality, it seems to be likely that group II mGluRs are fine-tuner of entorhinal cortex activity entering the DG, or, in the case of pathological changes, they might act protective to keep glutamate transmission with the physiological range to prevent hyper-excitability from interfering with normal brain functions.

6 Zusammenfassung

Das Resultat pharmakologischer Aktivierung präsynaptischer Gruppe II mGluRs lässt vermuten, dass jene Rezeptoren als Autorezeptoren fungieren und vorwiegend eine negative Rückkopplungsregulation synaptischer Signalübertragung bewirken (Ugolini and Bordi, 1995, Macek et al., 1996, Dietrich et al., 1997, Kilbride et al., 1998). Im Gegenzug dazu ist wenig bekannt über die physiologische Aktivierung Gruppe II mGluRs über den endogenen Liganden Glutamat. Das wenige Wissen darüber lässt jedoch große Zweifel an der Rolle präsynaptischer Gruppe II mGluRs als Autorezeptoren entstehen, da die synaptische Aktivierung dieser Rezeptoren über die Ausschüttung von Glutamat zu einer sehr viel geringeren Hemmung der Signalübertragung an Synapsen führt (Scanziani et al., 1997, Kew et al., 2001). Trotz dieser enormen Diskrepanz hatte bisher niemand versucht darüber Aufschluss zu geben. Würde sich die Annahme eines signifikanten Unterschiedes zwischen pharmakologischer und endogener Glutamat vermittelter Aktivierung präsynaptischer Gruppe II mGluRs verfestigen, müssten die potentiellen funktionelle Eigenschaften die diesen Rezeptoren angedacht sind, nochmals gründlich überdacht werden. In meiner Doktorarbeit nahm ich mich dieser Sache an und führte eine systematische Analyse über die synaptische Aktivierung Gruppe II mGluRs durch um herauszufinden, welche präsynaptischen Faktoren die Rezeptoraktivierung kontrollieren, wann die mGluR vermittelte Hemmung nach synaptischer Aktivierung maximal ist und wie die Aktivierung- und Deaktivierungskinetik der mGluR vermittelten Hemmung aussieht. Neben der Aktivität präsynaptischer Neurone spielen auch Faktoren wie Glutamataufnahme (Huang and Bergles, 2004), Diffusion (Asztely et al., 1997, Kullmann and Asztely, 1998, Min et al., 1998), subzelluläre Lokalisation (Lujan et al., 1997, Muly et al., 2007), Rezeptoraffinität (Conn and Pin, 1997) und Rezeptorkinetik (Parnas and Parnas, 2007) eine wesentliche Rolle bei der Aktivierung präsynaptischer Gruppe II mGluRs. Das Zusammenspiel all dieser Faktoren bestimmt im Wesentlichen die mGluR-Wirkung auf die neuronale Signalübertragung. Im Allgemeinen verläuft die Signalübertragung an exzitatorischen Synapsen von „Punkt zu Punkt". Ausgeschüttetes Glutamate bindet an hochaffine ionotrope Glutamatrezeptoren im synaptischen Spalt und wird simultan über Diffusion und astrozytäre Glutamataufnahme schnell aus dem

Extrazellulärraum entfernt (Scanziani et al., 1997). An Präsynapsen extrasynaptisch lokalisierte Rezeptoren, z.B. Gruppe II mGluRs, können nur aktivieren, wenn synaptisch ausgeschüttetes Glutamat die Homöostase zwischen Ausschüttung und Entfernung überwindet und die Chance erhält zu dem von synaptischen Spalt entfernter liegenden Rezeptor zu diffundieren. Zuallererst führten wir Feldpotentialmessungen durch und testeten Gruppe II mGluR Aktivierung mit einem bereits erfolgreich erprobten Stimulationsprotokoll (Kew et al., 2001). Eine Verlangsamung der Glutamat-Aufnahme durch eine partielle Blockade astrozytärer Glutamattransporter bewirkte eine Vergrößerung des mGluR vermittelten hemmenden Effekts auf die synaptische Signalübertragung. Dies verdeutlichte eine starke Abhängigkeit der mGluR Aktivierung von der Glutamataufnahme. Eine Erhöhung der Anzahl an Stimuli innerhalb der konditionierenden Bursts führte zu einer Steigerung der mGluR Aktivierung bis ein Plateau erreicht wurde, hauptsächlich hervorgerufen durch eine Erschöpfung der Präsynapsen während anhaltender Stimulation. Wurde das Inter-Stimulus-Intervall innerhalb einer konditionierenden Salve relative konstanter Dauer verändert, konnte zudem eine Abhängigkeit der mGluR Aktivierung von der Stimulationsfrequenz gezeigt werden. Die Gabe sich wiederholender Salven führte wider Erwarten zu keiner Steigerung der mGluR Aktivierung. Die Untersuchung des Zeitverlaufs des präsynaptischen Gruppe II mGluR vermittelten hemmenden Effekts auf die synaptische Signalübertragung verdeutlichte eine schnellere Aktivierungs- und eine langsamere Deaktivierungskinetik. Alles in allem zeigte die systematische Analyse synaptischer Gruppe II mGluR Aktivierung, dass der maximal erreichbare hemmende Effekt weit unter dem liegt, der über pharmakologische Gruppe II mGluR Aktivierung erreicht werden kann. Dies lässt Zweifel über die Funktionalität der mGluRs aufkommen. Möglicherweise fungieren sie nicht als Autorezeptoren, eine Starke und direkte Hemmung vermittelnd, sondern wahrscheinlicher als Rezeptoren die einen schwächeren, aber dauerhaften Einfluss auf synaptische Kommunikation ausüben. Aufgrund dieser Annahme untersuchten wir die mGluR-Kinetik mittels eines kombinatorischen Ca^{2+} imaging und Glutamat uncaging Ansatzes im Detail. Wohingegen die Zeitkonstante der Aktivierungskinetik bestimmt werden konnte (τ = 150ms), stellte sich die Bestimmung der Deaktivierungszeitkonstante als schwierig heraus. Eingeschränkt durch methodische Limitierungen musste für die Deaktivierung eine untere und obere Abschätzung gemacht werden (τ ~ 150 – 1870ms). Dennoch, trotz

dieser Einschränkungen, unterstützen diese Resultate unsere Annahme betreffend der Gruppe II mGluR Funktionalität die andeutet, dass jene Rezeptoren eher als Modulatoren agieren und einen schwächeren, aber lang anhaltenden hemmenden Effekt auf die synaptische Signalübertragung ausüben. Der Effekt muss nicht weniger wichtig sein im Vergleich zu einem Rezeptor, der z.B. eine starke und direkte Hemmung vermittelt, denn die integrale Hemmung könnte zwischen beiden Rezeptorwirkungsarten vergleichbar sein. Innerhalb des Gyrus dentatus könnten präsynaptische Gruppe II mGluRs als Fein-Modulierer eingehender entorhinaler Kortexaktivität dienen, oder, im Falle pathologischer Veränderungen, eine Schutzfunktion einnehmen indem sie die glutamaterge Signalübertragung in einem physiologischen Bereich halten, verhindernd, dass über-erregbare Neurone normale Hirnfunktionen stören.

7 Perspectives

In this study, we provided new insights about presynaptic inhibitory group II mGluR activation. Within the scope of our experiments, we were able to identify presynaptic and extrinsic factors controlling mGluR activation and to shed light on mGluR mediated inhibitory kinetics. However, many questions remain and the work on presynaptic group II mGluRs should be continued to answer open issues. Some important aspects I would like to mention here. For example, it would be important, especially to remove doubts, to find a technique to determine the deactivation kinetics as exactly as possible because we were only able to provide approximations. One suggestion would be to remove glutamate enzymatically after uncaging to minimize the probability of having persistent glutamate within the extracellular space which might keep glutamate receptors activated after uncaging. Moreover, other interesting aspects which should be brought in focus are how a change in transmitter release probability could affect mGluR activation. Also, studies to provide more evidence concerning the question of whether presynaptic group II mGluRs are activated self-sufficiently or cooperatively would be profitable. If the latter seems to be more likely, it should be clarified whether the activation is a homo- or hetero-synaptic mechanism. These are only a few ideas, but I think it is enough to highlight that the puzzle is still incomplete and more research on presynaptic mGluRs can and should be done to sharpen our understanding about mGlu receptor functionality and its context in brain function.

8 References

Alexander GM, Godwin DW (Metabotropic glutamate receptors as a strategic target for the treatment of epilepsy. Epilepsy Res 71:1-22.2006).

Altinbilek B, Manahan-Vaughan D (A specific role for group II metabotropic glutamate receptors in hippocampal long-term depression and spatial memory. Neuroscience 158:149-158.2009).

Amaral DG, Scharfman HE, Lavenex P (The dentate gyrus: fundamental neuroanatomical organization (dentate gyrus for dummies). Prog Brain Res 163:3-22.2007).

Amaral DG, Witter MP (The three-dimensional organization of the hippocampal formation: a review of anatomical data. Neuroscience 31:571-591.1989).

Amato A, Ballerini L, Attwell D (Intracellular pH changes produced by glutamate uptake in rat hippocampal slices. J Neurophysiol 72:1686-1696.1994).

Andersen P (2007) The hippocampus book. Oxford ; New York: Oxford University Press.

Anderson CM, Swanson RA (Astrocyte glutamate transport: review of properties, regulation, and physiological functions. Glia 32:1-14.2000).

Anwyl R (Metabotropic glutamate receptors: electrophysiological properties and role in plasticity. Brain Res Brain Res Rev 29:83-120.1999).

Arai A, Lynch G (AMPA receptor desensitization modulates synaptic responses induced by repetitive afferent stimulation in hippocampal slices. Brain Res 799:235-242.1998).

Araque A, Parpura V, Sanzgiri RP, Haydon PG (Tripartite synapses: glia, the unacknowledged partner. Trends Neurosci 22:208-215.1999).

Aronica E, van Vliet EA, Mayboroda OA, Troost D, da Silva FH, Gorter JA (Upregulation of metabotropic glutamate receptor subtype mGluR3 and mGluR5 in reactive astrocytes in a rat model of mesial temporal lobe epilepsy. Eur J Neurosci 12:2333-2344.2000).

Asztely F, Erdemli G, Kullmann DM (Extrasynaptic glutamate spillover in the hippocampus: dependence on temperature and the role of active glutamate uptake. Neuron 18:281-293.1997).

Asztely F, Gustafsson B (Ionotropic glutamate receptors. Their possible role in the expression of hippocampal synaptic plasticity. Mol Neurobiol 12:1-11.1996).

Awatramani GB, Slaughter MM (Intensity-dependent, rapid activation of presynaptic metabotropic glutamate receptors at a central synapse. J Neurosci 21:741-749.2001).

Balazs R, Miller S, Romano C, de Vries A, Chun Y, Cotman CW (Metabotropic glutamate receptor mGluR5 in astrocytes: pharmacological properties and agonist regulation. J Neurochem 69:151-163.1997).

Barbour B (An evaluation of synapse independence. J Neurosci 21:7969-7984.2001).

Bear MF, Abraham WC (Long-term depression in hippocampus. Annu Rev Neurosci 19:437-462.1996).

Bennett MV, Contreras JE, Bukauskas FF, Saez JC (New roles for astrocytes: gap junction hemichannels have something to communicate. Trends Neurosci 26:610-617.2003).

Bergles DE, Dzubay JA, Jahr CE (Glutamate transporter currents in bergmann glial cells follow the time course of extrasynaptic glutamate. Proc Natl Acad Sci U S A 94:14821-14825.1997).

Bergles DE, Jahr CE (Synaptic activation of glutamate transporters in hippocampal astrocytes. Neuron 19:1297-1308.1997).

Bischofberger J, Engel D, Frotscher M, Jonas P (Timing and efficacy of transmitter release at mossy fiber synapses in the hippocampal network. Pflugers Arch 453:361-372.2006).

Bleakman D, Alt A, Nisenbaum ES (Glutamate receptors and pain. Semin Cell Dev Biol 17:592-604.2006).

Bockaert J, Pin J, Fagni L (Metabotropic glutamate receptors: an original family of G protein-coupled receptors. Fundam Clin Pharmacol 7:473-485.1993).

Borg J, Balcar VJ, Mandel P (High affinity uptake in neuronal and glial cells. Brain Res 118:514-516.1976).

Bortolotto ZA, Fitzjohn SM, Collingridge GL (Roles of metabotropic glutamate receptors in LTP and LTD in the hippocampus. Curr Opin Neurobiol 9:299-304.1999).

Boulton CL, von Haebler D, Heinemann U (Tracing of axonal connections by rhodamine-dextran-amine in the rat hippocampal-entorhinal cortex slice preparation. Hippocampus 2:99-106.1992).

Bouvier M, Szatkowski M, Amato A, Attwell D (The glial cell glutamate uptake carrier countertransports pH-changing anions. Nature 360:471-474.1992).

Braak E (On the fine structure of the external glial layer in the isocortex of man. Cell Tissue Res 157:367-390.1975).

Bradley SR, Marino MJ, Wittmann M, Rouse ST, Awad H, Levey AI, Conn PJ (Activation of group II metabotropic glutamate receptors inhibits synaptic excitation of the substantia Nigra pars reticulata. J Neurosci 20:3085-3094.2000).

Bragin A, Jando G, Nadasdy Z, Hetke J, Wise K, Buzsaki G (Gamma (40-100 Hz) oscillation in the hippocampus of the behaving rat. J Neurosci 15:47-60.1995).

Brown RE, Reymann KG (Metabotropic glutamate receptor agonists reduce paired-pulse depression in the dentate gyrus of the rat in vitro. Neurosci Lett 196:17-20.1995).

Bruni JE, Clattenburg RE, Millar E (Tanycyte ependymal cells in the third ventricle of young and adult rats: a Golgi study. Anat Anz 153:53-68.1983).

Bushong EA, Martone ME, Ellisman MH (Examination of the relationship between astrocyte morphology and laminar boundaries in the molecular layer of adult dentate gyrus. J Comp Neurol 462:241-251.2003).

Buzsaki G (Theta oscillations in the hippocampus. Neuron 33:325-340.2002).

Byrnes KR, Loane DJ, Faden AI (Metabotropic glutamate receptors as targets for multipotential treatment of neurological disorders. Neurotherapeutics 6:94-107.2009).

Callaway EM, Katz LC (Photostimulation using caged glutamate reveals functional circuitry in living brain slices. Proc Natl Acad Sci U S A 90:7661-7665.1993).

Capogna M (Distinct properties of presynaptic group II and III metabotropic glutamate receptor-mediated inhibition of perforant pathway-CA1 EPSCs. Eur J Neurosci 19:2847-2858.2004).

Cartmell J, Schoepp DD (Regulation of neurotransmitter release by metabotropic glutamate receptors. J Neurochem 75:889-907.2000).

Carzoli KL, Hyson RL (In vivo analysis of the role of metabotropic glutamate receptors in the afferent regulation of chick cochlear nucleus neurons. Hear Res 272:49-57.2011).

Castillo PE, Malenka RC, Nicoll RA (Kainate receptors mediate a slow postsynaptic current in hippocampal CA3 neurons. Nature 388:182-186.1997).

Chaki S, Yoshikawa R, Hirota S, Shimazaki T, Maeda M, Kawashima N, Yoshimizu T, Yasuhara A, Sakagami K, Okuyama S, Nakanishi S, Nakazato A (MGS0039: a potent and selective group II metabotropic glutamate receptor antagonist with antidepressant-like activity. Neuropharmacology 46:457-467.2004).

Chang PY, Jackson MB (Interpretation and optimization of absorbance and fluorescence signals from voltage-sensitive dyes. J Membr Biol 196:105-116.2003).

Chavis P, Shinozaki H, Bockaert J, Fagni L (The metabotropic glutamate receptor types 2/3 inhibit L-type calcium channels via a pertussis toxin-sensitive G-protein in cultured cerebellar granule cells. J Neurosci 14:7067-7076.1994).

Chen CY, Bonham AC (Glutamate suppresses GABA release via presynaptic metabotropic glutamate receptors at baroreceptor neurones in rats. J Physiol 562:535-551.2005).

Chou KC (Prediction of G-protein-coupled receptor classes. J Proteome Res 4:1413-1418.2005).

Chrobak JJ, Lorincz A, Buzsaki G (Physiological patterns in the hippocampo-entorhinal cortex system. Hippocampus 10:457-465.2000).

Clements JD (Transmitter timecourse in the synaptic cleft: its role in central synaptic function. Trends Neurosci 19:163-171.1996).

Clements JD, Lester RA, Tong G, Jahr CE, Westbrook GL (The time course of glutamate in the synaptic cleft. Science 258:1498-1501.1992).

Cochilla AJ, Alford S (Metabotropic glutamate receptor-mediated control of neurotransmitter release. Neuron 20:1007-1016.1998).

Conn PJ, Battaglia G, Marino MJ, Nicoletti F (Metabotropic glutamate receptors in the basal ganglia motor circuit. Nat Rev Neurosci 6:787-798.2005).

Conn PJ, Pin JP (Pharmacology and functions of metabotropic glutamate receptors. Annu Rev Pharmacol Toxicol 37:205-237.1997).

Cosgrove KE, Galvan EJ, Barrionuevo G, Meriney SD (mGluRs modulate strength and timing of excitatory transmission in hippocampal area CA3. Mol Neurobiol 44:93-101.2011).

Cotman CW, Flatman JA, Ganong AH, Perkins MN (Effects of excitatory amino acid antagonists on evoked and spontaneous excitatory potentials in guinea-pig hippocampus. J Physiol 378:403-415.1986).

Danbolt NC (Glutamate uptake. Prog Neurobiol 65:1-105.2001).

Das GD (Differentiation of Bergmann glia cells in the cerebellum: a golgi study. Brain Res 110:199-213.1976).

Diamond JS (Deriving the glutamate clearance time course from transporter currents in CA1 hippocampal astrocytes: transmitter uptake gets faster during development. J Neurosci 25:2906-2916.2005).

Diamond JS, Jahr CE (Transporters buffer synaptically released glutamate on a submillisecond time scale. J Neurosci 17:4672-4687.1997).

Diamond JS, Jahr CE (Synaptically released glutamate does not overwhelm transporters on hippocampal astrocytes during high-frequency stimulation. J Neurophysiol 83:2835-2843.2000).

Dietrich D, Beck H, Kral T, Clusmann H, Elger CE, Schramm J (Metabotropic glutamate receptors modulate synaptic transmission in the perforant path: pharmacology and localization of two distinct receptors. Brain Res 767:220-227.1997).

Dietrich D, Kirschstein T, Kukley M, Pereverzev A, von der Brelie C, Schneider T, Beck H (Functional specialization of presynaptic Cav2.3 Ca2+ channels. Neuron 39:483-496.2003).

Dietrich D, Kral T, Clusmann H, Friedl M, Schramm J (Presynaptic group II metabotropic glutamate receptors reduce stimulated and spontaneous transmitter release in human dentate gyrus. Neuropharmacology 42:297-305.2002).

Dittman JS, Regehr WG (Mechanism and kinetics of heterosynaptic depression at a cerebellar synapse. J Neurosci 17:9048-9059.1997).

Doherty JJ, Alagarsamy S, Bough KJ, Conn PJ, Dingledine R, Mott DD (Metabotropic glutamate receptors modulate feedback inhibition in a developmentally regulated manner in rat dentate gyrus. J Physiol 561:395-401.2004).

Doumazane E, Scholler P, Zwier JM, Eric T, Rondard P, Pin JP (A new approach to analyze cell surface protein complexes reveals specific heterodimeric metabotropic glutamate receptors. FASEB J 25:66-77.2011).

Dube GR, Marshall KC (Activity-dependent activation of presynaptic metabotropic glutamate receptors in locus coeruleus. J Neurophysiol 83:1141-1149.2000).

Dudek FE, Hellier JL, Williams PA, Ferraro DJ, Staley KJ (The course of cellular alterations associated with the development of spontaneous seizures after status epilepticus. Prog Brain Res 135:53-65.2002).

Ellis-Davies GC (Caged compounds: photorelease technology for control of cellular chemistry and physiology. Nat Methods 4:619-628.2007).

Emsley JG, Macklis JD (Astroglial heterogeneity closely reflects the neuronal-defined anatomy of the adult murine CNS. Neuron Glia Biol 2:175-186.2006).

Eng LF (Glial fibrillary acidic protein (GFAP): the major protein of glial intermediate filaments in differentiated astrocytes. J Neuroimmunol 8:203-214.1985).

Erdmann E, Rupprecht V, Matthews E, Kukley M, Schoch S, Dietrich D (Depression of Release by mGluR8 Alters Ca2+ Dependence of Release Machinery. Cereb Cortex.2011).

Errington AC, Di Giovanni G, Crunelli V, Cope DW (mGluR control of interneuron output regulates feedforward tonic GABAA inhibition in the visual thalamus. J Neurosci 31:8669-8680.2011).

Fernandes LG, Jin YH, Andresen MC (Heterosynaptic crosstalk: GABA-glutamate metabotropic receptors interactively control glutamate release in solitary tract nucleus. Neuroscience 174:1-9.2011).

Fernandez-Alfonso T, Ryan TA (The kinetics of synaptic vesicle pool depletion at CNS synaptic terminals. Neuron 41:943-953.2004).

Fonnum F (Glutamate: a neurotransmitter in mammalian brain. J Neurochem 42:1-11.1984).

Forsythe ID, Westbrook GL (Slow excitatory postsynaptic currents mediated by N-methyl-D-aspartate receptors on cultured mouse central neurones. J Physiol 396:515-533.1988).

Fredriksson R, Lagerstrom MC, Lundin LG, Schioth HB (The G-protein-coupled receptors in the human genome form five main families. Phylogenetic analysis, paralogon groups, and fingerprints. Mol Pharmacol 63:1256-1272.2003).

Fremeau RT, Jr., Troyer MD, Pahner I, Nygaard GO, Tran CH, Reimer RJ, Bellocchio EE, Fortin D, Storm-Mathisen J, Edwards RH (The expression of vesicular glutamate transporters defines two classes of excitatory synapse. Neuron 31:247-260.2001).

Frotscher M, Drakew A, Heimrich B (Role of afferent innervation and neuronal activity in dendritic development and spine maturation of fascia dentata granule cells. Cereb Cortex 10:946-951.2000).

Furtak SC, Wei SM, Agster KL, Burwell RD (Functional neuroanatomy of the parahippocampal region in the rat: the perirhinal and postrhinal cortices. Hippocampus 17:709-722.2007).

Gadea A, Lopez-Colome AM (Glial transporters for glutamate, glycine and GABA I. Glutamate transporters. J Neurosci Res 63:453-460.2001).

Gloveli T, Schmitz D, Empson RM, Heinemann U (Frequency-dependent information flow from the entorhinal cortex to the hippocampus. J Neurophysiol 78:3444-3449.1997).

Gonzalez-Maeso J, Ang RL, Yuen T, Chan P, Weisstaub NV, Lopez-Gimenez JF, Zhou M, Okawa Y, Callado LF, Milligan G, Gingrich JA, Filizola M, Meana JJ, Sealfon SC (Identification of a serotonin/glutamate receptor complex implicated in psychosis. Nature 452:93-97.2008).

Grueter BA, McElligott ZA, Robison AJ, Mathews GC, Winder DG (In vivo metabotropic glutamate receptor 5 (mGluR5) antagonism prevents cocaine-induced disruption of postsynaptically maintained mGluR5-dependent long-term depression. J Neurosci 28:9261-9270.2008).

Hansson E (Regional heterogeneity among astrocytes in the central nervous system. Neurochem Int 16:237-245.1990).

Hildebrand C, Remahl S, Waxman SG (Axo-glial relations in the retina-optic nerve junction of the adult rat: electron-microscopic observations. J Neurocytol 14:597-617.1985).

Hirono M, Yoshioka T, Konishi S (GABA(B) receptor activation enhances mGluR-mediated responses at cerebellar excitatory synapses. Nat Neurosci 4:1207-1216.2001).

Hjorth-Simonsen A, Jeune B (Origin and termination of the hippocampal perforant path in the rat studied by silver impregnation. J Comp Neurol 144:215-232.1972).

Hollmann M, Heinemann S (Cloned glutamate receptors. Annu Rev Neurosci 17:31-108.1994).

Huang LQ, Rowan MJ, Anwyl R (mGluR II agonist inhibition of LTP induction, and mGluR II antagonist inhibition of LTD induction, in the dentate gyrus in vitro. Neuroreport 8:687-693.1997).

Huang YH, Bergles DE (Glutamate transporters bring competition to the synapse. Curr Opin Neurobiol 14:346-352.2004).

Huang YH, Sinha SR, Tanaka K, Rothstein JD, Bergles DE (Astrocyte glutamate transporters regulate metabotropic glutamate receptor-mediated excitation of hippocampal interneurons. J Neurosci 24:4551-4559.2004).

Huettner JE (Kainate receptors and synaptic transmission. Prog Neurobiol 70:387-407.2003).

Jarrard LE (Selective hippocampal lesions: differential effects on performance by rats of a spatial task with preoperative versus postoperative training. J Comp Physiol Psychol 92:1119-1127.1978).

Jessen KR (Glial cells. Int J Biochem Cell Biol 36:1861-1867.2004).

Johnston D, Wu SM-s (1995) Foundations of cellular neurophysiology. Cambridge, Mass.: MIT Press.

Jouvet M (Biogenic amines and the states of sleep. Science 163:32-41.1969).

Kammermeier PJ, Davis MI, Ikeda SR (Specificity of metabotropic glutamate receptor 2 coupling to G proteins. Mol Pharmacol 63:183-191.2003).

Kaupmann K, Huggel K, Heid J, Flor PJ, Bischoff S, Mickel SJ, McMaster G, Angst C, Bittiger H, Froestl W, Bettler B (Expression cloning of GABA(B) receptors uncovers similarity to metabotropic glutamate receptors. Nature 386:239-246.1997).

Kerr DI, Ong J (GABAB receptors. Pharmacol Ther 67:187-246.1995).

Kew JN, Ducarre JM, Pflimlin MC, Mutel V, Kemp JA (Activity-dependent presynaptic autoinhibition by group II metabotropic glutamate receptors at the perforant path inputs to the dentate gyrus and CA1. Neuropharmacology 40:20-27.2001).

Kilbride J, Huang LQ, Rowan MJ, Anwyl R (Presynaptic inhibitory action of the group II metabotropic glutamate receptor agonists, LY354740 and DCG-IV. Eur J Pharmacol 356:149-157.1998).

Kilbride J, Rush AM, Rowan MJ, Anwyl R (Presynaptic group II mGluR inhibition of short-term depression in the medial perforant path of the dentate gyrus in vitro. J Neurophysiol 85:2509-2515.2001).

Kojima S, Nakamura T, Nidaira T, Nakamura K, Ooashi N, Ito E, Watase K, Tanaka K, Wada K, Kudo Y, Miyakawa H (Optical detection of synaptically induced glutamate transport in hippocampal slices. J Neurosci 19:2580-2588.1999).

Konnerth A, Obaid AL, Salzberg BM (Optical recording of electrical activity from parallel fibres and other cell types in skate cerebellar slices in vitro. J Physiol 393:681-702.1987).

Kosaka T, Hama K (Three-dimensional structure of astrocytes in the rat dentate gyrus. J Comp Neurol 249:242-260.1986).

Krebs HA (Metabolism of amino-acids: The synthesis of glutamine from glutamic acid and ammonia, and the enzymic hydrolysis of glutamine in animal tissues. Biochem J 29:1951-1969.1935).

Kullmann DM, Asztely F (Extrasynaptic glutamate spillover in the hippocampus: evidence and implications. Trends Neurosci 21:8-14.1998).

Kupchik YM, Barchad-Avitzur O, Wess J, Ben-Chaim Y, Parnas I, Parnas H (A novel fast mechanism for GPCR-mediated signal transduction--control of neurotransmitter release. J Cell Biol 192:137-151.2011).

Kwon HB, Castillo PE (Role of glutamate autoreceptors at hippocampal mossy fiber synapses. Neuron 60:1082-1094.2008).

Ladera C, del Carmen Godino M, Jose Cabanero M, Torres M, Watanabe M, Lujan R, Sanchez-Prieto J (Pre-synaptic GABA receptors inhibit glutamate release through GIRK channels in rat cerebral cortex. J Neurochem 107:1506-1517.2008).

Larson J, Lynch G (Role of N-methyl-D-aspartate receptors in the induction of synaptic potentiation by burst stimulation patterned after the hippocampal theta-rhythm. Brain Res 441:111-118.1988).

Lee HG, Zhu X, O'Neill MJ, Webber K, Casadesus G, Marlatt M, Raina AK, Perry G, Smith MA (The role of metabotropic glutamate receptors in Alzheimer's disease. Acta Neurobiol Exp (Wars) 64:89-98.2004).

Lehre KP, Danbolt NC (The number of glutamate transporter subtype molecules at glutamatergic synapses: chemical and stereological quantification in young adult rat brain. J Neurosci 18:8751-8757.1998).

Lehre KP, Levy LM, Ottersen OP, Storm-Mathisen J, Danbolt NC (Differential expression of two glial glutamate transporters in the rat brain: quantitative and immunocytochemical observations. J Neurosci 15:1835-1853.1995).

Lenhossek Mv (1895) Der feinere Bau des Nervensystems im Lichte neuester Forschungen: Fischers Medizinische Buchhandlung H. Kornfeld.

Lerma J (Roles and rules of kainate receptors in synaptic transmission. Nat Rev Neurosci 4:481-495.2003).

Lu Y (Endogenous mGluR activity suppresses GABAergic transmission in avian cochlear nucleus magnocellularis neurons. J Neurophysiol 97:1018-1029.2007).

Lujan R, Roberts JD, Shigemoto R, Ohishi H, Somogyi P (Differential plasma membrane distribution of metabotropic glutamate receptors mGluR1 alpha, mGluR2 and mGluR5, relative to neurotransmitter release sites. J Chem Neuroanat 13:219-241.1997).

Luscher C, Jan LY, Stoffel M, Malenka RC, Nicoll RA (G protein-coupled inwardly rectifying K+ channels (GIRKs) mediate postsynaptic but not presynaptic transmitter actions in hippocampal neurons. Neuron 19:687-695.1997).

Macek TA, Winder DG, Gereau RWt, Ladd CO, Conn PJ (Differential involvement of group II and group III mGluRs as autoreceptors at lateral and medial perforant path synapses. J Neurophysiol 76:3798-3806.1996).

Maejima T, Hashimoto K, Yoshida T, Aiba A, Kano M (Presynaptic inhibition caused by retrograde signal from metabotropic glutamate to cannabinoid receptors. Neuron 31:463-475.2001).

Malenka RC (Synaptic plasticity in the hippocampus: LTP and LTD. Cell 78:535-538.1994).

Manahan-Vaughan D, Kulla A, Frey JU (Requirement of translation but not transcription for the maintenance of long-term depression in the CA1 region of freely moving rats. J Neurosci 20:8572-8576.2000).

Manzoni OJ, Castillo PE, Nicoll RA (Pharmacology of metabotropic glutamate receptors at the mossy fiber synapses of the guinea pig hippocampus. Neuropharmacology 34:965-971.1995).

Marcaggi P, Mutoh H, Dimitrov D, Beato M, Knopfel T (Optical measurement of mGluR1 conformational changes reveals fast activation, slow deactivation, and sensitization. Proc Natl Acad Sci U S A 106:11388-11393.2009).

Masu M, Tanabe Y, Tsuchida K, Shigemoto R, Nakanishi S (Sequence and expression of a metabotropic glutamate receptor. Nature 349:760-765.1991).

Mateo Z, Porter JT (Group II metabotropic glutamate receptors inhibit glutamate release at thalamocortical synapses in the developing somatosensory cortex. Neuroscience 146:1062-1072.2007).

Mathis C, Ungerer A (The retention deficit induced by (RS)-alpha-methyl-4-carboxyphenylglycine in a lever-press learning task is blocked by selective

agonists of either group I or group II metabotropic glutamate receptors. Exp Brain Res 129:147-155.1999).

Matyash V, Kettenmann H (Heterogeneity in astrocyte morphology and physiology. Brain Res Rev 63:2-10.2010).

Mayer ML, Westbrook GL (The physiology of excitatory amino acids in the vertebrate central nervous system. Prog Neurobiol 28:197-276.1987).

McCool BA, Pin JP, Brust PF, Harpold MM, Lovinger DM (Functional coupling of rat group II metabotropic glutamate receptors to an omega-conotoxin GVIA-sensitive calcium channel in human embryonic kidney 293 cells. Mol Pharmacol 50:912-922.1996).

McNaughton BL (Evidence for two physiologically distinct perforant pathways to the fascia dentata. Brain Res 199:1-19.1980).

Meldrum BS (Glutamate as a neurotransmitter in the brain: review of physiology and pathology. J Nutr 130:1007S-1015S.2000).

Milner B (Visually-Guided Maze-Learning in Man - Effects of Bilateral Hippocampal, Bilateral Frontal, and Unilateral Cerebral-Lesions. Neuropsychologia 3:317-338.1965).

Milner B, Corkin S, Teuber HL (Further Analysis of Hippocampal Amnesic Syndrome - 14-Year Follow-up Study of Hm. Neuropsychologia 6:215-&.1968).

Min MY, Rusakov DA, Kullmann DM (Activation of AMPA, kainate, and metabotropic receptors at hippocampal mossy fiber synapses: role of glutamate diffusion. Neuron 21:561-570.1998).

Mintz IM, Bean BP (GABAB receptor inhibition of P-type Ca2+ channels in central neurons. Neuron 10:889-898.1993).

Mitchell SJ, Silver RA (Glutamate spillover suppresses inhibition by activating presynaptic mGluRs. Nature 404:498-502.2000).

Model PG, Highstein SM, Bennett MV (Depletion of vesicles and fatigue of transmission at a vertebrate central synapse. Brain Res 98:209-228.1975).

Moghaddam B (Targeting metabotropic glutamate receptors for treatment of the cognitive symptoms of schizophrenia. Psychopharmacology (Berl) 174:39-44.2004).

Monaghan DT, Bridges RJ, Cotman CW (The excitatory amino acid receptors: their classes, pharmacology, and distinct properties in the function of the central nervous system. Annu Rev Pharmacol Toxicol 29:365-402.1989).

Montgomery DL (Astrocytes: form, functions, and roles in disease. Vet Pathol 31:145-167.1994).

Muller R (A quarter of a century of place cells. Neuron 17:813-822.1996).

Muly EC, Mania I, Guo JD, Rainnie DG (Group II metabotropic glutamate receptors in anxiety circuitry: correspondence of physiological response and subcellular distribution. J Comp Neurol 505:682-700.2007).

Mutel V, Adam G, Chaboz S, Kemp JA, Klingelschmidt A, Messer J, Wichmann J, Woltering T, Richards JG (Characterization of (2S,2'R,3'R)-2-(2',3'-[3H]-

dicarboxycyclopropyl)glycine binding in rat brain. J Neurochem 71:2558-2564.1998).

Nadel L (The hippocampus and space revisited. Hippocampus 1:221-229.1991).

Nakajima Y, Iwakabe H, Akazawa C, Nawa H, Shigemoto R, Mizuno N, Nakanishi S (Molecular characterization of a novel retinal metabotropic glutamate receptor mGluR6 with a high agonist selectivity for L-2-amino-4-phosphonobutyrate. J Biol Chem 268:11868-11873.1993).

Nakanishi S (Molecular diversity of glutamate receptors and implications for brain function. Science 258:597-603.1992).

Nakanishi S (Metabotropic glutamate receptors: synaptic transmission, modulation, and plasticity. Neuron 13:1031-1037.1994).

Nedergaard M, Ransom B, Goldman SA (New roles for astrocytes: redefining the functional architecture of the brain. Trends Neurosci 26:523-530.2003).

Neki A, Ohishi H, Kaneko T, Shigemoto R, Nakanishi S, Mizuno N (Pre- and postsynaptic localization of a metabotropic glutamate receptor, mGluR2, in the rat brain: an immunohistochemical study with a monoclonal antibody. Neurosci Lett 202:197-200.1996).

Nicoll RA, Schmitz D (Synaptic plasticity at hippocampal mossy fibre synapses. Nat Rev Neurosci 6:863-876.2005).

Nikolenko V, Poskanzer KE, Yuste R (Two-photon photostimulation and imaging of neural circuits. Nat Methods 4:943-950.2007).

Nimmerjahn A, Kirchhoff F, Kerr JN, Helmchen F (Sulforhodamine 101 as a specific marker of astroglia in the neocortex in vivo. Nat Methods 1:31-37.2004).

Niswender CM, Conn PJ (Metabotropic glutamate receptors: physiology, pharmacology, and disease. Annu Rev Pharmacol Toxicol 50:295-322.2010).

Nomura A, Shigemoto R, Nakamura Y, Okamoto N, Mizuno N, Nakanishi S (Developmentally regulated postsynaptic localization of a metabotropic glutamate receptor in rat rod bipolar cells. Cell 77:361-369.1994).

O'Keefe J, Conway DH (Hippocampal place units in the freely moving rat: why they fire where they fire. Exp Brain Res 31:573-590.1978).

O'Keefe J, Dostrovsky J (The hippocampus as a spatial map. Preliminary evidence from unit activity in the freely-moving rat. Brain Res 34:171-175.1971).

Ohishi H, Neki A, Mizuno N (Distribution of a metabotropic glutamate receptor, mGluR2, in the central nervous system of the rat and mouse: an immunohistochemical study with a monoclonal antibody. Neurosci Res 30:65-82.1998).

Ohishi H, Shigemoto R, Nakanishi S, Mizuno N (Distribution of the mRNA for a metabotropic glutamate receptor (mGluR3) in the rat brain: an in situ hybridization study. J Comp Neurol 335:252-266.1993).

Olive MF (Metabotropic glutamate receptor ligands as potential therapeutics for addiction. Curr Drug Abuse Rev 2:83-98.2009).

Olton DS, Walker JA, Gage FH (Hippocampal connections and spatial discrimination. Brain Res 139:295-308.1978).

Ozawa S, Kamiya H, Tsuzuki K (Glutamate receptors in the mammalian central nervous system. Prog Neurobiol 54:581-618.1998).

Parnas H, Parnas I (The chemical synapse goes electric: Ca2+- and voltage-sensitive GPCRs control neurotransmitter release. Trends Neurosci 30:54-61.2007).

Paulsen O, Sejnowski TJ (Natural patterns of activity and long-term synaptic plasticity. Curr Opin Neurobiol 10:172-179.2000).

Perea G, Navarrete M, Araque A (Tripartite synapses: astrocytes process and control synaptic information. Trends Neurosci 32:421-431.2009).

Petralia RS, Wang YX, Niedzielski AS, Wenthold RJ (The metabotropic glutamate receptors, mGluR2 and mGluR3, show unique postsynaptic, presynaptic and glial localizations. Neuroscience 71:949-976.1996).

Pfrieger FW, Gottmann K, Lux HD (Kinetics of GABAB receptor-mediated inhibition of calcium currents and excitatory synaptic transmission in hippocampal neurons in vitro. Neuron 12:97-107.1994).

Pilc A, Chaki S, Nowak G, Witkin JM (Mood disorders: regulation by metabotropic glutamate receptors. Biochem Pharmacol 75:997-1006.2008).

Pin JP, Duvoisin R (The metabotropic glutamate receptors: structure and functions. Neuropharmacology 34:1-26.1995).

Pin JP, Galvez T, Prezeau L (Evolution, structure, and activation mechanism of family 3/C G-protein-coupled receptors. Pharmacol Ther 98:325-354.2003).

Pin JP, Kniazeff J, Goudet C, Bessis AS, Liu J, Galvez T, Acher F, Rondard P, Prezeau L (The activation mechanism of class-C G-protein coupled receptors. Biol Cell 96:335-342.2004).

Pinheiro PS, Mulle C (Presynaptic glutamate receptors: physiological functions and mechanisms of action. Nat Rev Neurosci 9:423-436.2008).

Poschel B, Manahan-Vaughan D (Group II mGluR-induced long term depression in the dentate gyrus in vivo is NMDA receptor-independent and does not require protein synthesis. Neuropharmacology 49 Suppl 1:1-12.2005).

Price CJ, Karayannis T, Pal BZ, Capogna M (Group II and III mGluRs-mediated presynaptic inhibition of EPSCs recorded from hippocampal interneurons of CA1 stratum lacunosum moleculare. Neuropharmacology 49 Suppl 1:45-56.2005).

Raff MC, Fields KL, Hakomori SI, Mirsky R, Pruss RM, Winter J (Cell-type-specific markers for distinguishing and studying neurons and the major classes of glial cells in culture. Brain Res 174:283-308.1979).

Ransom B, Behar T, Nedergaard M (New roles for astrocytes (stars at last). Trends Neurosci 26:520-522.2003).

Rao VL, Baskaya MK, Dogan A, Rothstein JD, Dempsey RJ (Traumatic brain injury down-regulates glial glutamate transporter (GLT-1 and GLAST) proteins in rat brain. J Neurochem 70:2020-2027.1998).

Reichenbach A (2004) Astrocytes and Ependymal Glia. In: Neuroglia: Oxford University Press.

Riedel G, Platt B, Micheau J (Glutamate receptor function in learning and memory. Behav Brain Res 140:1-47.2003).

Robbe D, Alonso G, Chaumont S, Bockaert J, Manzoni OJ (Role of p/q-Ca2+ channels in metabotropic glutamate receptor 2/3-dependent presynaptic long-term depression at nucleus accumbens synapses. J Neurosci 22:4346-4356.2002).

Rodriguez-Moreno A, Lerma J (Kainate receptor modulation of GABA release involves a metabotropic function. Neuron 20:1211-1218.1998).

Romano C, Yang WL, O'Malley KL (Metabotropic glutamate receptor 5 is a disulfide-linked dimer. J Biol Chem 271:28612-28616.1996).

Rusakov DA, Kullmann DM (Extrasynaptic glutamate diffusion in the hippocampus: ultrastructural constraints, uptake, and receptor activation. J Neurosci 18:3158-3170.1998).

Ruth RE, Collier TJ, Routtenberg A (Topography between the entorhinal cortex and the dentate septotemporal axis in rats: I. Medial and intermediate entorhinal projecting cells. J Comp Neurol 209:69-78.1982).

Sabatini BL, Regehr WG (Detecting changes in calcium influx which contribute to synaptic modulation in mammalian brain slice. Neuropharmacology 34:1453-1467.1995).

Sabatini BL, Regehr WG (Timing of neurotransmission at fast synapses in the mammalian brain. Nature 384:170-172.1996).

Sabatini BL, Regehr WG (Optical measurement of presynaptic calcium currents. Biophys J 74:1549-1563.1998).

Salin PA, Scanziani M, Malenka RC, Nicoll RA (Distinct short-term plasticity at two excitatory synapses in the hippocampus. Proc Natl Acad Sci U S A 93:13304-13309.1996).

Scanziani M, Gahwiler BH, Thompson SM (Presynaptic inhibition of excitatory synaptic transmission by muscarinic and metabotropic glutamate receptor activation in the hippocampus: are Ca2+ channels involved? Neuropharmacology 34:1549-1557.1995).

Scanziani M, Salin PA, Vogt KE, Malenka RC, Nicoll RA (Use-dependent increases in glutamate concentration activate presynaptic metabotropic glutamate receptors. Nature 385:630-634.1997).

Schaffhauser H, Richards JG, Cartmell J, Chaboz S, Kemp JA, Klingelschmidt A, Messer J, Stadler H, Woltering T, Mutel V (In vitro binding characteristics of a new selective group II metabotropic glutamate receptor radioligand, [3H]LY354740, in rat brain. Mol Pharmacol 53:228-233.1998).

Scharfman HE, Witter MP, Schwarcz R (The parahippocampal region. Implications for neurological and psychiatric diseases. Introduction. Ann N Y Acad Sci 911:ix-xiii.2000).

Schnitzer J (Retinal astrocytes: their restriction to vascularized parts of the mammalian retina. Neurosci Lett 78:29-34.1987).

Schoepp DD (Unveiling the functions of presynaptic metabotropic glutamate receptors in the central nervous system. J Pharmacol Exp Ther 299:12-20.2001).

Schwartz NE, Alford S (Physiological activation of presynaptic metabotropic glutamate receptors increases intracellular calcium and glutamate release. J Neurophysiol 84:415-427.2000).

Scoville WB, Milner B (Loss of Recent Memory after Bilateral Hippocampal Lesions. J Neurol Neurosur Ps 20:11-21.1957).

Segal M, Landis S (Afferents to the hippocampus of the rat studied with the method of retrograde transport of horseradish peroxidase. Brain Res 78:1-15.1974).

Seifert G, Rehn L, Weber M, Steinhauser C (AMPA receptor subunits expressed by single astrocytes in the juvenile mouse hippocampus. Brain Res Mol Brain Res 47:286-294.1997).

Shao LR, Dudek FE (Repetitive perforant-path stimulation induces epileptiform bursts in minislices of dentate gyrus from rats with kainate-induced epilepsy. J Neurophysiol 105:522-527.2011).

Shigemoto R, Kinoshita A, Wada E, Nomura S, Ohishi H, Takada M, Flor PJ, Neki A, Abe T, Nakanishi S, Mizuno N (Differential presynaptic localization of metabotropic glutamate receptor subtypes in the rat hippocampus. J Neurosci 17:7503-7522.1997).

Siegelbaum SA, Kandel ER (Learning-related synaptic plasticity: LTP and LTD. Curr Opin Neurobiol 1:113-120.1991).

Sladeczek F, Pin JP, Recasens M, Bockaert J, Weiss S (Glutamate stimulates inositol phosphate formation in striatal neurones. Nature 317:717-719.1985).

Sodickson DL, Bean BP (GABAB receptor-activated inwardly rectifying potassium current in dissociated hippocampal CA3 neurons. J Neurosci 16:6374-6385.1996).

Sontheimer H (Astrocytes, as well as neurons, express a diversity of ion channels. Can J Physiol Pharmacol 70 Suppl:S223-238.1992).

Spafford JD, Zamponi GW (Functional interactions between presynaptic calcium channels and the neurotransmitter release machinery. Curr Opin Neurobiol 13:308-314.2003).

Steward O, Scoville SA (Cells of origin of entorhinal cortical afferents to the hippocampus and fascia dentata of the rat. J Comp Neurol 169:347-370.1976).

Sugiyama H, Ito I, Hirono C (A new type of glutamate receptor linked to inositol phospholipid metabolism. Nature 325:531-533.1987).

Suzuki Y, Moriyoshi E, Tsuchiya D, Jingami H (Negative cooperativity of glutamate binding in the dimeric metabotropic glutamate receptor subtype 1. J Biol Chem 279:35526-35534.2004).

Swanson CJ, Bures M, Johnson MP, Linden AM, Monn JA, Schoepp DD (Metabotropic glutamate receptors as novel targets for anxiety and stress disorders. Nat Rev Drug Discov 4:131-144.2005).

Swanson RA, Liu J, Miller JW, Rothstein JD, Farrell K, Stein BA, Longuemare MC (Neuronal regulation of glutamate transporter subtype expression in astrocytes. J Neurosci 17:932-940.1997).

Takahashi M, Billups B, Rossi D, Sarantis M, Hamann M, Attwell D (The role of glutamate transporters in glutamate homeostasis in the brain. J Exp Biol 200:401-409.1997).

Takahashi T, Forsythe ID, Tsujimoto T, Barnes-Davies M, Onodera K (Presynaptic calcium current modulation by a metabotropic glutamate receptor. Science 274:594-597.1996).

Takayasu Y, Iino M, Ozawa S (Roles of glutamate transporters in shaping excitatory synaptic currents in cerebellar Purkinje cells. Eur J Neurosci 19:1285-1295.2004).

Tamamaki N, Nojyo Y (Projection of the entorhinal layer II neurons in the rat as revealed by intracellular pressure-injection of neurobiotin. Hippocampus 3:471-480.1993).

Tanabe Y, Nomura A, Masu M, Shigemoto R, Mizuno N, Nakanishi S (Signal transduction, pharmacological properties, and expression patterns of two rat metabotropic glutamate receptors, mGluR3 and mGluR4. J Neurosci 13:1372-1378.1993).

Tanaka K, Watase K, Manabe T, Yamada K, Watanabe M, Takahashi K, Iwama H, Nishikawa T, Ichihara N, Kikuchi T, Okuyama S, Kawashima N, Hori S, Takimoto M, Wada K (Epilepsy and exacerbation of brain injury in mice lacking the glutamate transporter GLT-1. Science 276:1699-1702.1997).

Theodosis DT, Poulain DA, Oliet SH (Activity-dependent structural and functional plasticity of astrocyte-neuron interactions. Physiol Rev 88:983-1008.2008).

Thompson SM, Capogna M, Scanziani M (Presynaptic inhibition in the hippocampus. Trends Neurosci 16:222-227.1993).

Toth K, Suares G, Lawrence JJ, Philips-Tansey E, McBain CJ (Differential mechanisms of transmission at three types of mossy fiber synapse. J Neurosci 20:8279-8289.2000).

Tyler EC, Lovinger DM (Metabotropic glutamate receptor modulation of synaptic transmission in corticostriatal co-cultures: role of calcium influx. Neuropharmacology 34:939-952.1995).

Ugolini A, Bordi F (Metabotropic glutamate group II receptors are responsible for the depression of synaptic transmission induced by ACPD in the dentate gyrus. Eur J Pharmacol 294:403-410.1995).

Valenti O, Conn PJ, Marino MJ (Distinct physiological roles of the Gq-coupled metabotropic glutamate receptors Co-expressed in the same neuronal populations. J Cell Physiol 191:125-137.2002).

Valverde F, Lopez-Mascaraque L (Neuroglial arrangements in the olfactory glomeruli of the hedgehog. J Comp Neurol 307:658-674.1991).

Vanderwolf CH (Hippocampal electrical activity and voluntary movement in the rat. Electroencephalogr Clin Neurophysiol 26:407-418.1969).

Vardi N, Duvoisin R, Wu G, Sterling P (Localization of mGluR6 to dendrites of ON bipolar cells in primate retina. J Comp Neurol 423:402-412.2000).

Varma N, Carlson GC, Ledent C, Alger BE (Metabotropic glutamate receptors drive the endocannabinoid system in hippocampus. J Neurosci 21:RC188.2001).

Ventura R, Harris KM (Three-dimensional relationships between hippocampal synapses and astrocytes. J Neurosci 19:6897-6906.1999).

von Gersdorff H, Schneggenburger R, Weis S, Neher E (Presynaptic depression at a calyx synapse: the small contribution of metabotropic glutamate receptors. J Neurosci 17:8137-8146.1997).

Wahl LM, Pouzat C, Stratford KJ (Monte Carlo simulation of fast excitatory synaptic transmission at a hippocampal synapse. J Neurophysiol 75:597-608.1996).

Witter AA (1995) Hippocampal formation. In: The rat nervous system(Paxinos, G., ed) San Diego, CA: Academic Press.

Witter MP (The perforant path: projections from the entorhinal cortex to the dentate gyrus. Prog Brain Res 163:43-61.2007).

Wostrack M, Dietrich D (Involvement of Group II mGluRs in mossy fiber LTD. Synapse 63:1060-1068.2009).

Wu LG, Saggau P (Presynaptic inhibition of elicited neurotransmitter release. Trends Neurosci 20:204-212.1997).

Yao Y, Pattabiraman N, Michne WF, Huang XP, Hampson DR (Molecular modeling and mutagenesis of the ligand-binding pocket of the mGlu3 subtype of metabotropic glutamate receptor. J Neurochem 86:947-957.2003).

Ylinen A, Soltesz I, Bragin A, Penttonen M, Sik A, Buzsaki G (Intracellular correlates of hippocampal theta rhythm in identified pyramidal cells, granule cells, and basket cells. Hippocampus 5:78-90.1995).

Yokoi M, Kobayashi K, Manabe T, Takahashi T, Sakaguchi I, Katsuura G, Shigemoto R, Ohishi H, Nomura S, Nakamura K, Nakao K, Katsuki M, Nakanishi S (Impairment of hippocampal mossy fiber LTD in mice lacking mGluR2. Science 273:645-647.1996).

Yoshino M, Kamiya H (Suppression of presynaptic calcium influx by metabotropic glutamate receptor agonists in neonatal rat hippocampus. Brain Res 695:179-185.1995).

Yoshino M, Sawada S, Yamamoto C, Kamiya H (A metabotropic glutamate receptor agonist DCG-IV suppresses synaptic transmission at mossy fiber pathway of the guinea pig hippocampus. Neurosci Lett 207:70-72.1996).

Zhang Y, Barres BA (Astrocyte heterogeneity: an underappreciated topic in neurobiology. Curr Opin Neurobiol 20:588-594.2010).

Zucker RS (Short-term synaptic plasticity. Annu Rev Neurosci 12:13-31.1989).

Vorträge:

Juni 2011

Internationales Symposium des Neurozentrums in Echternach (Luxemburg)
The functional role of presynaptic group II metabotropic glutamate receptors in the hippocampus

August 2009

Internationales Symposium des Neurozentrums in Marienheide
Role of receptors kinetics for synaptic activation of presynaptic metabotropic glutamate receptors

Poster:

Juli 2011

Neurobiologischer Doktoranden-Workshop (NeuroDoWo) in Bonn 2011
Vanessa Rupprecht, Dirk Dietrich
The functional role of presynaptic group II metabotropic glutamate receptors (mGluRs) in the dentate gyrus of the rat

November 2010

Jährliche Tagung der Society for Neuroscience in San Diego 2010
Vanessa Rupprecht, Dirk Dietrich
Slow receptor kinetics of presynaptic group II mGluRs cause a long lasting inhibition of glutamate release

März 2009

Tagung der Deutschen Neurowissenschaftlichen Gesellschaft in Göttingen 2009
Vanessa Rupprecht, Nevzat Güler, Dirk Dietrich
Synaptic activation of group II metabotropic glutamate receptors in the dentate gyrus of the rat

September 2007

Tagung der Deutschen Zoologische Gesellschaft (DZG) in Köln 2007
Vanessa Rupprecht, Gabriele Uhl
Male mate choice in the dwarf spider *Oedothorax retusus*

Veröffentlichungen:

September 2011

Evelyn Erdmann, Vanessa Rupprecht, Elizabeth Matthews, Maria Kukley, Susanne Schoch and Dirk Dietrich
Depression of Release by mGluR8 Alters Ca^{2+} Dependence of Release Machinery
Cerebral Cortex, September 7, 2011